

Prostor
kraj
čas

14

AIRBORNE LASER SCANNING RASTER DATA VISUALIZATION

A Guide to Good Practice

Žiga Kokalj and Ralf Hesse

PROSTOR, KRAJ, ČAS



ZALOŽBA
Z R C

PROSTOR, KRAJ, ČAS

**Airborne laser scanning raster data
visualization:
A Guide to Good Practice**

**Žiga Kokalj
Ralf Hesse**

Založba ZRC

Ljubljana, 2017

PROSTOR, KRAJ, ČAS 14

AIRBORNE LASER SCANNING RASTER DATA VISUALIZATION

A Guide to Good Practice

Žiga Kokalj and Ralf Hesse

Edited by: Nataša Gregorič Bon

Photography: Žiga Kokalj, Jovan Cukut, Forestry Commission Scotland, Boštjan Laharnar, Lawrence Goldman, Brian Lockett, Frank Numrich, Michael Wilson

Issued by: Institute of Anthropological and Spatial Studies, ZRC SAZU

For the Issuer: Ivan Šprajc

Publisher: Založba ZRC

For the Publisher: Oto Luthar

Reviewed by: Kevin Barton, Robert Shaw

CIP – Kataložni zapis o publikaciji
Narodna in univerzitetna knjižnica, Ljubljana
528.8.044.6:911.5(0.034.2)

KOKAJ, Žiga

Airborne laser scanning raster data visualization [Elektronski vir] : a guide to good practice / Žiga Kokalj, Ralf Hesse ; [photography Žiga Kokalj ... et al.]. - 1st e-ed. - El. knjiga. - Ljubljana : Založba ZRC, 2017. - (Prostor, kraj, čas, ISSN 2335-4208 ; 14)

ISBN 978-961-254-984-8 (pdf)

<https://doi.org/10.3986/9789612549848>

1. HESSE, Ralf

288463616



First e-edition.
Ljubljana 2017

© 2017, authors, Institute of Anthropological and Spatial Studies ZRC SAZU, Založba ZRC. All rights reserved. No part of this publication may be reproduced, stored in a retrieval system or transmitted, in any form or by any means, electronic, mechanical, photocopying, recording or otherwise, without the prior permission of the publisher.

The authors acknowledge the financial support from the Slovenian Research Agency (research core funding No. P6-0079 and project No. J6-7085).

Front Cover Image: An anisotropic sky-view factor image of the Rhône valley. SRTM Data © USGS. 2014. Shuttle Radar Topography Mission, 1 Arc-Second Global data, Sioux Falls, South Dakota, USA.

Endorsed by Archaeolandscapes International.

Abstract

This guide provides an insight into a range of visualization techniques for high-resolution digital elevation models (DEMs). It is provided in the context of investigation and interpretation of various types of historical and modern, cultural and natural small-scale relief features and landscape structures. It also provides concise guidance for selecting the best techniques when looking at a specific type of landscape and/or looking for particular kinds of forms.

The three main sections – descriptions of visualization techniques, guidance for selection of the techniques, and visualization tools – accompany examples of visualizations, exemplar archaeological and geomorphological case studies, a glossary of terms, and a list of references and recommendations for further reading. The structure facilitates people of different academic background and level of expertise to understand different visualizations, how to read them, how to manipulate the settings in a calculation, and choose the best suited for the purpose of the intended investigation.

Key Words

lidar, airborne laser scanning, visualization, interpretation, settings, techniques, tools, digital elevation model

Izveček

Monografija nudi vpogled v nabor tehnik prikaza visokoločljivih modelov višin. Napisana je v kontekstu preučevanja in interpretacije različnih tipov zgodovinskih in modernih, kulturnih in naravnih majhnih reliefnih oblik. Daje jedrnatte napotke za izbiro najboljših tehnik prikaza določenih tipov pokrajine in izrazitih oblik.

Tri glavna poglavja – opis tehnik prikazovanja digitalnih modelov višin, napotki za njihovo izbiro in orodja za izračun prikazov –, spremljajo izbrani primeri tipičnih arheoloških in geomorfoloških študij, slovarček pojmov ter seznam literature in priporočenega branja. Posameznikom z različnih znanstvenih področij in z različnim predznanjem o tematiki je struktura v pomoč pri razumevanju različnih tehnik prikazov, kako jih brati, kako izbrati prave nastavitve pri njihovem izračunu in kako prepoznati najbolj primerne za namen zasnovane raziskave.


Ključne besede

lidar, aerolasersko skeniranje, vizualizacija, prikaz prostorskih podatkov, interpretacija, nastavitve, tehnike, orodja, digitalni model višin

Contents

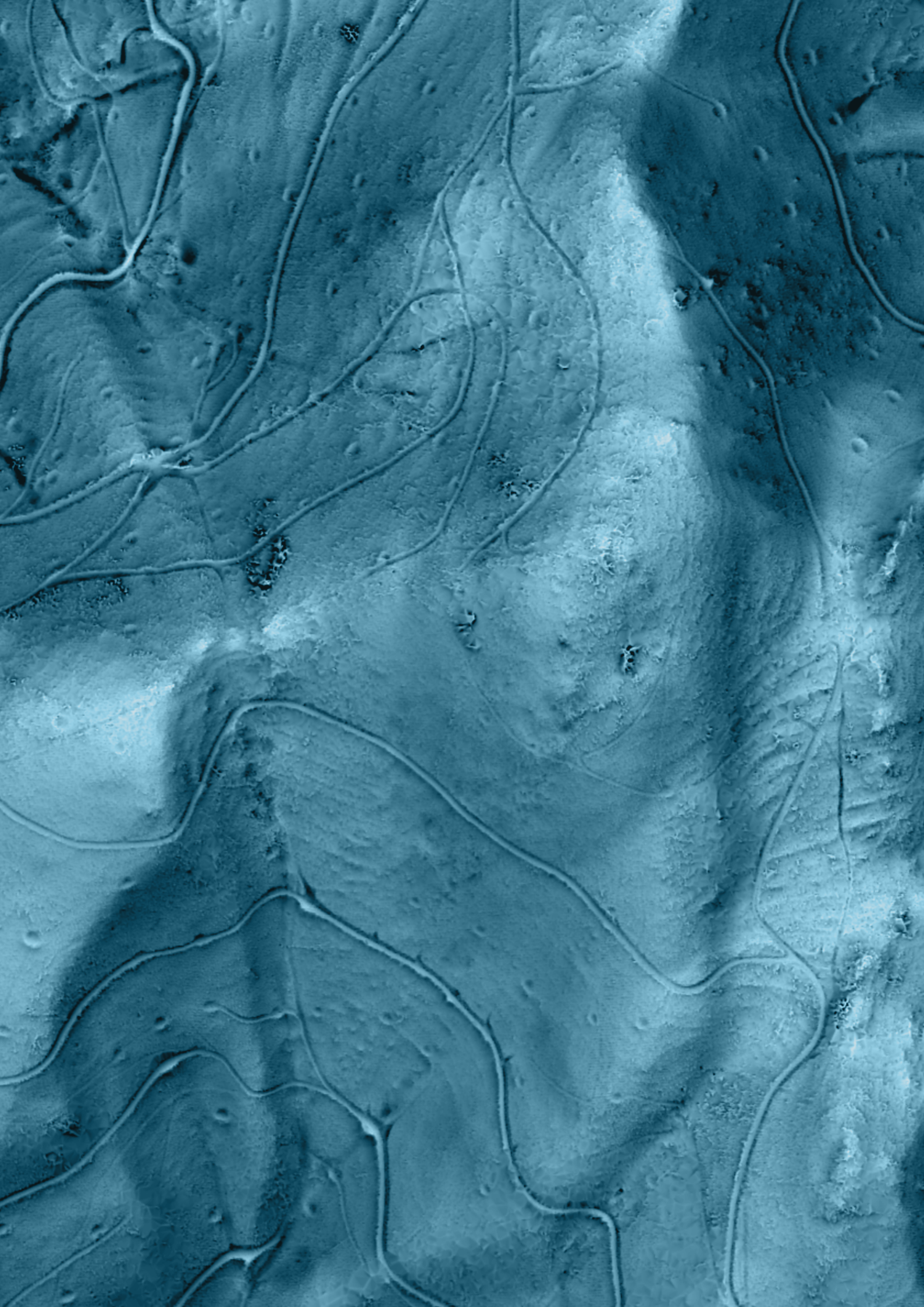
1	Introduction to the Guide	10
1.1	Aim and scope of this guide	12
1.2	How to use the guide	12
1.3	Applications of lidar visualizations	13
1.4	Free data access	13
2	Description of techniques	14
2.1	Analytical hillshading and hillshading from multiple directions	16
2.2	Slope	19
2.3	Elevation differentiation	20
2.4	Trend removal and local relief model	20
2.5	Sky-view factor and anisotropic sky-view factor	22
2.6	Openness	24
2.7	Local dominance	25
2.8	Cumulative visibility	25
2.9	Accessibility	26
2.10	Multi-scale integral invariants (MSII)	26
2.11	Laplacian-of-Gaussian (LoG)	27
2.12	Visualizing uncertainty	27
3	Guidance for selection of techniques	30
3.1	Preparing the images for detection and interpretation	32
3.2	Reading and presenting the images	34
3.2.1	Choosing appropriate visualisations	34
3.2.2	Personal preferences and intercomparability	35
3.2.3	Perception	35
3.3	Visualization of datasets other than lidar	37
3.4	What's in a name?	39
4	Tools	46
4.1	Relief Visualization Toolbox (RVT)	48
4.2	Lidar Visualisation Toolbox (LiVT)	48

5	Case studies	50
5.1	WWII anti-glider defences at Culbin, Scotland	52
5.2	Hollow ways at Volčji Potok, Slovenia	54
5.3	Prehistoric and Roman settlement above Knežak, Slovenia	56
5.4	Barrow cemetery in Pivola, Slovenia	58
5.5	Alluvial fan at Craig canyon, Saline Valley, California, USA	60
5.6	Geological features in the Julian Alps, Slovenia	62
5.7	The Granite Dells, USA	64
5.8	Cinder cones and lava flows on Mauna Loa, Hawaii, USA	66
5.9	Blind valley Odolina, Slovenia	68
5.10	Lake floor morphology, Lake Constance, Germany, Switzerland, and Austria	70
5.11	High-rise buildings in New York, USA	72
	Glossary of terms and abbreviations	74
	Bibliography and further reading	78
	List of figures	83
	List of tables	88



1

Introduction to the Guide



1

This guide aims to help specialists and interested public to produce or ask for such lidar products that will facilitate ‘reading and exploring’ the landscape for meaningful information.

1|1 Aim and scope of this guide

The aim of this Guide to good practice in airborne laser scanning (ALS) raster data visualization (hereafter called ‘the guide’) is to help specialists and interested public to produce or ask for such lidar products that will facilitate ‘reading and exploring’ the landscape for meaningful information. This guide provides an insight into a range of visualization techniques for high-resolution digital elevation models (DEMs) with their specifics, advantages and weaknesses. It is provided in the context of investigation and interpretation of various types of historical and modern, cultural and natural small-scale relief features and landscape structures. It also provides concise guidance for selecting the best techniques when looking at a specific type of landscape and/or looking for particular kinds of small-scale structures. It does not, however, provide insight into other, equally important, areas of lidar data acquisition, processing, and management. While the examples mainly relate to archaeological relief features on scales from several metres to a few hundred metres, the techniques presented in this guide are equally suitable for the visualisation of many other features on scales from microscopic to continental. Furthermore, while the focus is on DEMs based on airborne lidar, the techniques are applicable for any DEM-like raster data set, *e.g.* based on Synthetic Aperture Radar or Structure-from-Motion (SfM).

1|2 How to use the guide

The guide is aimed at everyone who is interested in visual exploration of rasterized elevation data (DEM) which can be the product of airborne lidar or other techniques. Scientists, professionals and the public are all fascinated by the details lidar data offer. While automatic feature detection is gaining importance, it is still indispensable that a human observer asks, thinks about, and answers the questions. Visual exploration and inspection is the only way to comprehend the existence, intricate relations, and context of small-scale structures in lidar data. The guide is structured so that people of different academic background and level of expertise can understand different visualizations, how to read them, how to manipulate the settings in a calculation, and which techniques to use to help answer the questions. Throughout the guide, reference is made to more detailed explanations, comparisons, observations, and further studies.

The guide is comprised of three main sections accompanied by examples of visualizations of small-scale features, exemplar archaeological and geomorphological case studies, a glossary of terms, and a list of references and recommendations for further reading.

- Descriptions of visualization techniques provide a brief

introduction to a variety of processing methods that help create meaningful images for observation, exploration, and interpretation of rasterized lidar data. A special chapter describes how to recognize and visualize uncertainty in data.

- The guidance is meant to lead the keen explorer through the main steps of the process from preparing the data to answering all the relevant questions regarding the selection of techniques that are best suited for the purpose of the intended investigation.
- The tools section briefly explains and compares the main settings and workflows of the freely available RVT and LiVT toolboxes for calculation of visualization techniques. Anyone wishing to visualize their digital elevation model (DEM) with one or several of the techniques described in the chapter Description of techniques should be able to do so with these tools, regardless of their current knowledge in image processing.

1|3 Applications of lidar visualizations

Digital elevation models are raster datasets containing elevation values. Because these numerical datasets are not readable as such, visualisation techniques are necessary to convert the DEM into human-readable greyscale or colour images. The obvious use of different visualizations is for visual examination of data. They facilitate the interpretation of terrain data and are used for visual validation of the geomorphologic quality of the DEMs *e.g.* in geography, geomorphology, cartography, archaeology, hydrology, glaciology, forestry, and disaster management. Often we use them for discovering new features, especially in archaeology, but also to better delineate and more precisely position already known objects, such as riverbanks, levees, cultural terraces, parcel divisions, stone walls, or areas of erosion. However, techniques, particularly the ones directly related to physical quantities, are also used for different other purposes. Sky-view factor, for example, is used in meteorology, because it is fundamental for modelling solar insolation, and it can be used even in engineering applications such as predicting the availability of the GPS signal in urban areas. Techniques that remove the general topography, typical examples are local relief modelling and openness, are also well suited for automatic feature extraction.

While this guide focuses on raster elevation data, it is worth mentioning the emergence and fast adaptation of pseudo and real 3D techniques for presentation of lidar point clouds or generated 3D models. These offer a whole new world of opportunities, not only for visual examination, but even more so for scientific exploration.

1|4 Free data access

Getting lidar data for research purposes is becoming increasingly simple as a growing number of science groups, governmental agencies, city councils, counties, regions, and even countries publish their data with a free and unlimited use license. Datasets come in various formats and states of processing. Gridded digital surface and terrain models are usually available, either as ASCII text files or already rasterized

files in a TIFF or other similar geospatial format. More and more classified point clouds are also shared. Table 1 lists some of the possible sources where practice experimental data (and more) can be accessed. Some portals are easier to use than others, with the more user friendly being those of Slovenia, England, and Wales.

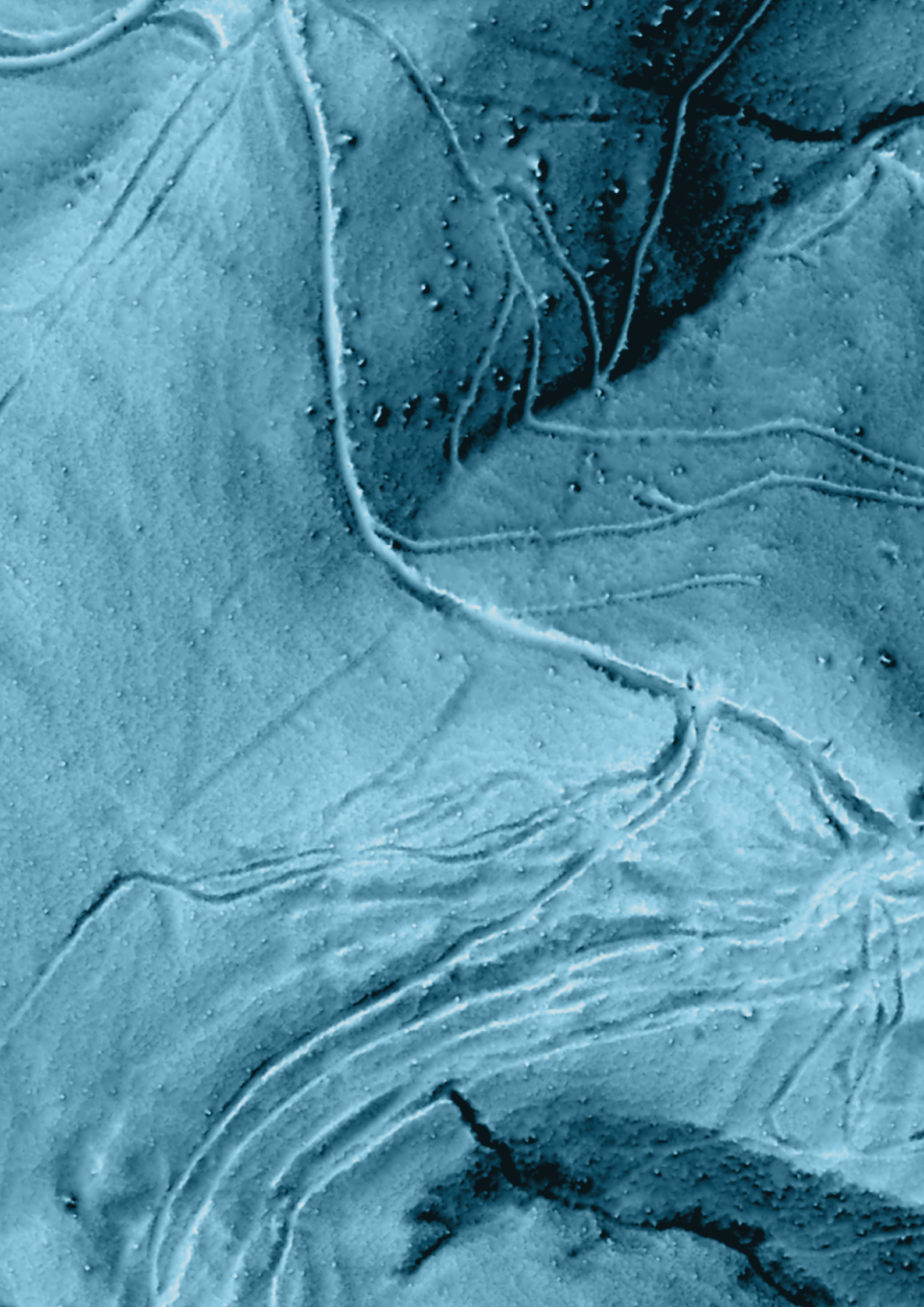
Table 1: Some useful resources to go search for free lidar datasets. Host sites will inevitably change and new datasets are becoming available regularly, so use your favourite search engine.

a list of sources	Terrain Data · openterrain Wiki · GitHub https://github.com/openterrain/openterrain/wiki/Terrain-Data
Denmark	Agency for Data Supply and Efficiency http://download.kortforsyningen.dk
England	Environment Agency http://environment.data.gov.uk/ds/survey/#/survey
Finland	National Land Survey of Finland open map data download ftp://tiedostot.kartat.kapsi.fi/laser/etrs-tm35finn2000/mara_2m
Netherlands	Dutch National SDI (PDOK) https://www.pdok.nl/nl/producten/downloaden-van-data-pdok http://geodata.nationaalgeoregister.nl/ahn2/atom/ahn2_gefilterd.xml https://geodata.nationaalgeoregister.nl/ahn2/atom/ahn2_05m_int.xml
Norway	Høydedata https://hoydedata.no/LaserInnsyn/
Spain	Plan Nacional de Observación del Territorio http://pnoa.ign.es/coberturalidar
Slovenia	Ministry of the Environment and Spatial Planning. http://gis.arso.gov.si/evode/profile.aspx?id=atlas_voda_Lidar@Arso
Sweden	Lantmäteriet http://www.lantmateriet.se/en/Maps-and-geographic-information/Elevation-data-
USA	OpenTopography http://www.opentopography.org USGS http://earthexplorer.usgs.gov ftp://rockyftp.cr.usgs.gov/vdelivery/Datasets/Staged/NED/LPC/projects NOAA - Coastal Topographic Lidar https://coast.noaa.gov/dataregistry/search/collection/info/coastallidar NASA - G-LiHT: Goddard's LiDAR, Hyperspectral & Thermal Imager http://gliht.gsfc.nasa.gov/ext/maps/index.html Search also for data of individual states as many provide them integrated into their own distribution systems.
Wales	Natural Resources Wales http://lle.gov.wales/Catalogue/Item/LidarCompositeDataset/?lang=en

A microscopic image of plant tissue, likely a leaf cross-section, showing various cellular structures. A large white number '2' is overlaid on the left side of the image. The background is a blue-tinted micrograph showing cell walls, veins, and a prominent, textured, fan-shaped structure in the lower center.

2

Description of techniques



2

The explorational value of different visualizations varies significantly with respect to characteristics of structures observed; their size, shape, orientation, concavity or convexity, degree of prominence, and edge type.

By transforming the DEM into greyscale or colour images, different types of visualizations help us make sense of lidar data. Some visualization techniques produce results that can be related to physical quantities (e.g. sky-view factor – SVF, and local relief model – LRM) while others only have a presentational value (e.g. principal components of hillshading from multiple directions). Some work better on an almost flat terrain (elevation differentiation), or topography with gentle slopes (LRM), while others on rugged or mixed terrain (SVF). Their explorational value varies significantly with respect to characteristics of structures observed; their size, shape, orientation, concavity or convexity, degree of prominence, and edge type. Not all methods can be recommended for interpretation when relative or absolute comparisons need to be judged. This is because most can change the observable properties of structures, depending on the settings used in the calculation. The DEM can be either a subset of the digital terrain model (DTM) (representing the elevations of bare-earth, in the text we regard it as such) or a digital surface model (DSM) (representing elevations of terrain or objects on it, whichever the higher), or anything between the two. See the glossary of terms (p. 76) for further details.

2|1 Analytical hillshading and hillshading from multiple directions

Relief shading (also known as hillshading or shaded relief) provides the most 'natural', i.e. intuitively readable, visual impression of all techniques. It is a description of how the relief surface reflects incoming illumination based on physical laws or empirical experience. There are numerous analytical hillshading techniques (Horn 1981; Blinn 1977; Batson *et al.* 1975; Minnaert 1961), although only the method developed by Yoëli (1965) has become a standard feature in most GIS software. Therefore, when analytical hillshading (or hillshading in general) is discussed it is the method developed by Yoëli that is implemented.

Standard analytical hillshading is easy to compute and straightforward to interpret even by non-experts and without training. It has a basic assumption that the relief is a Lambertian surface illuminated by direct light from a fictive light source at an infinite distance (the light beam has a constant azimuth and elevation angle for the entire area). The computed grey value is proportional to the cosine of the illumination incidence angle on the relief surface – the angle between the surface normal and the light beam. Areas perpendicular to the light beam are the most illuminated, while areas with an incidence angle equal or greater than

90° are dark (Figure 1A). Under very low light source angles (below 10°) features of extreme subtleness can be made visible, but this is useful for exploratory purposes in areas with only slight variations in general topography (Table 2, Figure 2).

Areas facing directly towards or away from illumination are commonly saturated (homogeneously bright or dark, respectively), and no or very little detail can be perceived there. A single light beam also fails to reveal linear structures that lie parallel to it, which can be problematic in some applications, especially in archaeology (Devereux *et al.* 2008).

Producing multiple relief shading outputs by illuminating a surface from multiple directions enhances visualization of topography (Figure 1). Hill-shaded images are sometimes used to guide ground surveys, but comparing multiple images in the field is extremely inconvenient. A step towards an improved understanding of the results is combining multiple shadings by considering only the mean (Hobbs 1995), the maximum, or the range of values, for each pixel. In order to display the areas with a low range of values more clearly, the result can be square rooted.

A common example is also a combination of standard hillshading (315° azimuth) with vertical illumination (Imhof 1982; Hobbs 1995). Hill-shades from three different directions can be used to create an RGB colour composite image by assigning the three greyscale images

to the red, green and blue colour channel (Devereux *et al.* 2008; Hobbs 1999) and this often works well indeed (Figure 3A). Because images created by illumination from several angles are highly correlated (the same scene is viewed), it is possible to 'summarize' information by a mathematical transformation with principal component analysis (PCA) (Devereux *et al.* 2008). The first three components computed from multiple (*e.g.* 16) directions usually contain a high percentage (typically over 99 %) of the variability in the original dataset. They can thus be expected to provide a basis for the visualization with minimal loss of small-scale features. The PCA – especially the combination of the first and second principal components (Figure 3B), or the RGB colour composite image of the first three (Figure 3C) – simplifies the interpretation of the multiple shading data. However, it does not provide consistent results with different datasets.

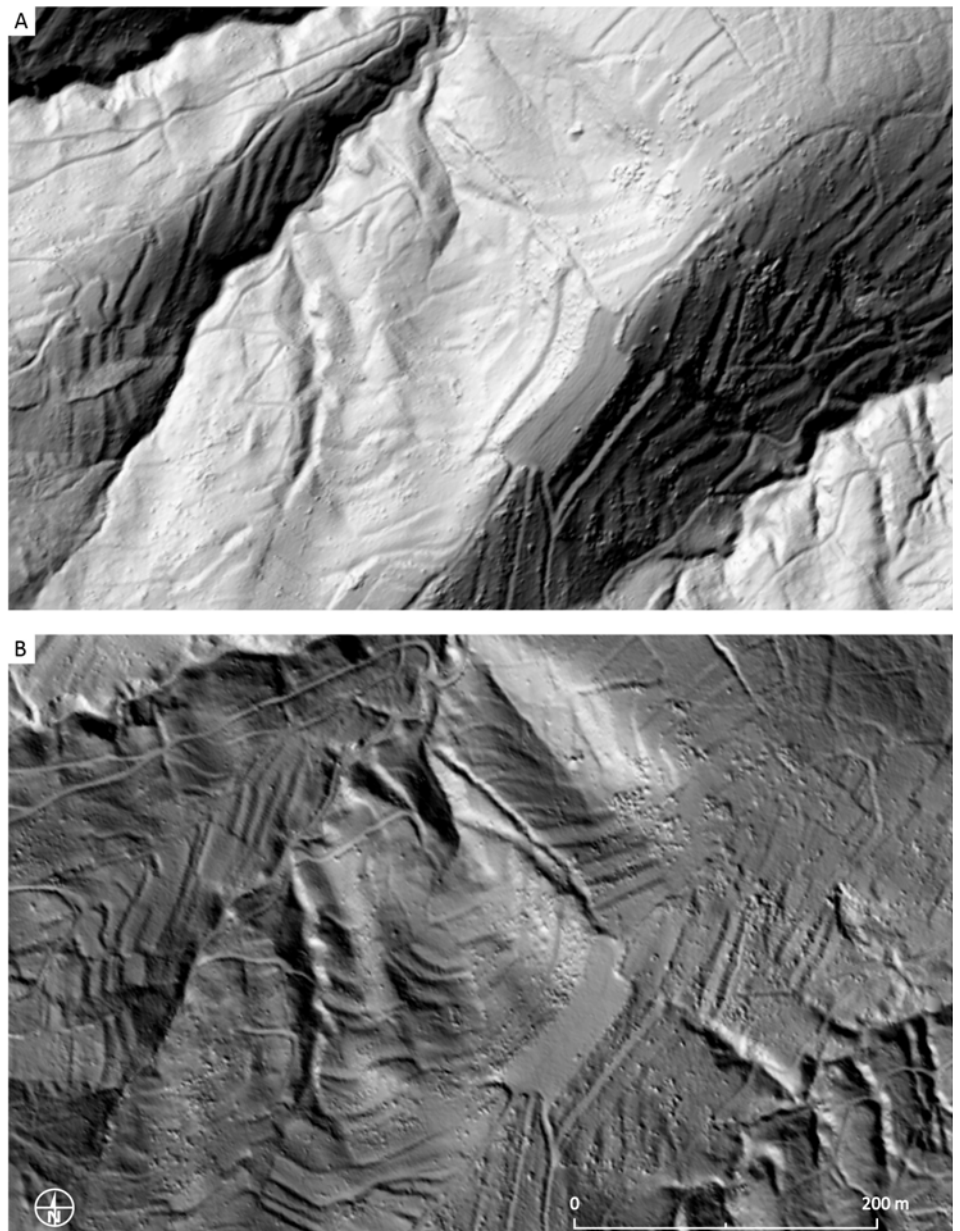


Figure 1: Angle dependence of analytical hill-shading: 315° azimuth illumination (A), and 225° azimuth (B), both with 35° Sun elevation. Note the difference of the relief perception and the structures that can be observed. Overgrown cultural terraces near Koboli in Slovenia as evidenced by 1 m spatial resolution terrain model. Data © ARSO, Slovenia. See also Figure 23.

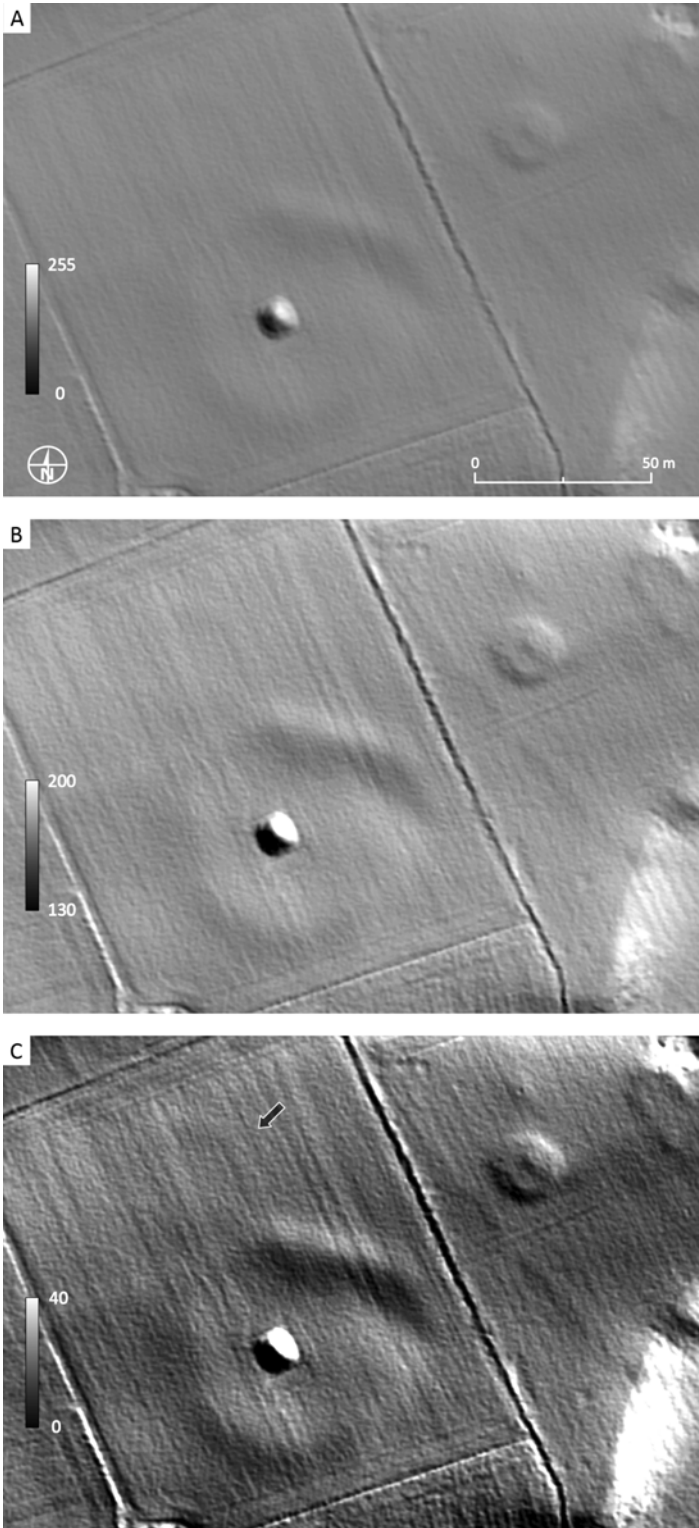


Figure 2: Very low light source angles expose features of extreme subtlety: a standard 45° Sun elevation (A) and (B), and low light 5° Sun elevation (C), all with 45° azimuth. However, this only works in areas with very gentle relief morphology, such as this example of the Site A embanked enclosure(s) in Brú na Bóinne World Heritage Site in Ireland. 1 m spatial resolution lidar data used with permission of Meath County Council and the Discovery Programme. Local histogram saturation is used to present (B) and (C). The first to show the difference this makes when compared with normally presented shaded relief (A), and the second because the image is otherwise too dark to expose any details. A hint of a small circular enclosure can be observed to the NW of the bigger one on (C).

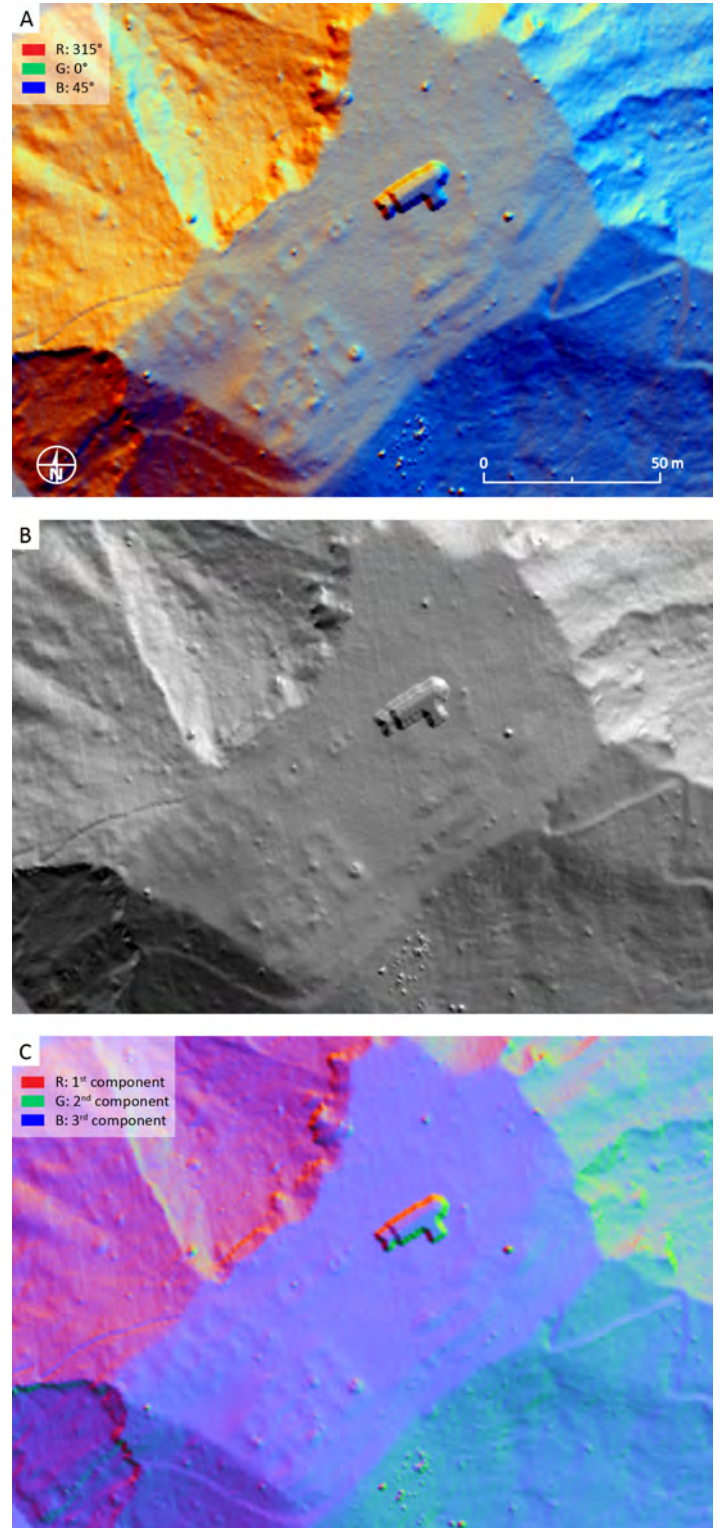


Figure 3: An RGB image of hill-shadings from three directions (315°, 0°, and 45° azimuth with 35° Sun elevation) (A), a composite of the first two components (B) and an RGB composite of the first three components of a principal component analysis of analytical hill-shading from 16 directions with 35° Sun elevation (C). A late Roman camp at St. Helena, west of Kobarid, Slovenia. 0.5 m spatial resolution lidar data © Walks of Peace in the Soča river Foundation.

Table 2: Typical settings for calculation and visualization of hillshading.

visualization parameter	general	very flat terrain	steep or complex terrain
Sun azimuth [°]	315	315	315
Sun elevation angle [°]	35	5	> 45
recommended histogram stretch	linear stretch, 2 % cut-off	linear stretch, 2 % cut-off	linear stretch, 2 % cut-off

Table 3: Typical settings for calculation and visualization of principal components analysis of hillshading images from multiple directions.

visualization parameter	general	very flat terrain	steep or complex terrain
Sun elevation angle [°]	35	5	45
number of directions	16	16	16
recommended histogram stretch	linear stretch, 2 % cut-off	linear stretch, 2 % cut-off	linear stretch, 2 % cut-off

2|2 Slope

Slope (gradient) is the first derivative of a DEM and is aspect independent. It represents the maximum rate of change between each cell and its neighbours and can be calculated either as percentage of slope or degree of slope.

Challis *et al.* (2011) found slope the best visualization technique for most circumstances among the methods they analysed. If presented in an inverted greyscale (steep slopes are darker), slope retains a very plastic representation of morphology (Table 4). However, additional information is needed to distinguish between positive/convex (*e.g.* banks) and negative/concave (*e.g.* ditches) features since slopes of the same gradient (regardless of rising or falling) are presented with the same colour (Figure 4).

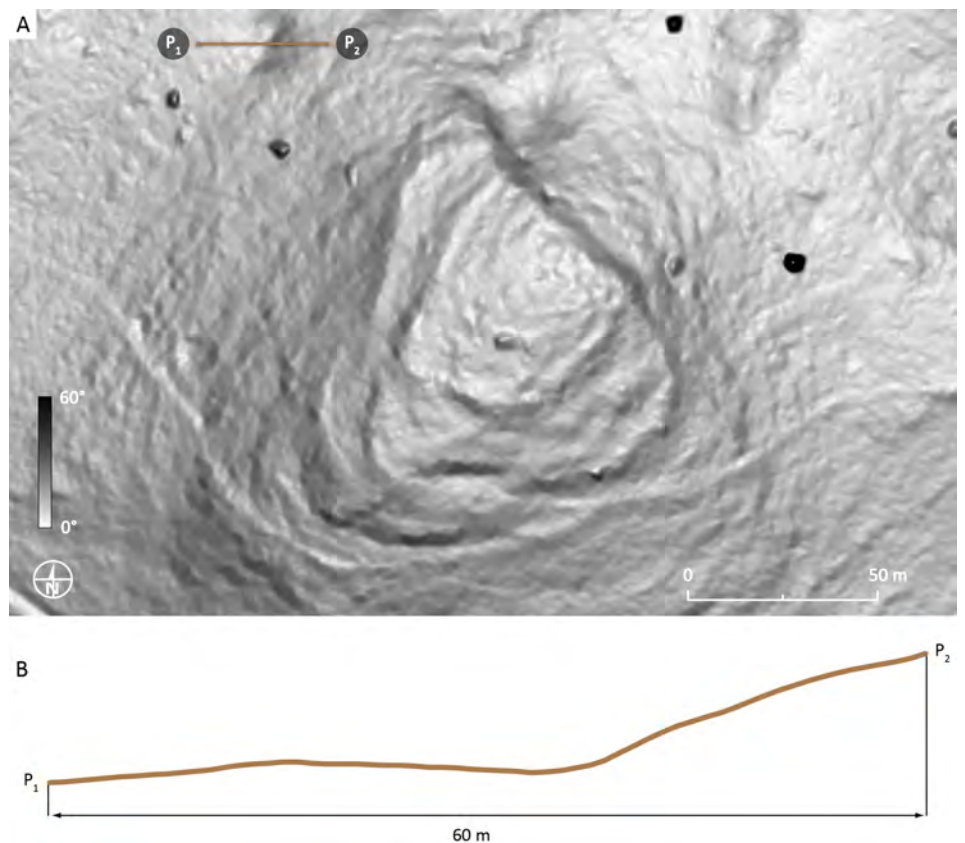


Figure 4: Slope image of Žerovinšček Iron Age hillfort near Bločice, Slovenia (A). The elevation profile (B) refers to the P₁-P₂ line in (A). Note that the structure the profile line crosses can be quite easily – and wrongly – interpreted as convex instead of concave. 1 m spatial resolution lidar data © ZRC SAZU, Slovenia.

Table 4: Typical settings for visualization of slope.

visualization parameter	general	very flat terrain	steep or complex terrain
recommended histogram stretch*	linear stretch, 0-50°	linear stretch, 0-15°	linear stretch, 0-60°

*Inverted grayscale (white to black) presentation works best

2|3 Elevation differentiation

Elevation differentiation (also referred to as colour coding, colour cast, or constrained colour ramps method) controls the range of values that are presented over a given range of greyscale tones or colours. The technique applied is a histogram stretch, whereby the range of elevation values of interest is stretched to the whole range of greyscale (or colour) values of the resulting image (Figure 5, Table 5). This can strongly enhance the contrast between pixels or areas of different elevation.

There are many variants of histogram stretch that can be applied to enhance contrast and emphasize detail. Besides the simple linear stretch between lower and upper cut-off values, these include nonlinear enhancements such as logarithmic stretch, square root enhancement, exponential stretch, and histogram equalization. However, if the preservation of the relative differences between the values (elevations) is important, the basic method known as linear stretch with saturation (cut-off of extreme values in the upper and lower parts of the histogram, also known as histogram clipping) is preferable. The histogram is linearly stretched to fill the whole range of values between the defined minimum and maximum value. For more information on how to use histogram stretch for visualization see section 3.1 Preparing the images for detection and interpretation.

Elevation differentiation is very useful for visualization of features of interest in flat landscapes and is very easy to interpret, especially when an appropriate colour ramp is used (Figure 6). It is also the only visualization technique presented that retains the original information about relief elevation. It is therefore easy to assess factors such as the depth of ditches or height of tumuli. However, even with slight variations in the general morphology of terrain, the technique becomes less useful, because archaeological earthworks are obscured by the variation in topography and because intensive manipulation of the histogram is required. For the same reasons the technique completely fails in rugged terrain.

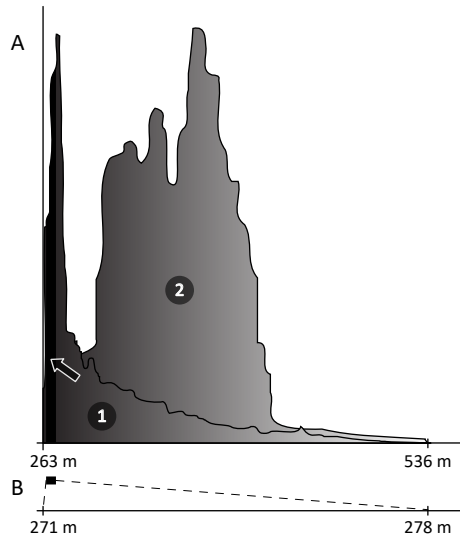


Figure 5: [A 1] A histogram of the whole data range – elevations between 263 m and 536 m. Because we are only interested in a very narrow range of values between 271 m and 278 m – marked by a dark arrow on (A) –, it makes sense to stretch only this range to the whole 'colour' palette (B). [A 2] A histogram of stretched values of the area shown on Figure 5. Instead of everything being concentrated in a 'dark corner' of the histogram, the values are much more evenly distributed and differences in colour shade can be more easily perceived.

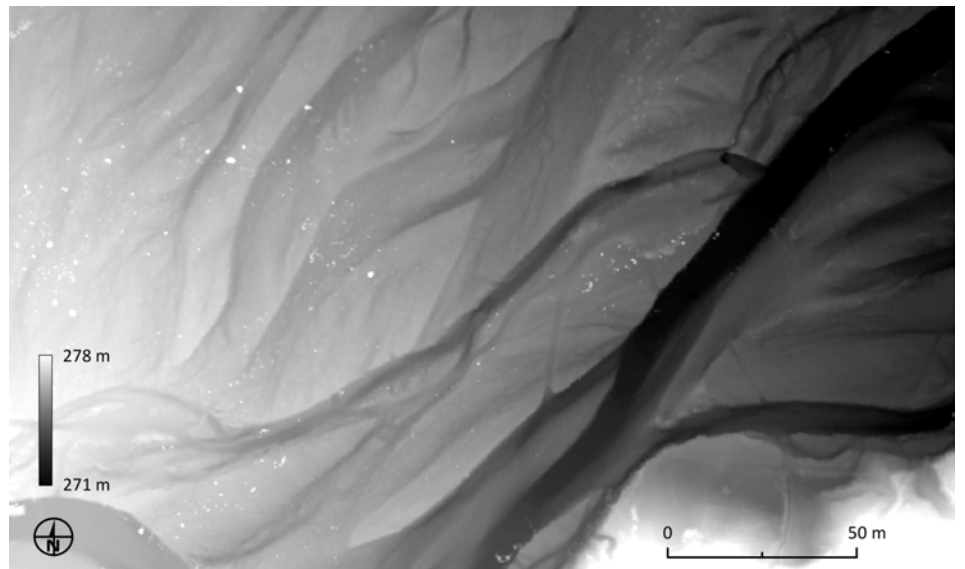


Figure 6: Histogram stretch to a narrow range of values. Past riverbeds of Nadiža. 0.5 m spatial resolution lidar data, West of Kobarid in NW Slovenia. 0.5 m spatial resolution lidar data © Walks of Peace in the Soča river Foundation.

Table 5: Typical settings for displaying elevation differentiation.

visualization parameter	general
recommended histogram stretch	linear stretch with minimum and maximum cut-off

2|4 Trend removal and local relief model

Archaeological features are generally of a much smaller scale than the landforms on which they lie. It is therefore necessary to adjust visualization techniques appropriately, for example defining a small search radius for sky-view factor calculation or set a suitable range for elevation differentiation, although this is not possible with all techniques. A procedure that separates local small-scale features from large-scale landscape forms is called trend removal. When working with a DEM, the trend (*i.e.* the larger landscape forms) is represented by a smoothed (generalized) version of that DEM. The smoothing can be accomplished by applying a low pass convolution filter. A Gaussian low pass filter produces a smoother transition between features, but is computationally more demanding (Reitberger *et al.* 2008; Wagner *et al.* 2008). Trend removal is then accomplished by subtracting the smoothed DEM from the original DEM. The resulting difference map contains only the local deviations from the overall landscape forms.

Because small-scale features are smoothed rather than eliminated by the low-pass filter, the derived trend removal map is biased towards small features, *i.e.* the local relative relief elevations are progressively underestimated as the spatial extent of the features increases. Hesse (2010) has therefore proposed to refine the process by introducing a 'purged DEM'. This is produced by creating zero contours in the trend removal map (*i.e.* find all points for which the values of smoothed DEM and the original DEM are equal). DEM elevation data are assigned to all points along these contours. A new approximation of the generalized DEM is then interpolated from the points to create a purged DEM. Finally, the difference map between the original DEM and the purged DEM is a local relief model (LRM). The LRM derived using this approach results in a less biased representation of small-scale topographic features and reflects more truthfully the relative heights and depths of these features with respect to the surrounding landscape (Figure 7).

The level of smoothing is defined by a kernel size of the low pass filter, where a smaller kernel exposes smaller features and vice versa. The precise kernel size should reflect the size of the small-scale landforms while a generally safe bet is a kernel size of about 25 m. The method works best on terrain with gradual slopes, while it produces artefacts such as artificial banks and ditches where relief is diverse and/or changing abruptly.

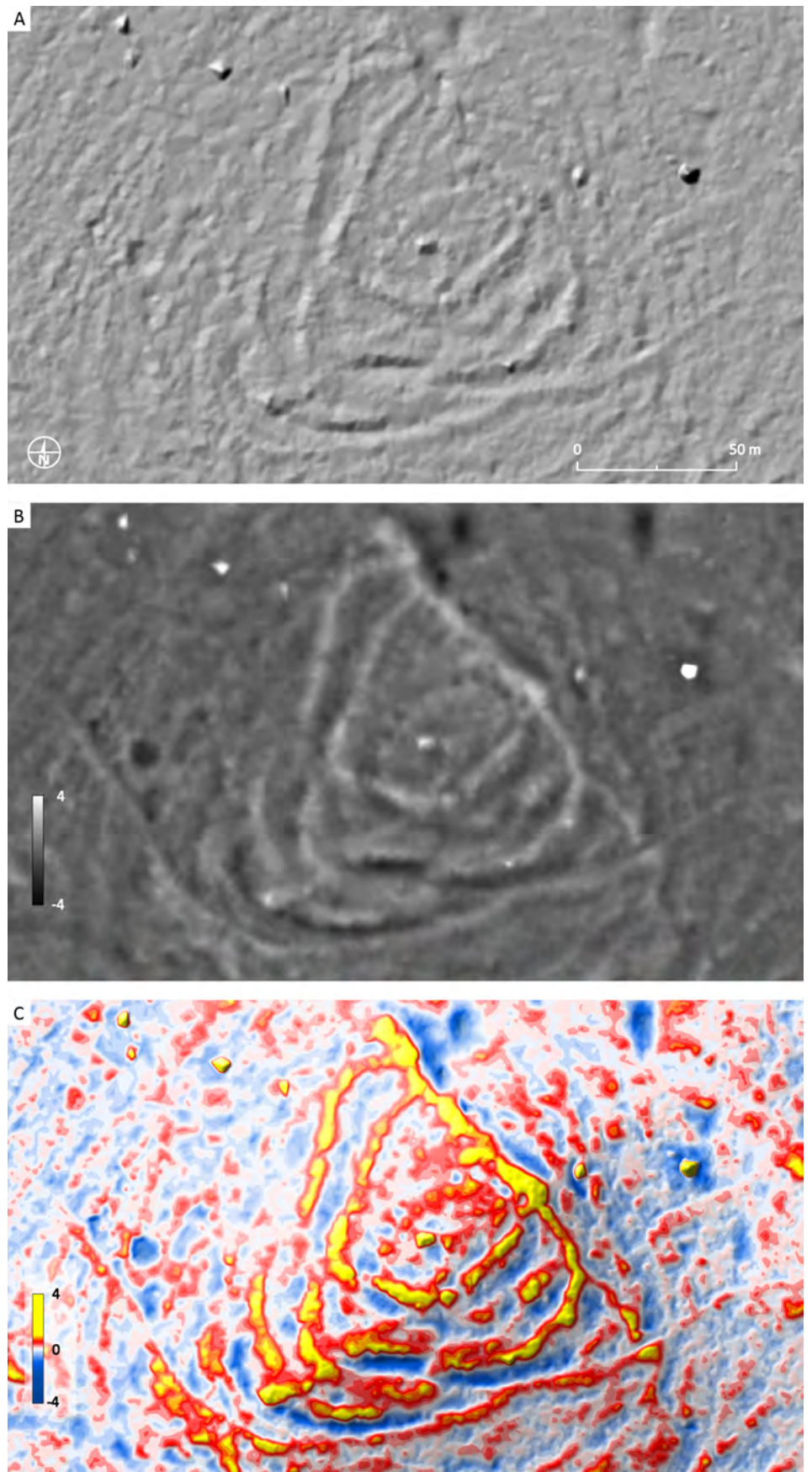


Figure 7: A hill-shaded image (A) and a histogram stretch (B) of a local relief model, and the LRM presented with a purposely designed colour ramp overlaid on a hill-shaded image (Hesse 2010) (C). 1 m spatial resolution lidar data of Žerovinšček Iron Age hillfort near Bločice, Slovenia © ZRC SAZU.

2|5 Sky-view factor and anisotropic sky-view factor

Sky-view factor (SVF) can be used as an alternative method of relief mapping in order to overcome the directional problems of hillshading (Kokalj *et al.* 2011; Zakšek *et al.* 2011). SVF is a geophysical parameter (if we do not manipulate elevation data by vertical exaggeration) that represents the portion of the sky visible from a certain point (considering a hemisphere centred above each pixel and ignoring any direction below the mathematical horizon). Diffuse solar insolation rasters can be used to visualize archaeological features as well (Challis *et al.* 2011), but require additional calculations and the results are more generalized. In contrast to shading techniques based on directional illumination, features visualized by SVF (or by openness) do not contain any horizontal displacements.

SVF has a range between 0 and 1. Values close to 1 indicate that almost the entire hemisphere above the pixel is visible, which is the case in exposed features (planes, ridges, and peaks), while values close to 0 are present in deep sinks and lower parts of deep valleys where almost no sky is visible. Like hillshading images, SVF images are intuitively readable. While hillshading simulates directional illumination of a surface ('sun'), SVF simulates diffuse illumination ('overcast sky').

The computation of SVF is influenced by the search radius of the horizon – the larger the search radius, the more generalized the results. In contrast, a small search radius can be used to visualize and classify local morphological forms. For example, a 10 km search radius can be used in meteorological studies, while a 10 m search radius is suitable for discrimination of archaeological features. Locally flat terrain, ridges and earthworks (e.g. building walls, cultivation ridges, burial mounds) which receive more illumination are highlighted and appear in light to white colours on a SVF image, while depressions (e.g. trenches, moats, ploughing furrows, mining pits) are dark because they receive less illumination.

Various software solutions provide different algorithms to compute the SVF. The difference between results, especially for visualization purposes, can be enormous. For example, the code given by ZRC SAZU (2010) that is implemented in LiVT and RVT (see Chapter 4 Tools) has no saturations, while the implementations in SAGA GIS (Conrad *et al.* 2015) usually give very saturated areas with low SVF. This means no details can be perceived in valleys.

Anisotropic (directional) SVF considers an unevenly bright sky. The brightness can depend on the azimuth and solar distance from the imaginary light source (Zakšek

et al. 2012). This brings back some of the 'plasticity' of hill shading and gives better details on very flat areas.

Both, SVF and anisotropic SVF are very good general visualization techniques, because they enhance visibility of simple and complex small-scale features whatever their orientation and shape, on most types of terrain.

Omitting the closest neighbour pixels in the SVF calculation greatly improves the visibility of archaeological features where the data are noisy due to strip misalignment or overambitious resolution setting.

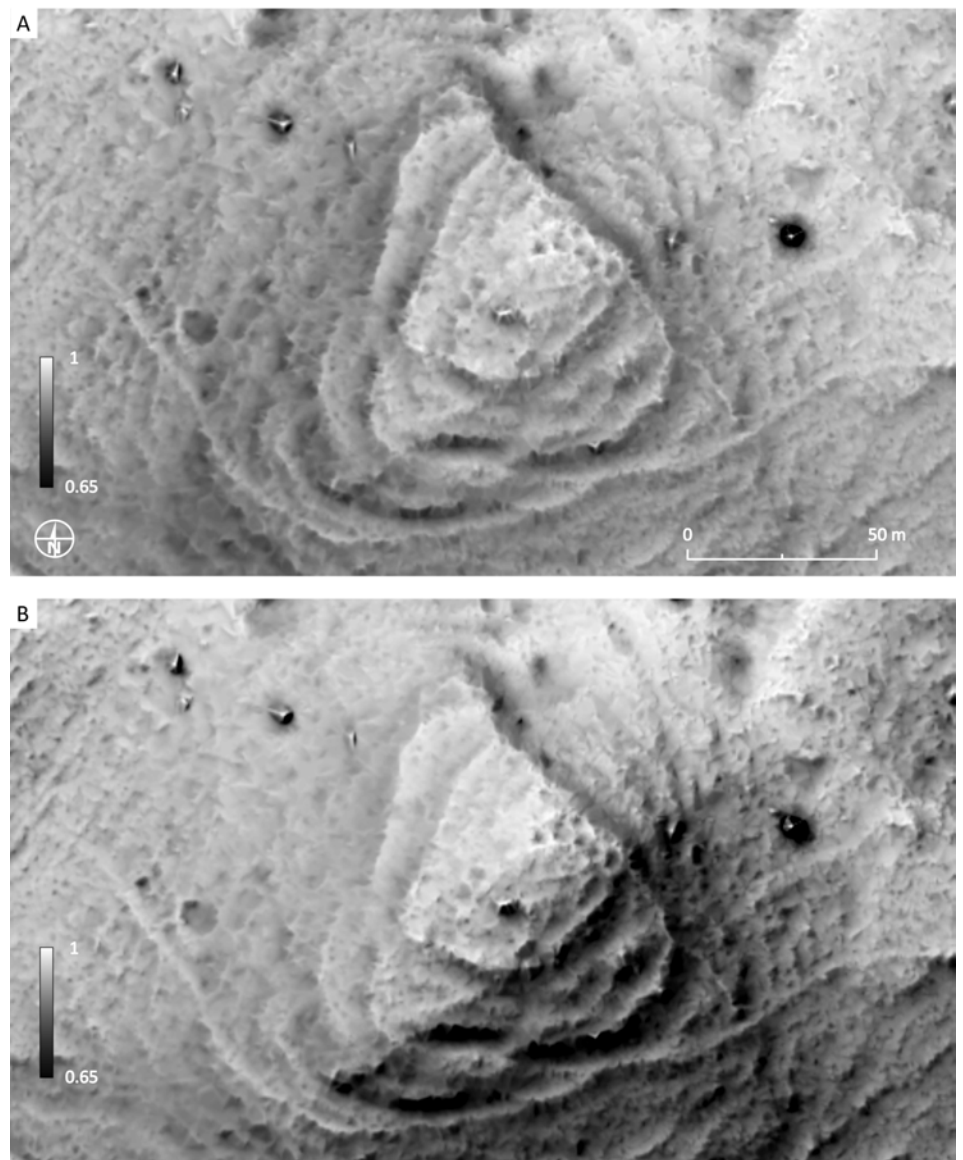


Figure 8: Sky-view factor image (10 m search radius in 16 directions) (A) and anisotropic sky-view factor image (B) of Žerovnišček Iron Age hillfort. Many details can be perceived despite the variable relief morphology. 1 m spatial resolution lidar data © ZRC SAZU.

Table 6: Typical settings for trend removal and Local Relief Modelling.

visualization parameter	general	very flat terrain	steep or complex terrain
filter radius [m]	10	5	25
recommended histogram stretch*	linear stretch, minimum -1.0 m, maximum 1.0 m	linear stretch, minimum -0.5 m, maximum 0.5 m	linear stretch, minimum -2.0 m, maximum 2.0 m

*Depends also on the height and depth of the observed features.

Figure 9: Sky-view factor image (10 m search radius in 16 directions) of ridge and furrow near Neudingen, Germany (A). Omitting the nearest pixels from the calculation can reduce the noise in the data so that features of interest can be perceived more clearly (B). 1 m spatial resolution lidar data © LGL in Baden-Württemberg.

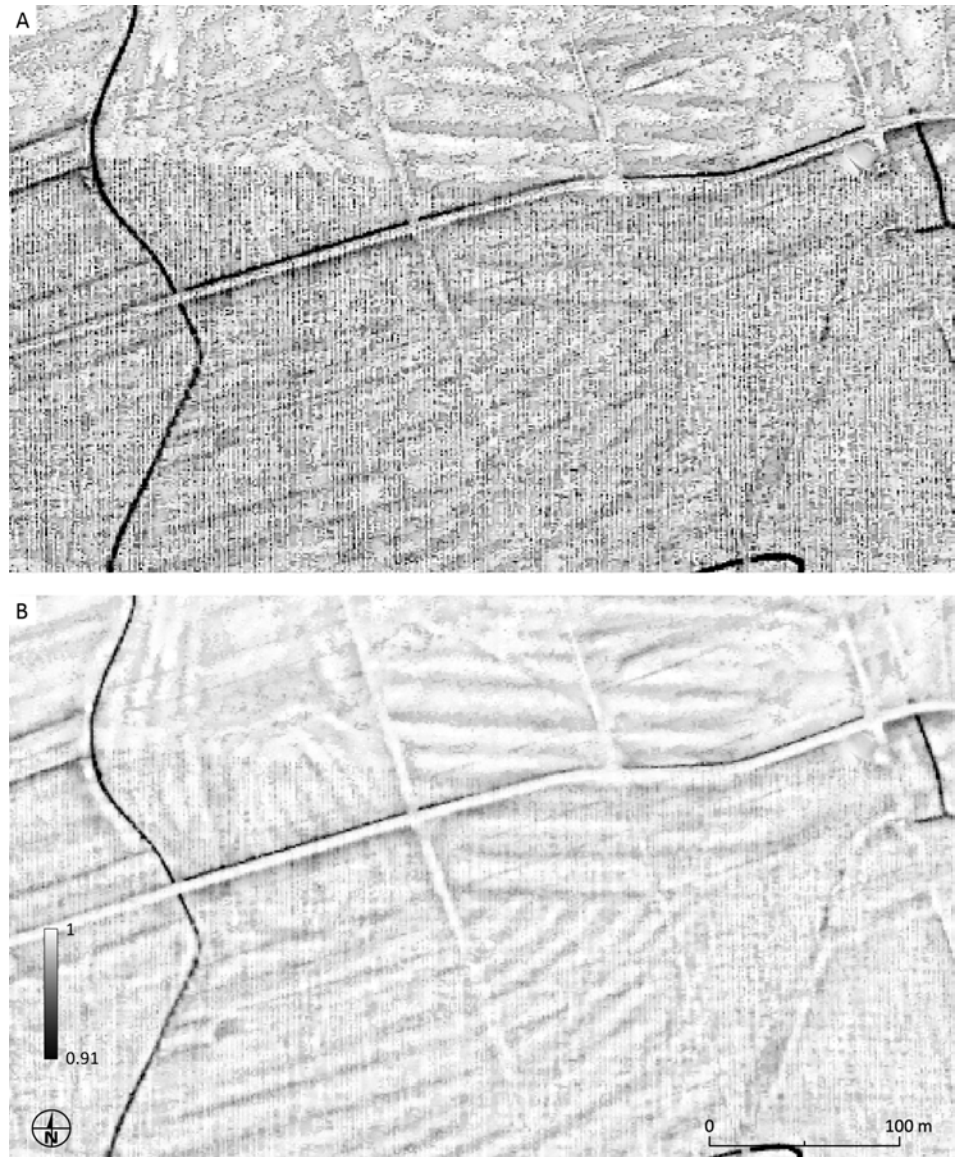


Table 7: Typical settings for calculation and visualization of sky-view factor.

visualization parameter	general	very flat terrain	steep or complex terrain
radius [m]	10	10	10
number of directions	16	16	16
recommended histogram stretch	linear stretch, minimum 0.65, maximum 1.0	linear stretch, minimum 0.9, maximum 1.0	linear stretch, minimum 0.55, maximum 1.0

2|6 Openness

Openness is another proxy for diffuse relief illumination. The method is based on estimating the mean horizon elevation angle within a defined search radius (Yokoyama *et al.* 2002). Positive openness equals the mean zenith angle of all determined horizons, while the negative openness is based on nadir angles. Openness does not limit the estimation of each zenith angle by the mathematical horizon (as SVF does). In other words, openness considers the whole sphere and not only the celestial hemisphere. As a result, the maximum value of openness can be greater than 90° . In addition, a plane (a long slope or a horizontal plane) without any obstacles will always have an openness value of 90° irrespective of its slope. Therefore, interpreting openness results is sometimes difficult because a slope is visualized in the same manner as a horizontal plane. However, because openness considers the whole sphere for calculation, the result is a much 'flatter' image, devoid of general topography – a kind of trend-removed image. It has the same valuable properties for visualization as the SVF with the exception that the visual impression of the general topography is lost. Interpretation is therefore a bit trickier, but openness has a big advantage for automatic feature detection because 'signatures' of features are more homogeneous because they are the same irrespective of their location on a plane or slope (Doneus 2013).

Negative openness is not the inverse of positive openness and it provides additional information. While positive openness highlights topographic convexities, *e.g.* ridges between hollow ways and rims of bomb craters, negative openness emphasizes the lowest parts of concavities, *e.g.* the actual hollow ways, the lowest parts of gorges and the lower edges of cliffs. For consistent readability, it is recommended that negative openness is displayed with inverted greyscale (*i.e.* darker for higher values). Thereby, concave features are always presented by dark tones.

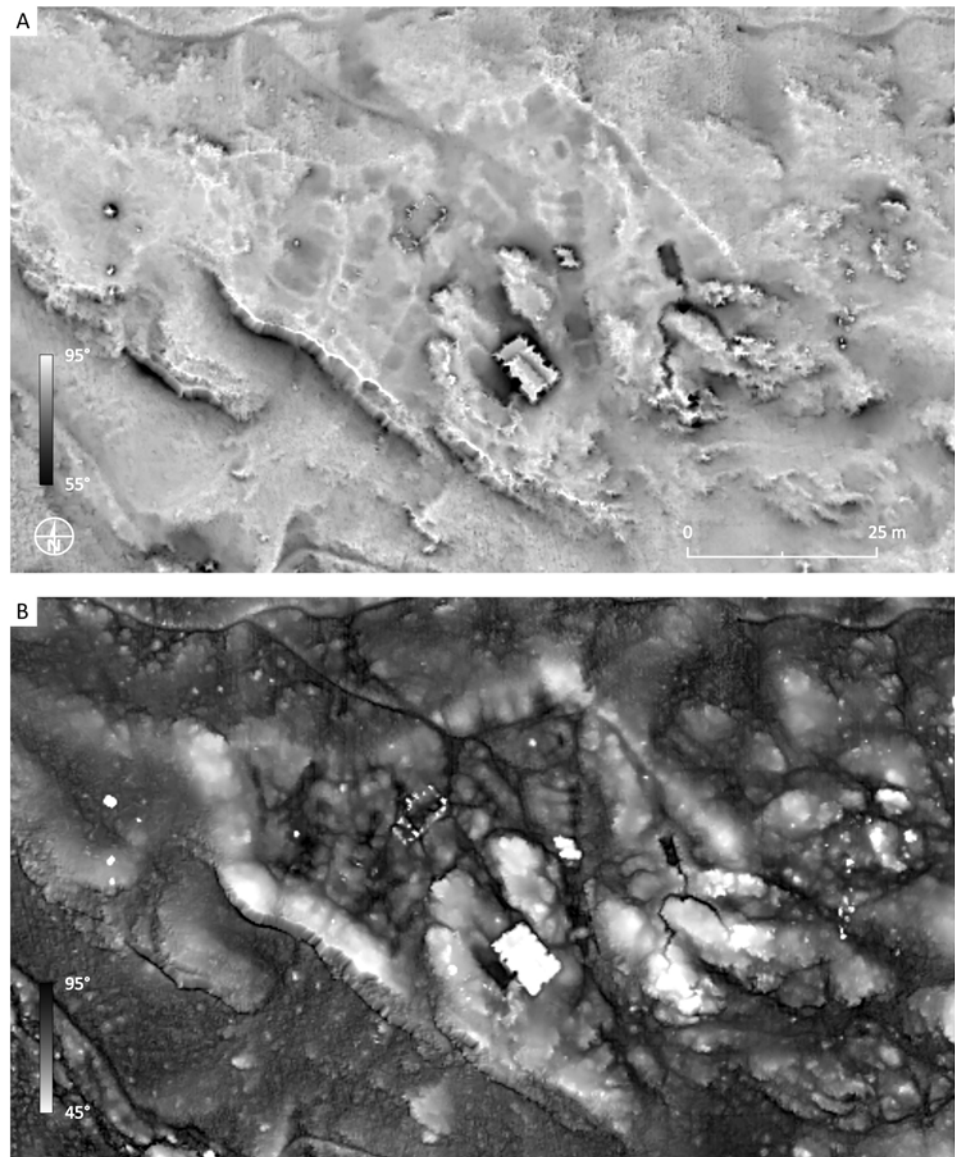


Figure 10: Positive (A) and negative (B) openness image (10 m search radius in 16 directions) of a late Antiquity settlement of Tonovcov grad, Slovenia. The very complex terrain seems flattened. Tops of protruding features are well delineated on positive openness image, while negative openness delineates the bottoms of hollows and lower edges of cliffs. 0.5 m spatial resolution lidar data © Walks of Peace in the Soča river Foundation.

Table 8: Typical settings for calculation and visualization of positive and negative openness.

visualization parameter	general	very flat terrain	steep or complex terrain
radius [m]	10	10	10
number of directions	16	16	16
recommended histogram stretch for positive openness	linear stretch, minimum 65° , maximum 95°	linear stretch, minimum 85° , maximum 91°	linear stretch, minimum 55° , maximum 95°
recommended histogram stretch for negative openness*	linear stretch, minimum 60° , maximum 95°	linear stretch, minimum 75° , maximum 95°	linear stretch, minimum 45° , maximum 95°

*Inverted grayscale (white to black) presentation works best.

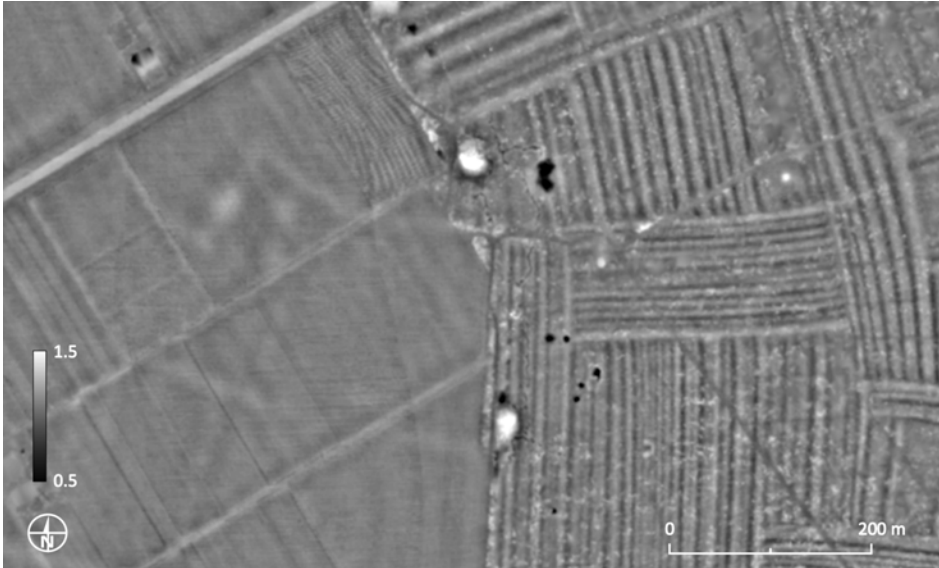


Figure 11: Local dominance image (10-20 m search radius) of former field boundaries, roads, and ridge and furrow near Hügelsheim, Germany. Ridge and furrow is only preserved in areas that are today covered by forest. Some other features on the image include bomb craters, earth covered bunkers, and trenches. 1 m resolution lidar data © LGL in Baden-Württemberg.

Table 9: Typical settings for calculation and visualization of local dominance.

visualization parameter	general	very flat terrain	steep or complex terrain
search radius [m]	10-20	10-20	10
observer height [m]	1.7	1.7	16
recommended histogram stretch	linear stretch, minimum 0.5, maximum 1.8	linear stretch, minimum 0.5, maximum 3.0	linear stretch, minimum 55°, maximum 95°

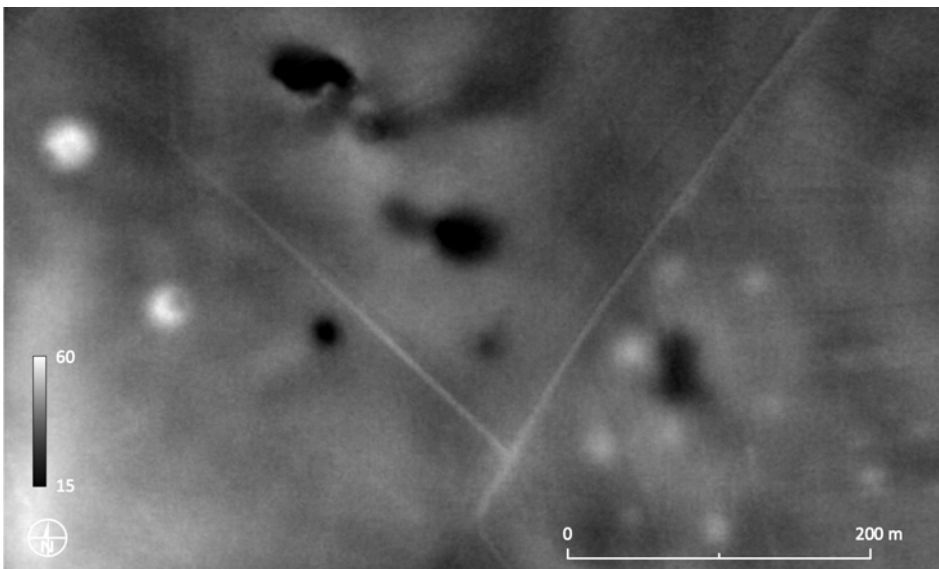


Figure 12: Cumulative visibility image of burial mounds (high values) and dolines (low values) on the Swabian Alb. 1 m resolution lidar data © LGL in Baden-Württemberg.

Table 10: Typical settings for calculation and visualization of cumulative visibility.

visualization parameter	general	very flat terrain	steep or complex terrain
radius [m]	1-100	1-100	1-100
angular resolution [°]	10	10	10
observer height [m]	1.7	1.7	1.7
target height [m]	0.0	0.0	0.0
recommended histogram stretch	linear stretch, minimum 15, maximum 55	linear stretch, minimum 0, maximum 25	linear stretch, minimum 10, maximum 65

2|7 Local dominance

Local dominance visualisation of a DEM is based on computing, for every pixel of the DEM, how dominant an observer standing on that point would be for a local surrounding area (Hesse 2016). Dominance as used here is the average steepness of the angle at which the observer looks down at the surrounding land surface. It is higher for points on local elevations as well as on slopes and lower for points in local depressions.

Local dominance is computed for pixels within a specified maximum radius and a specified observer height above the surface. To reduce the noisy appearance of the resulting image due to small-scale surface roughness, a minimum radius can be specified. Pixel brightness is derived from the local dominance values by applying an appropriate greyscale histogram stretch.

This visualisation is well suited for very subtle positive relief features such as former field boundaries or strongly eroded burial mounds, but also delivers very good results for topographic depressions such as dolines, mining traces, or hollow ways.

2|8 Cumulative visibility

A viewshed is the area visible from a given vantage point. The viewshed area depends on the topographic position of the vantage point and the surrounding topography, but also on the height of the observer standing on the vantage point, the height of the objects that should be visible to the observer, and the radius under consideration.

Cumulative visibility, on the other hand, specifies the size of the area from which a point in the DEM (or an object on that point) is visible to observers of a certain height. DEM visualisation by cumulative visibility is based on computing, for each pixel of the DEM, the size of the area within a specified radius from which an object is visible (Hesse 2016). Because the surrounding topography plays a dominant role for intervisibility, the resulting raster map can also be a suitable technique to

visualise that topography. Besides this, such a visualisation can be used as a tool for analysing for example the locations of archaeological sites.

The resulting raster map contains percentage values (0...100) of the size of the cumulative visibility area relative to the entire area within the specified radius.

2|9 Accessibility

DEM data can be visualised by computing surface accessibility. This means that an algorithm determines, for every pixel of the DEM, the maximum radius of a sphere that could be placed on the surface at this position without being impeded by the heights of surrounding pixels (Miller 1994). To reduce computation time, the algorithm only takes into account surrounding pixels within a pre-defined radius. Computation time can be further reduced by taking into account only surrounding pixels along a small number of radial lines rather than all pixels.

The range of values in the resulting accessibility raster map corresponds to the range of sphere radii. Greyscale or colour mapping is used to display the results as an image. Accessibility can be used for visualising negative relief features (e.g. pits, hollow ways) and features on slopes (e.g. agricultural terraces). Subtle relief features on more or less horizontal surfaces show up only poorly or not at all.

2|10 Multi-scale integral invariants (MSII)

Multi-scale integral invariants is a visualisation technique which has previously been applied to enhance readability and approach automatic interpretation of cuneiform tablets (Mara *et al.* 2010), but which is equally valuable for the visualisation of elevation models. To compute MSII, *n* spheres of different diameters are centred on each pixel in the DEM. The percentage of the volume of these spheres, which lies above/below the DEM surface is computed. The result is

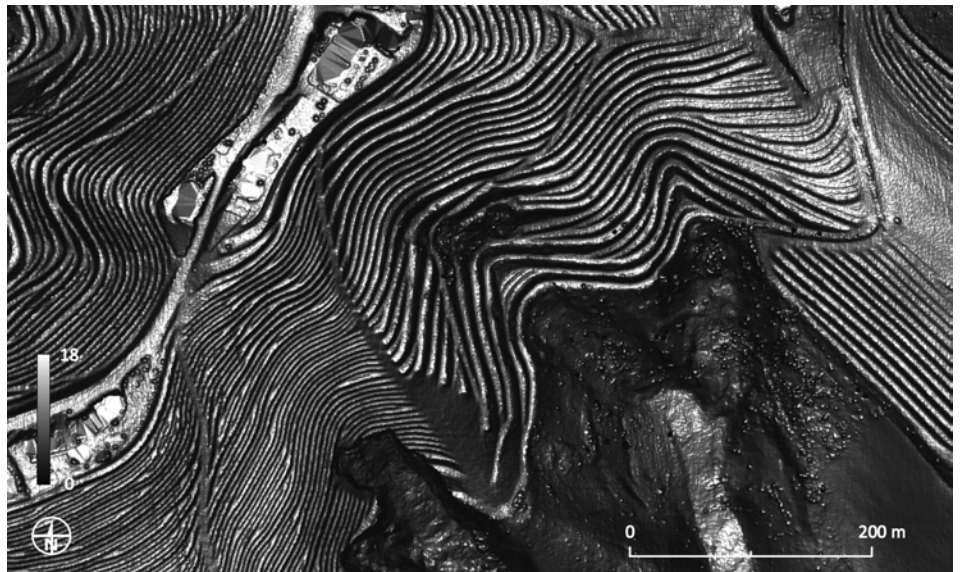


Figure 13: Accessibility image (20 m maximum radius) of very narrow agricultural terraces with vineyards near Jeruzalem, Slovenia. 0.5 m resolution lidar data © ARSO, Slovenia.

Table 11: Typical settings for calculation and visualization of accessibility.

visualization parameter	general
radius [m]	10
number of directions	16
recommended histogram stretch	linear stretch, minimum 0, maximum = radius



Figure 14: Multi-scale integral invariants image of a late Roman camp at St. Helena, west of Kobarid, Slovenia. 0.5 m resolution lidar data © Walks of Peace in the Soča river Foundation.

Table 12: Typical settings for calculation and visualization of multi-scale integral invariants.

visualization parameter	general	very flat terrain	steep or complex terrain
number of scales	8	8	8
minimum radius [m]	1	1	1
maximum radius [m]	11	11	11
recommended histogram stretch	linear stretch, minimum 1.2, maximum 1.8	linear stretch, minimum 1.3, maximum 1.5	linear stretch, minimum 1.2, maximum 2.5

a set of n values (volume fractions above the DEM surface) for each DEM pixel. These sets of n values are interpreted as n -dimensional vectors. By computing the distance of these n -dimensional vectors from a reference vector, the data can be reduced to a raster map containing a single value for each pixel. Low values (low vector distance) indicate high similarity with the reference vector and vice versa. Using an appropriate greyscale histogram stretch, this raster map can be displayed as an image. The reference vector can, for example, be determined by extracting the vector values for a specific relief feature or a point within a cuneiform character or simply by choosing the origin of the n -dimensional coordinate system (*i.e.* zero).

MSII is almost equally suitable for very diverse terrains from plains to mountains. Because it is a multi-scale approach, it is able to visualize relief features within a wide range of sizes, *i.e.* it can clearly show very small features while at the same time preserving at least some impression of the landscape forms. It can be quite susceptible to data noise. This can be avoided by setting a larger minimum radius; however, this in turn partly compromises the depiction of small details.

2|11 Laplacian-of-Gaussian (LoG)

The discrete Laplacian filter computes the second derivative of elevation, *i.e.* the change of slope. It is a measure of convexity and can therefore be valuable for the visualisation of edges. The Laplacian filter is often applied to an image that has first been smoothed with something approximating a Gaussian smoothing filter in order to reduce its sensitivity to noise and this combination is known as Laplacian-of-Gaussian (LoG).

2|12 Visualizing uncertainty

Information about how raw data has been acquired and processed, and about the method and settings for its presentation, has a great impact on the feature detection

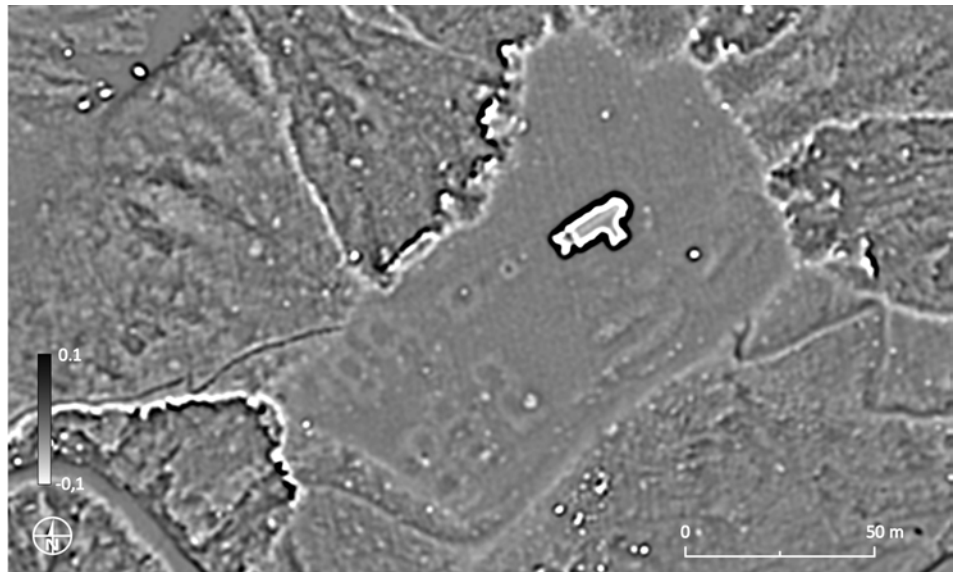


Figure 15: Image of a late Roman camp at St. Helena, west of Kobarid, Slovenia as evident on a 0.5 m resolution lidar data filtered by a Laplacian-of-Gaussian convolution filter with a radius of 3 pixels (*i.e.* 1.5 by 1.5 m).

Table 13: Typical settings for calculation and visualization of Laplacian-of-Gaussian.

visualization parameter	general
laplacian filter radius [px]	3
low pass filter radius [px]	25
recommended histogram stretch*	linear stretch, minimum -0.05, maximum 0.05

*Inverted grayscale (white to black) presentation works best.

and interpretation processes. For example, if the interpreter knows the original scanning density, the method of point cloud filtering, and the method of digital elevation model generation, they can judge and take decisions about the various artefacts that can be found in the data.

The occurrence of different artefacts or unnaturally smooth terrain can be effectively predicted by mapping the density of laser points representing the ground and density of the vegetation canopy above them. It can be seen from Figure 16C that the density of ground points is in places insufficient (data gaps in red) to accurately map the ground under forest at 0.5 m resolution, despite the high scanning density. In such cases the rasterization algorithm has to interpolate (infer from neighbouring points) the representation of the ground. The appearance of these interpolated surfaces varies from algorithm to algorithm, but the most important is influence on the general smoothness and preservation (clarity) of edges (Figure 17). The artefacts produced by some interpolation algorithms may be seen as unattractive and inappropriate for display. However, we recommend to use

such algorithms in particular when the goal is visual interpretation: the artefacts are very recognizable and thus help to avoid misinterpretation of 'pretty' surfaces that are based on insufficient data.

If point density maps, data gap masks, or actual point cloud data are unavailable, forest masks or topographical maps can be used as a rough guide. In absence of these, very simplified vegetation density maps can be approximated with vegetation indices (*e.g.* Normalised Difference Vegetation Index) derived from freely available high-resolution satellite data (Landsat-8 or Sentinel-2, available at earthexplorer.usgs.gov and scihub.copernicus.eu respectively).

There are several types of artefacts that are commonly found in lidar-based DEMs. It is useful to know that 'fish scales' sometimes found in forest datasets (Figure 18A), are a result of a direct point cloud rasterization (*i.e.* without help of a Triangulated Irregular Network – TIN), and that wave-like features (resembling, at first glance, tightly spaced ridge and furrow) are a consequence of poor registration of scan lines (Figure 19A).

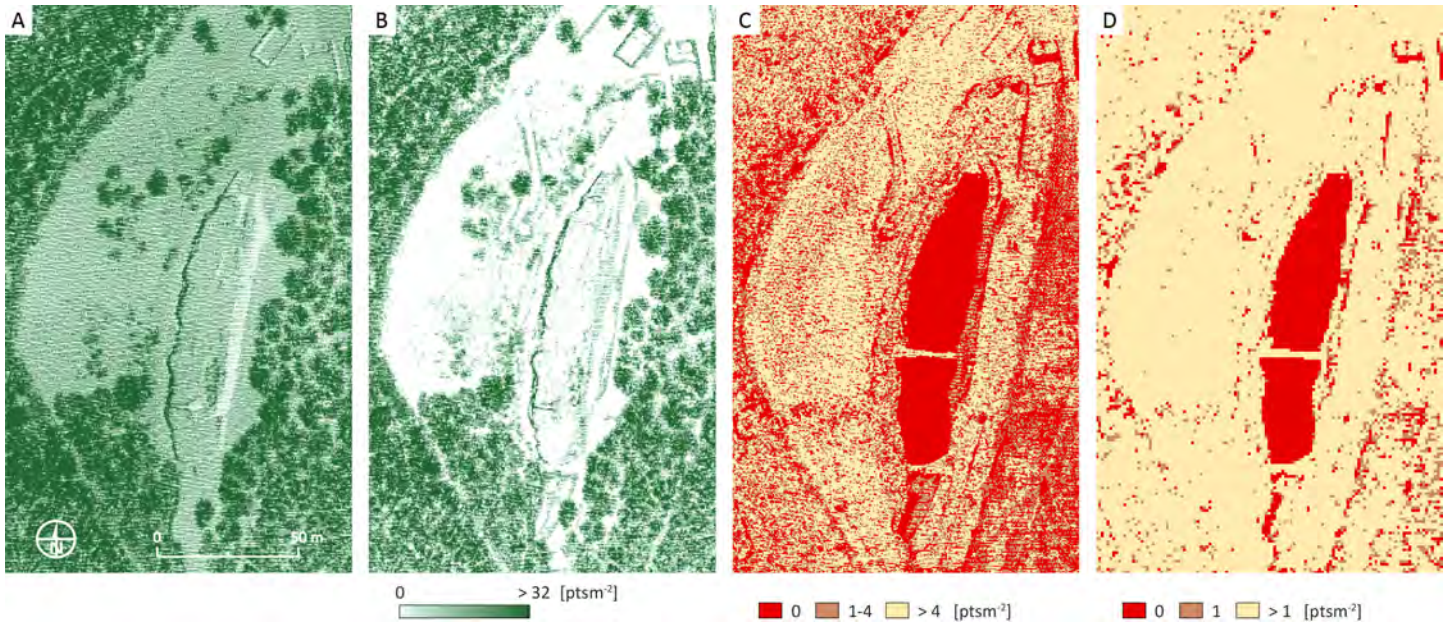


Figure 16: Lidar data density maps of Castle Montfaucon east of Besancon, France. Density of all points (A), vegetation points (B) and ground points (C) calculated per every pixel (0.5 m) but plotted per m². Density of ground points calculated and plotted per m² (D).

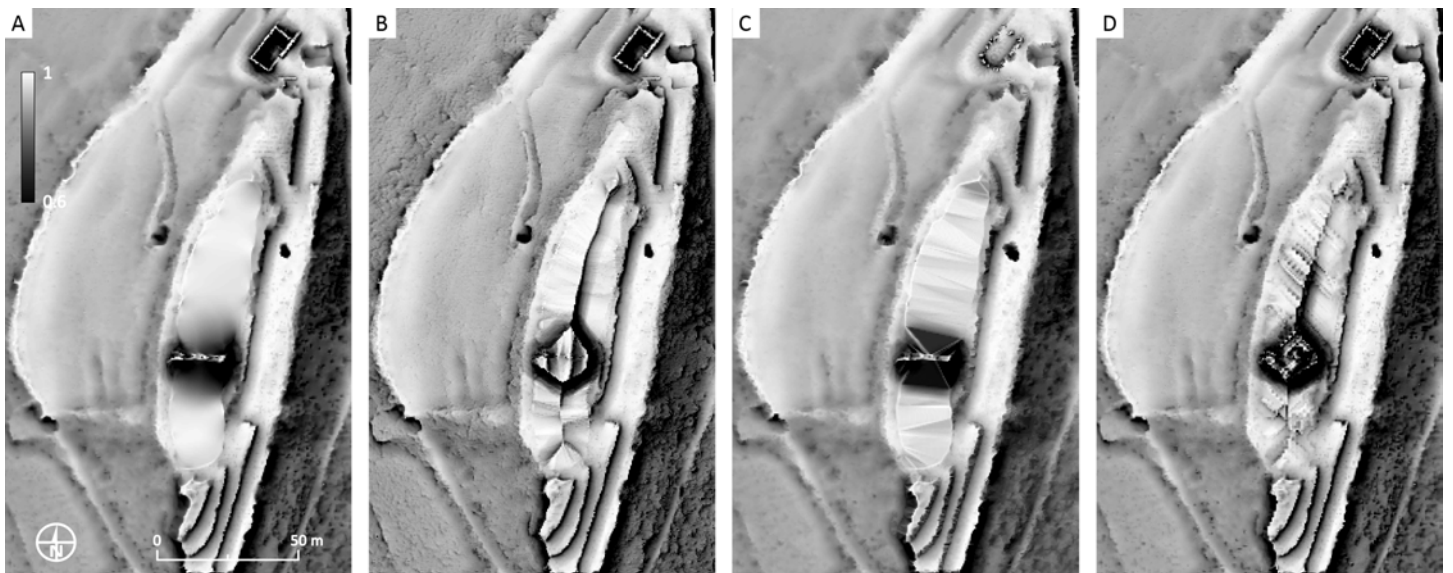


Figure 17: Anisotropic sky-view factor image of elevation models produced with different rasterization (interpolation) algorithms. Note the difference in interpolation of the castle area and the south-eastern slope leading to it. Natural Neighbours (NN) (A) generates a very smooth terrain, Inverse Distance Weighted (IDW) (B) introduces steps, TIN with Repetitive Interpolation (REIN) (C) introduces triangles, and splines (D) create a range of artefacts.

Black stars, sometimes seen in a sky-view factor image, can be linked to dedicated processing, where the point-cloud filtering process has been optimized to leave the archaeology as intact as possible. Eight or sixteen-pointed black stars may be formed around very small (in area) ‘bumps’ that are the unfiltered remains of conifer trees (Figure 18B) or other uprights (Figure 42). This occurs where conifers are too dense for a laser pulse to reach the ground and filtering is set so as not to over smooth the derived elevation model. Stars are generated by the fact that sky-view factor is usually calculated in eight or sixteen

directions. Additional artefacts are shown in Figures 18C, 19B and 19C. Artefacts and anomalies are not only aesthetic but also affect the accuracy of analyses based on the terrain surface.

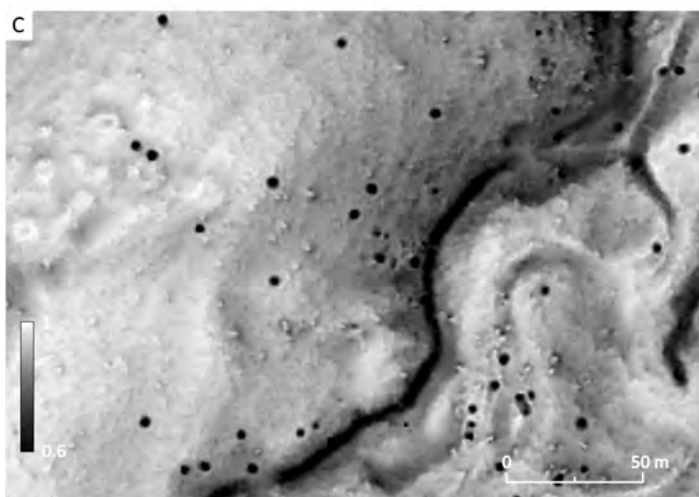
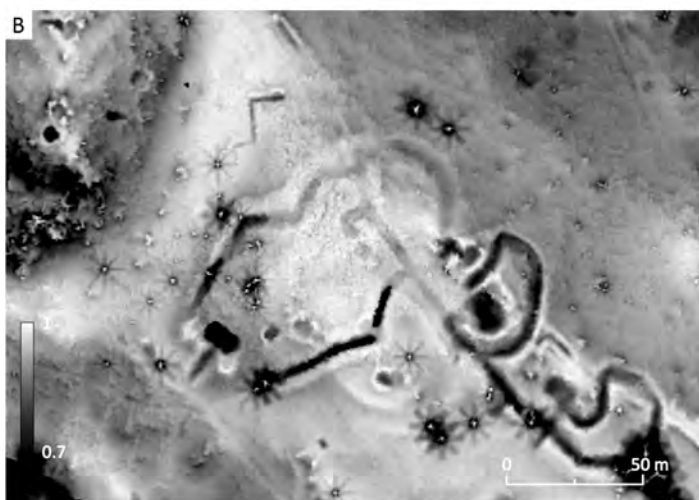
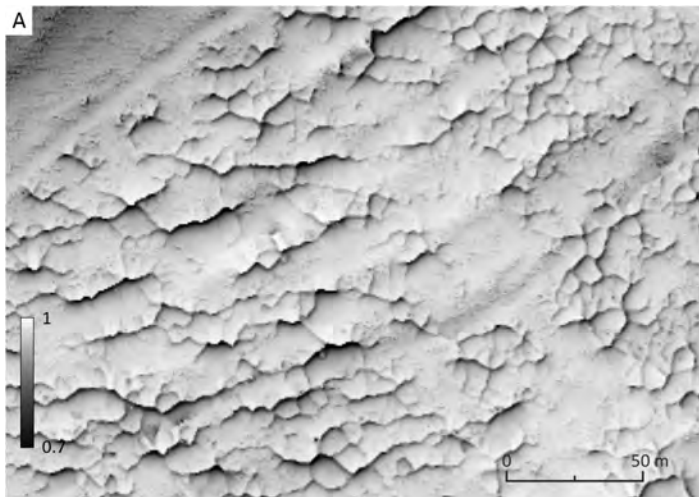


Figure 18: (A) ‘Fish scales’ are a result of direct point cloud rasterization. 0.5 m spatial resolution lidar data of an area around Besancon, France, © University of Franche-Comte. (B) Black stars typically form around small protruding features on a sky-view factor (SVF) image when calculating it with 8 or 16 directions. 0.5 m spatial resolution lidar data of World War I trenches near Kobariid in Slovenia. © Walks of Peace in the Soča river Foundation. (C) 1 m spatial resolution lidar data full of false depressions (C). They are a result of poor data processing that classified many below-ground lidar points as true ground. Poštela burial mounds can be seen in the upper left corner of (C). © ARSO, Slovenia. All images display SVF calculated in 8 directions with a 10 m search radius.

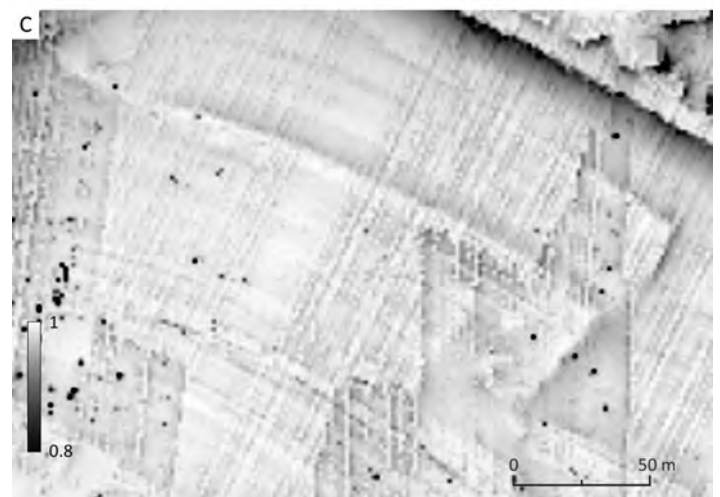
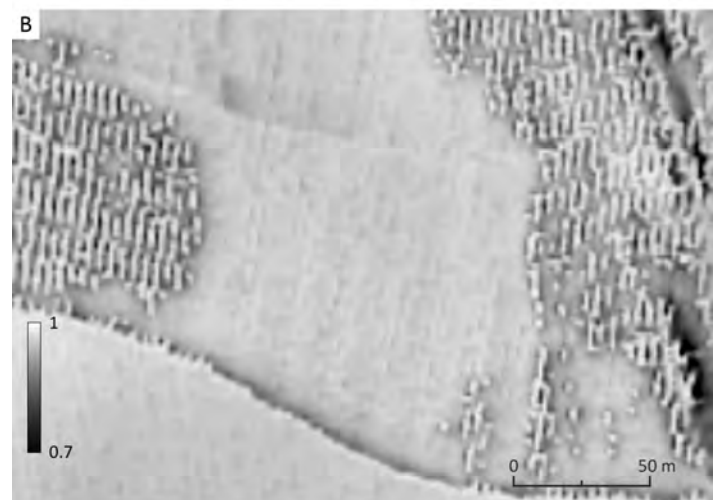
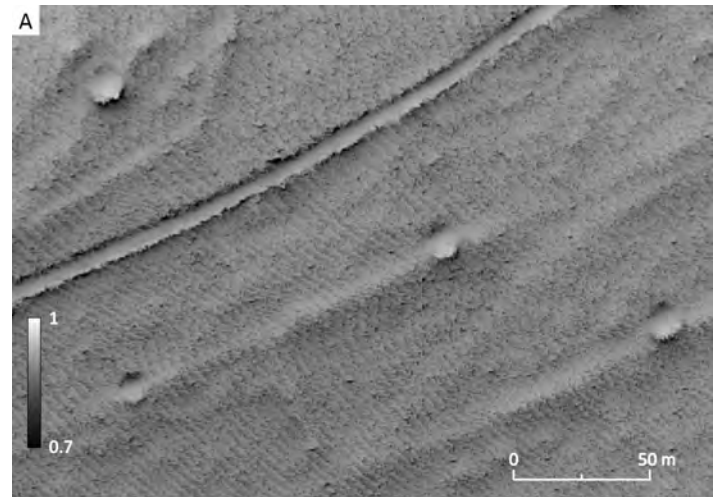
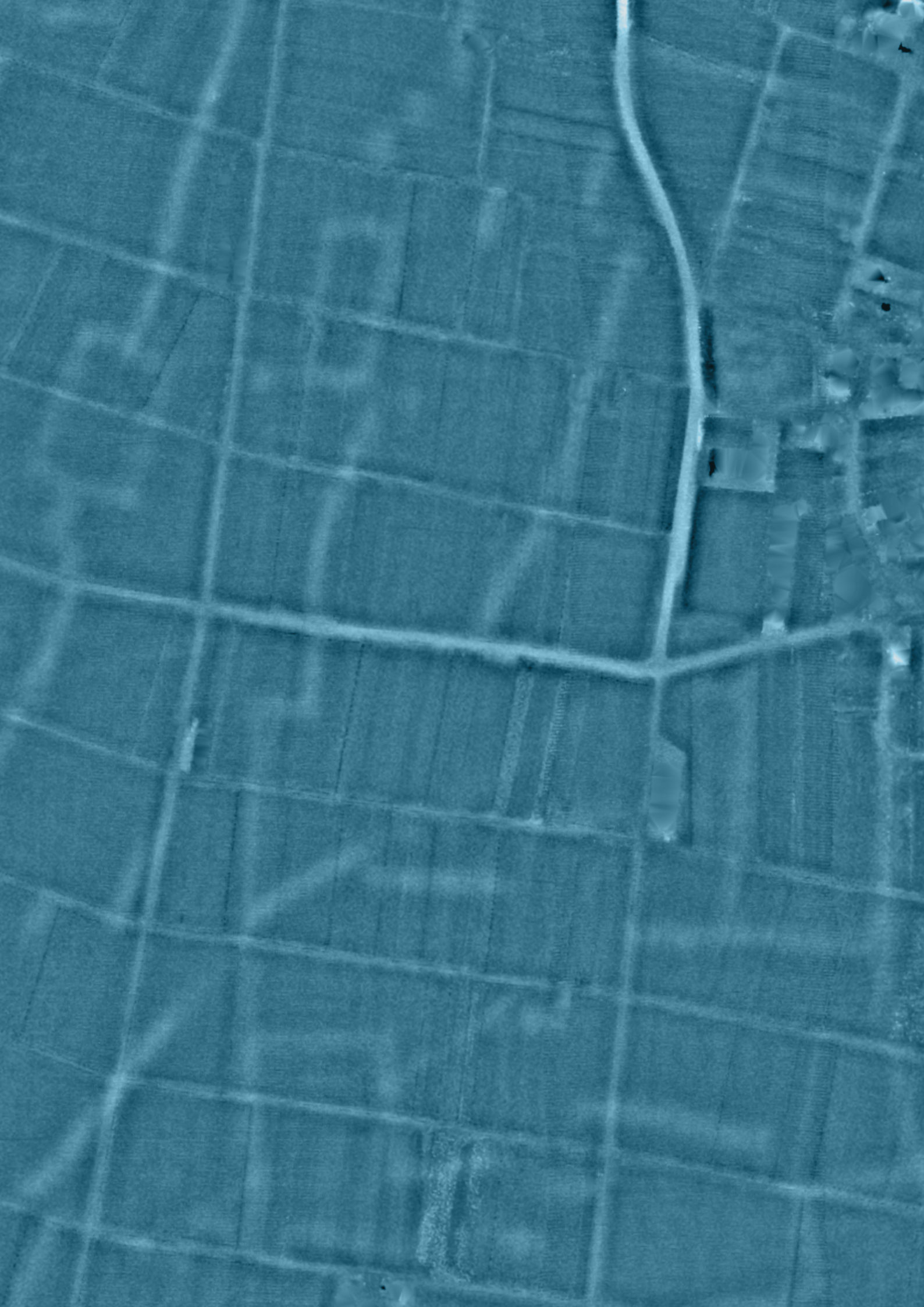


Figure 19: Wave-like features are a consequence of poor registration of scan lines (A). Charcoal burning platforms can be seen. 0.5 m spatial resolution lidar data of an area around Besancon, France, © University of Franche-Comte. Severe strip misalignment and over-ambitious resolution setting result in scrub-like artefacts and fictional steps in terrain (B). 1 m spatial resolution lidar data of an area close to Tauberbischofsheim © LGL in Baden-Württemberg. Poor raw data preprocessing resulted in a whole range of artefacts imprinted in terrain NW of Volarje, Slovenia (C). 1 m spatial resolution lidar data © ARSO, Slovenia. All images display SVF calculated in 8 directions with a 10 m search radius.

3

Guidance for selection of techniques



3

As the complexity of research questions increases so does the need for visualizations to convey not only what is there in screaming colour, but also the correct shape, size, relative elevation, degree of preservation, and the context of the immediate environment.

There are usually several important types of questions you want answered when using lidar data for archaeological prospection. Is there anything out there? Is there anything beside it? What is it? Why is it there? Which one is older/younger? The complexity is getting higher with each one of these questions and so is the knowledge you need to choose the appropriate visualization. As the complexity increases so does the need for visualizations to convey not only what is there in screaming colour, but also the correct shape, size, relative elevation, degree of preservation, and the context of the immediate environment.

There are two fundamental questions when creating visualizations. How many do you need to accomplish your task, and which ones are the best suited to do it as quickly and accurately as possible? Primarily, the choice of visualization depends on the characteristics of the sought-after relief features (*e.g.* size, shape, convexity/concavity) and the overall landscape forms (*e.g.* smooth, rolling, rugged). Further factors that can influence the choice of visualization can range from computation time to personal preferences.

3|1 Preparing the images for detection and interpretation

As mentioned in the introduction, DEMs contain numerical elevation data and have to be transformed into human-readable images for visual interpretation. Likewise, most of the visualisation techniques described in the previous chapters produce raster maps containing numerical values. To display these raster maps as images, greyscale or colour cast as well as contrast stretch have to be applied. Such a greyscale cast is for example achieved by assigning the colour black (pixel value of zero) to the lowest and white (pixel value of 255) to the highest numerical value found in the computed raster file. However, in many cases extreme values occur (in particular along the edges of DEMs) which can result in a very low contrast images. Therefore, extreme low and high values usually have to be cut-off/clipped (*i.e.* saturated).

While the use of a greyscale cast is generally the best choice, a colour cast is preferred in some cases, in particular when a clear distinction between positive and negative relief features is required. For trend removal and local relief model, the use of blue tones for negative and red/yellow tones for positive values has been found to be useful.

To display features more clearly – *i.e.* with a higher contrast – a histogram stretch is usually required. A histogram stretch transforms a narrow range of input values (*e.g.* elevation values from 523.2 to 542.7 m for a hypothetical elevation differentiation) onto the whole range of output values (*e.g.* from 0=black to 255=white). There are many types of histogram stretch, with the most frequently used being a linear minimum-maximum stretch (with or without clipping of values below and/or above a certain value or a certain percentage), histogram equalization, standard deviation stretch, and custom histogram stretch, based on a user defined frequency curve. Only the linear stretches preserve the relative distribution of values between the displayed minimum and maximum, while the others do not. The effect of non-linear stretch is that we cannot precisely compare different features or areas. For visual interpretation, however, they can nevertheless be useful as they can ‘pull apart’ very similar values and thereby enable a visual differentiation.

Some software allows the user to automatically adjust histogram stretch in real time, based only on the values currently displayed on-screen. This means that the displayed range of values changes when we move around the landscape, which is not very useful for comparison of features, but works very well for their detection.

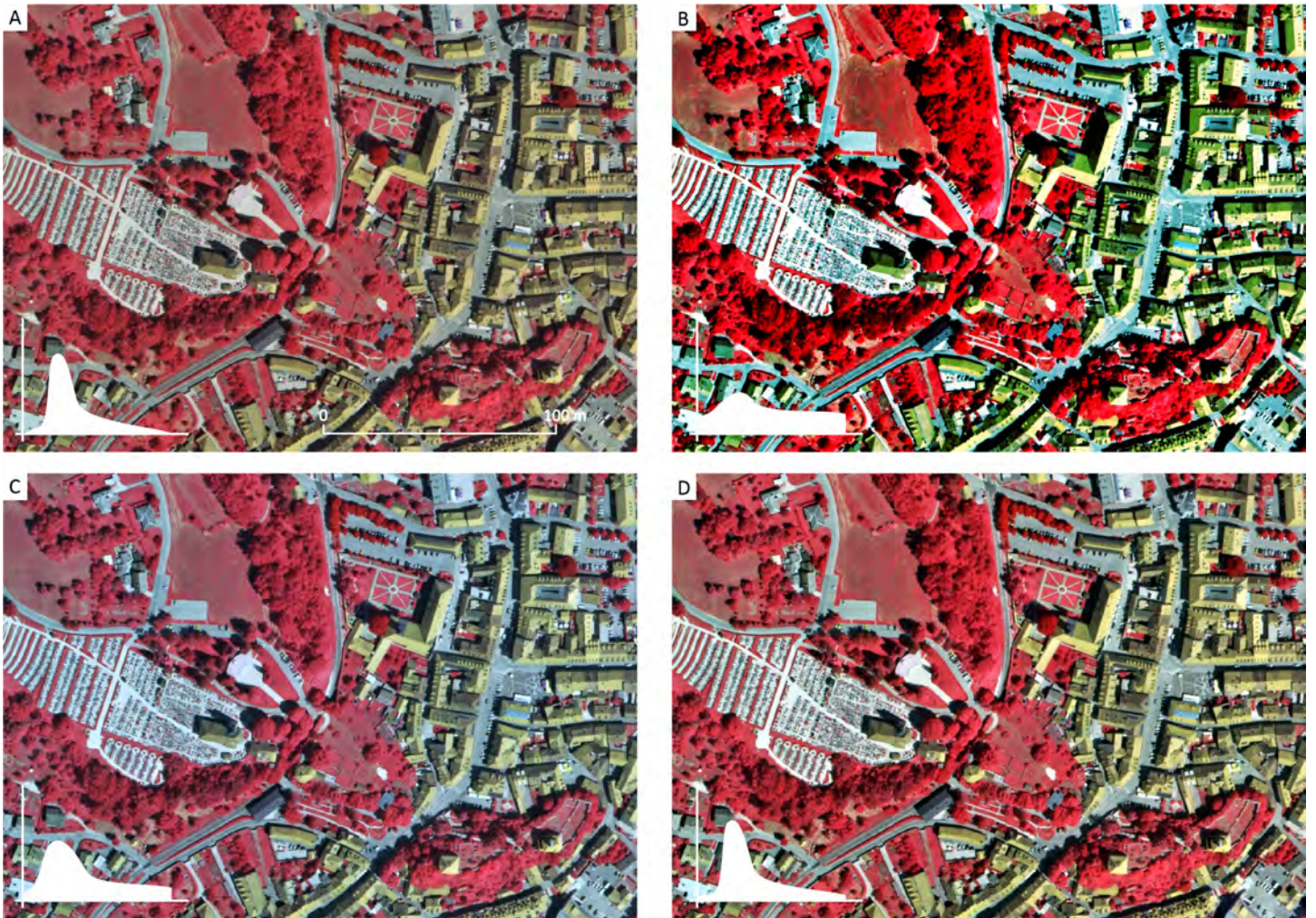


Figure 20: An original image where only a minimum-maximum histogram stretch has been applied – a whole range of values is displayed with relative differences between values preserved (A). Images displayed with different techniques of histogram stretch: histogram equalisation (B), standard deviation 2.5σ (C), 0.5 % saturation of minimum and maximum (D).

A histogram stretch with saturation of minimum for a SVF or a positive openness image renders narrow valley floors, very steep slopes, and the vicinity of high objects (such as buildings) black, which can be useful when delineating concave features on flat or undulating terrain. If this is undesirable because features of interest can be 'hidden' in such areas, a standard deviation stretch or a standard minimum-maximum stretch provide a visualization with no or minimal saturation, but less contrast.

Two or more visualisations can be combined into a single image. This can be a useful approach to enhance the visual

representation of landscapes or features and/or to reduce the number of images to be analysed. Such combinations are usually applied to greyscale or colour images rather than to the numerical output of the visualisation algorithms. Computing the greyscale or colour average of two or more images results in a translucent overlay of one image over the other; a weighted average can be used to adjust the translucency. Alternatively, images can be multiplied with each other (and the range of values subsequently re-scaled to the 0 to 255 range). Three greyscale images can be combined into a RGB composite image where the different input images are displayed as

the red, green and blue components of the resulting colour image (Figure 3A and C).

Combining results of various visualizations in a meaningful and deliberate way builds upon their strengths. Some examples are presented in the Case studies chapters. We can not only play with different histogram stretches and colour tables, but also with the degree of transparency and the mathematical operations to combine the layers. Play was deliberately left out of brackets, as the process of creating an expressive visualization is indeed as much art as it is work.

3|2 Reading and presenting the images

3|2|1 Choosing appropriate visualisations

The choice of a visualisation technique depends on a number of factors; the most important are the topography of the landscape, and morphology and size of the sought after features. This is because different techniques can preferentially emphasize small-scale depressions or elevations, low relief features on horizontal or sloping planes, or structures on slopes. The type of visualisation often also depends on the task at hand and the current stage in an overall workflow (e.g. general overview, feature mapping, analysis of details). In almost all cases, a single visualisation technique will not be sufficient to extract the full amount of information from the data. This entails that for a given area, several techniques have to be applied. In the following, an attempt is made to reduce the complexity of multiple visualisation techniques and to provide guidance regarding their selection.

It is recommended to always begin by looking at shaded relief overview images of the area under investigation, because they provide the most 'natural' visual appearance of the topography and can thus help decide which other techniques could work well (Table 14).

In areas of gentle to moderately steep topography, shaded relief can be successfully used to investigate relief details. However, care has to be taken to apply several illumination directions and to avoid the drawbacks of shaded relief such as poor representation of linear features parallel to illumination azimuth,

low contrast in areas facing towards (homogeneously bright) or away from (homogeneously dark) the light source, as well as optical illusions (inverted relief). While very low illumination elevation angles ($< 10^\circ$) can and should be used to highlight low relief features in areas of low slopes and flat terrain, higher illumination elevation angles ($> 35^\circ$) are required in steeper topography. To investigate features on moderate to steep slopes, shaded relief should be used with (almost) vertical illumination to minimize saturated bright/dark areas on slopes facing towards/away from the illumination. In such cases, shaded relief images become similar to Slope images, which can be a useful alternative in moderate to steep topography.

In areas of moderate to steep topography, sky-view factor works best to highlight surface depressions and features on slopes. Depending on the range of slopes in a given area under study, different histogram stretches may be necessary to avoid bright saturation in gentle topography and dark saturation on steep slopes. In areas with flat or very gentle topography, sky-view factor is generally limited to the presentation of negative relief features (pits, ditches, quarries, erosion areas, dolines...) and becomes very sensitive to DEM noise. A good general rule is to use a histogram stretch of 0.65 to 1.0 for diverse terrain and 0.9 to 1.0 for very flat terrain.

In areas with flat or very gentle to moderate topography, local dominance, trend removal, and local relief model are very helpful to highlight very low relief features such as former field boundaries or levelled burial mounds. On very flat horizontal planes (coastal plains or broad river valleys), elevation differentiation (greyscale or colour coding of the DEM) can be a very simple and effective alternative; however, it fails as

soon as the overall topography deviates from nearly horizontal. Trend removal, local relief model, and local dominance are interchangeable to a certain extent. The advantage of simple trend removal over local relief model is that it is a much simpler and faster algorithm. On the other hand, local relief model produces more realistic relative elevation values of relief anomalies. Local dominance retains a (limited) visual impression of the overall landscape forms as it produces higher values on slopes than on horizontal planes. This entails that on steeper slopes, local dominance will require a different histogram stretch than in areas with gentle topography.

Laplacian-of-Gaussian is a very useful technique to highlight edges and can be used on its own for this purpose. It works well as an overlay over other visualisations to strongly enhance edges and thereby to emphasize relief features. When combined in a (weighted) greyscale average with local dominance or sky-view factor, it helps to overcome saturation on steeper slopes that arises when histogram stretch for local dominance or sky-view factor is adjusted so as to be suitable for gentle to moderate topography.

Positive and negative openness are very useful to highlight positive and negative relief features, respectively. As openness removes the visual impression of overall landscape forms, it is not affected by saturation due to gentle or steep slopes and may be used in a varied topography. Because of the ability to differentially highlight positive and negative relief features, it is particularly suitable for targeted detection of these features.

Like openness, multi-scale integral invariants may be used in varied topography because it is relatively little affected by saturation due to overall topography. Because it is a multi-scale

Table 14: Matrix for the suitability of visualisation techniques for selected archaeological relief features in different topographic settings. Begin with a shaded relief overview image then try/add techniques from left to right

flat terrain	Shaded relief (sun elevation $< 10^\circ$)	Trend removal / LRM (filter radius ~ 20 m)	Local dominance (radius 10-20 m)	Openness or MSII (radius 10 m)	
gentle slopes	Shaded relief (sun elevation ~ 30°)	Sky-view factor (radius ~ 10 m)	Trend removal / LRM (filter radius ~ 20 m)	Local dominance (radius 10-20 m)	Openness or MSII (radius 10 m)
moderate slopes	Shaded relief (sun elevation ~ 45°)	SVF (& LoG) (radius ~ 10 m)	Trend removal / LRM (filter radius ~ 20 m)	LD (&LoG) (radius 10-20 m)	Openness or MSII (radius 10 m)
complex topography	Shaded relief (sun elevation $> 45^\circ$)	SVF (& LoG) (radius ~ 10 m)	LD (&LoG) (radius 10-20 m)	Openness or MSII (radius 10 m)	

approach it results in good representation of features within a range of scales; however, very wide ranges of scale are computationally intensive and can result in reduced contrast.

Further visualisation techniques may be employed on a case-by-case basis; however, most if not all tasks can be performed with the selection described above.

3|2|2 Personal preferences and intercomparability

While landscape topography and feature morphology are important factors that limit the suitability of any given visualisation technique, user preferences also play a role in the selection. While some users prefer to look at visualisations that retain as much as possible a 'natural' appearance of the terrain (*e.g.* shaded relief or sky-view factor), others prefer visualisations that provide a greater level of abstraction from terrain to image (*e.g.* techniques that reduce or remove the visual impression of the overall landscape topography such as trend removal or openness). Other personal preferences may relate to the display as either greyscale or colour images, the combination of several visualisations (or several variants of one visualisation with different parameter settings) as RGB composite or the type and strength of histogram stretch that is applied. When producing colour images, the relatively high prevalence of various degrees of colour vision deficiency should be considered (*e.g.* in particular transitions from green to brown or from blue to purple may be not readable for many people). Colour transitions should always be transitions in both hue and brightness, not in hue alone.

In all cases, it is very helpful to ensure consistency with visualizing the same technique, *e.g.* inverted greyscale for negative openness and for Laplacian-of-Gaussian to retain dark representation of low/concave and bright representation of high/convex relief elements. Preferences for specific visualisation techniques also depend on the task at hand. While some techniques are particularly suitable for

Table 15: Suitability of visualisation techniques for representing selected archaeological topographical features.

	mining pits	former field boundaries	burial mounds	terraces	hollow ways	ridge and furrow
shaded relief	-	-	+	0	0	-
slope	-	0	0	+	+	++
principal components analysis	-	-	+	0	+	++
trend removal and LRM	++	+	++	+	+	++
sky-view factor	++	+	0	++	++	++
openness	++	+	+	+	++	++
local dominance	++	++	++	+	++	++
cumulative visibility	-	-	+	0	+	0
accessibility	-	0	-	0	0	-
multi-scale integral invariants	+	+	0	+	+	+
Laplacian-of-Gaussian	+	+	++	+	+	++

- not suitable; 0 indistinct; + suitable; ++ very suitable

the visual detection of features (*i.e.* they help to see something *is there*), others are more suitable for the interpretation of these features (*i.e.* they help recognize and interpret *what it is*).

Training and experience as well as new methods may over time change the preferences of a given user. While the adaptation and development of personal preferences can generally be expected to improve the quality of the interpretation and the rate of detection, it also entails a limited intercomparability of mapping results between different users and even between areas mapped by the same user at different times of their skills development. As intercomparability of results is very important in scientific work, efforts should be made to improve or at least quantify it. Ideally, repeated mapping by different persons or paired mapping would have the potential to greatly reduce intercomparability issues. However, these options are usually prohibited by workload and lack of staff.

3|2|3 Perception

DEM visualisation is a long process chain. We start with numerical elevation data, transform these by diverse visualization algorithms into raster maps of numerical values, visualize the numerical data with greyscale/colour mapping and contrast/histogram stretch, and present these images on computer displays or print them out to the final physical image that is perceived by the human eye. All this has

to happen before the image can be read by a human observer. Thus, understanding the entire process chain is necessary to be able to correctly interpret the images and to be able to purposefully modify/adjust the data processing parameters. Producing varied visualisations from a DEM is only the prelude to the equally important process of reading and interpreting the images. Because it happens in our brain (where, contrary to the software we have used up to this step, we do not have much control over algorithms and parameters), this process of reading and interpreting is commonly taken for granted. However, despite the limited control, which we have over our own brain, it is important to at least develop an awareness of *how* we see.

Perhaps counterintuitively, perception is an active rather than a passive process. The high-resolution fovea in the human eye covers only a very small portion of the field of view. The fact necessitates eye movements, which in turn require a complex feedback between the eye and brain. These eye movements amount to scan paths by which a scene or an image is scanned (Yarbus 1967). Furthermore, Yarbus (1967) noted that the scan paths depend on the question or task related to the images. Because the scan path interactions between our brain-eye system and the image are subconscious, they entail that high-resolution coverage of a given image is likely incomplete unless the observer makes a cognitive effort to look at all parts of the image. This effort can be facilitated by applying a (visible or imaginary) grid to the image.

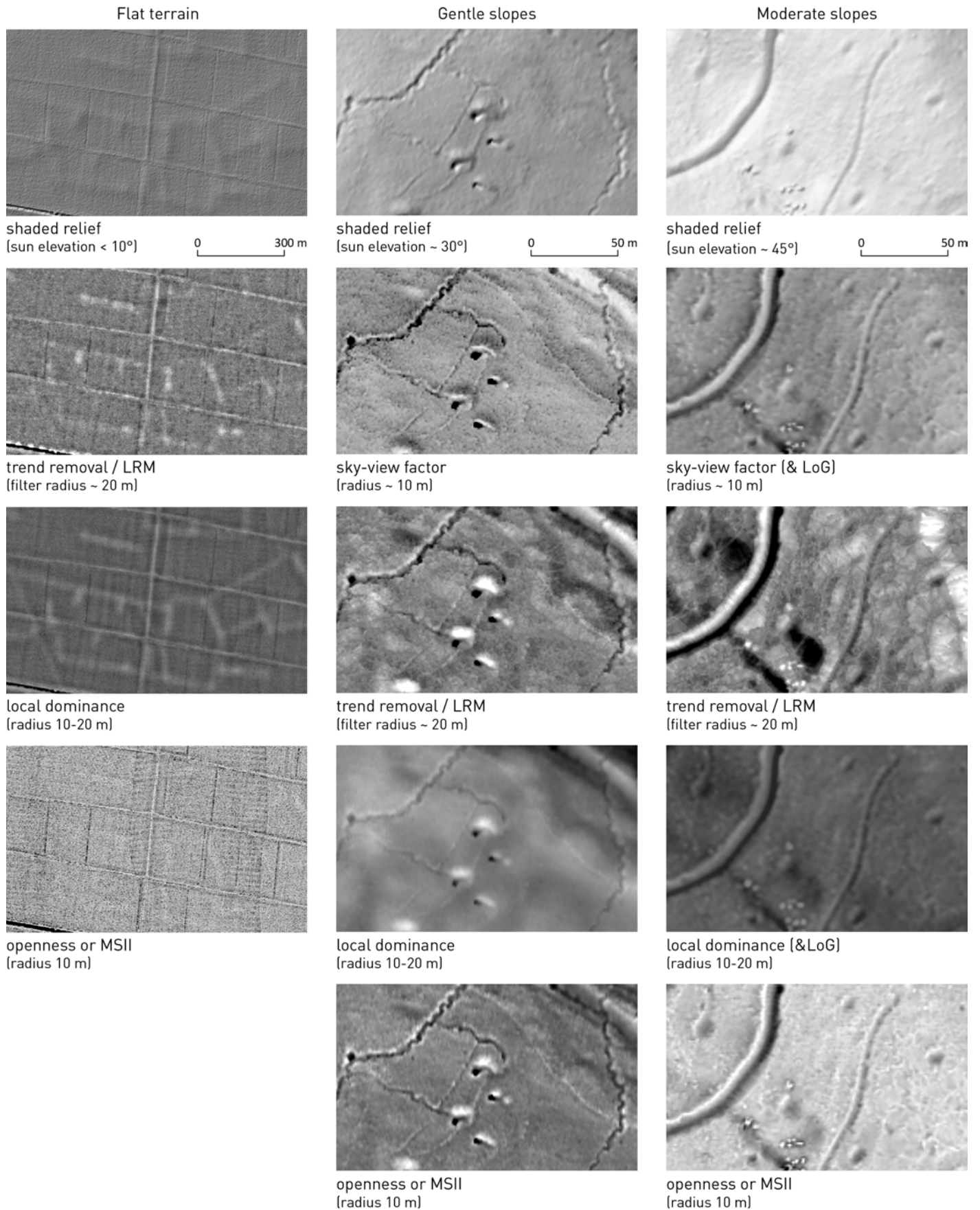
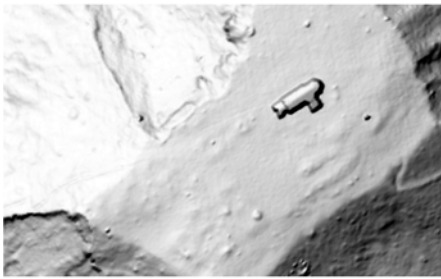
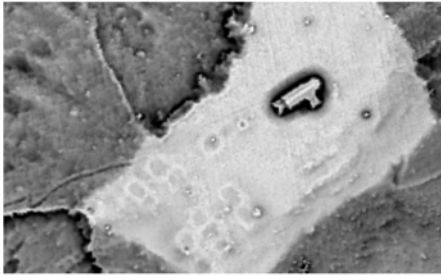
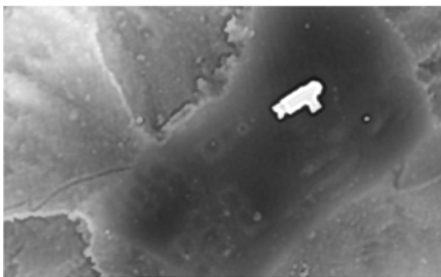
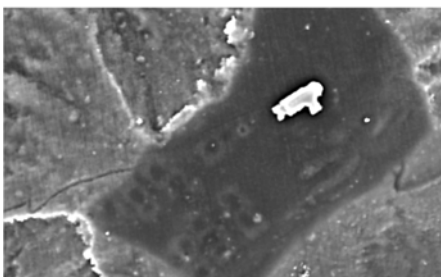


Figure 21: Visualization techniques in different topographic settings. (A) Plough headlands on a flat plain near Endingen am Kaiserstuhl. 1 m lidar data © LGL in Baden-Württemberg. (B) Three different types of World War I trenches with shelters on gentle NE slopes of Črni hribi, near Renče, Slovenia. 1 m lidar data © ARSO, Slovenia. (C) Charcoal burning platforms in the hills of the Black forest. 1 m lidar data © LGL in Baden-Württemberg. (D) A late Roman campo on a rocky outcrop with a church of St. Helena, west of Kobarid, Slovenia. 0.5 m lidar data © Walks of Peace in the Soča river Foundation.

Steep slopes or complex topography

shaded relief
(sun elevation > 45°)

0 50 m

sky-view factor (& LoG)
(radius ~ 10 m)local dominance (& LoG)
(radius 10-20 m)openness or MSII
(radius 10 m)

Yet even if we do consciously force ourselves to look at every portion of an image, we will commonly only see those features which we know and recognize and which we are looking for. Adams (1982) has wonderfully described this as a 'Somebody Else's Problem field' (SEP):

"An SEP[...] is something we can't see, or don't see, or our brain doesn't let us see, because we think that it's somebody else's problem [...] The brain just edits it out, it's like a blind spot. If you look at it directly you won't see it unless you know precisely what it is. Your only hope is to catch it by surprise out of the corner of your eye [...] It relies on people's natural predisposition not to see anything they don't want to, weren't expecting, or can't explain" (Adams 1982).

The subconscious pre-interpretation of what we see, e.g. the fact that we tend to close gaps or group objects based on similarity or proximity to form a 'gestalt' (Boeree 2009), can allow us to recognize relief features which are only partially preserved. However, the very same effect can also be misleading and can result in misinterpretations. The human eye-brain system is a remarkably efficient and adaptable pattern recognition system, but it needs to be trained to detect these patterns. Its efficiency can also be a hindrance, because it might see pattern where there is none. A possible approach to counteracting such limitations may, for example, be paired mapping – i.e. two persons have to agree on what they see. Besides understanding the described visualization algorithms and consciously counteracting the limitations of our visual perception, training and experience in reading DEM visualizations are therefore key for correct and (in times of overwhelming amounts of data and very limited manpower) rapid interpretation. Yet, having looked very purposefully at the same lidar image again and again, you can sometimes still discover something new 'out of the corner of your eye'.

3|3 Visualization of datasets other than lidar

The described visualization techniques and guidance for their selection are applicable to raster elevation data of different sources and resolutions, applied at various scales, and for observation of a range of entities (landscape, site object). Raster elevation models can be derived from aerial laser scanning (ALS) with a spatial resolution of 10 cm at best, but more frequently in the range of 0.5 m to 1 m. ALS data are most frequently used for a site or regional scale projects. Much higher resolution DEMs can be derived from, for example, terrestrial laser scanning, Structure-from-Motion (SfM) modelling (also referred to as close range photogrammetry), or structured light scanning. The resolution of such DEMs varies from a few centimetres to sub-millimetre and they are best for observation of smaller areas or individual objects.

Coarser DEMs, for example traditional national and world-wide datasets produced with surveying, photogrammetry, or interferometry, have a spatial resolution ranging from 5 m to 30 m. Free sources of global datasets are SRTM Global and ASTER Global DEM, both with approximately 30 m resolution and available at earthexplorer.usgs.gov. These are appropriate for national, continental, and global environmental studies.

Figure 21 continued.

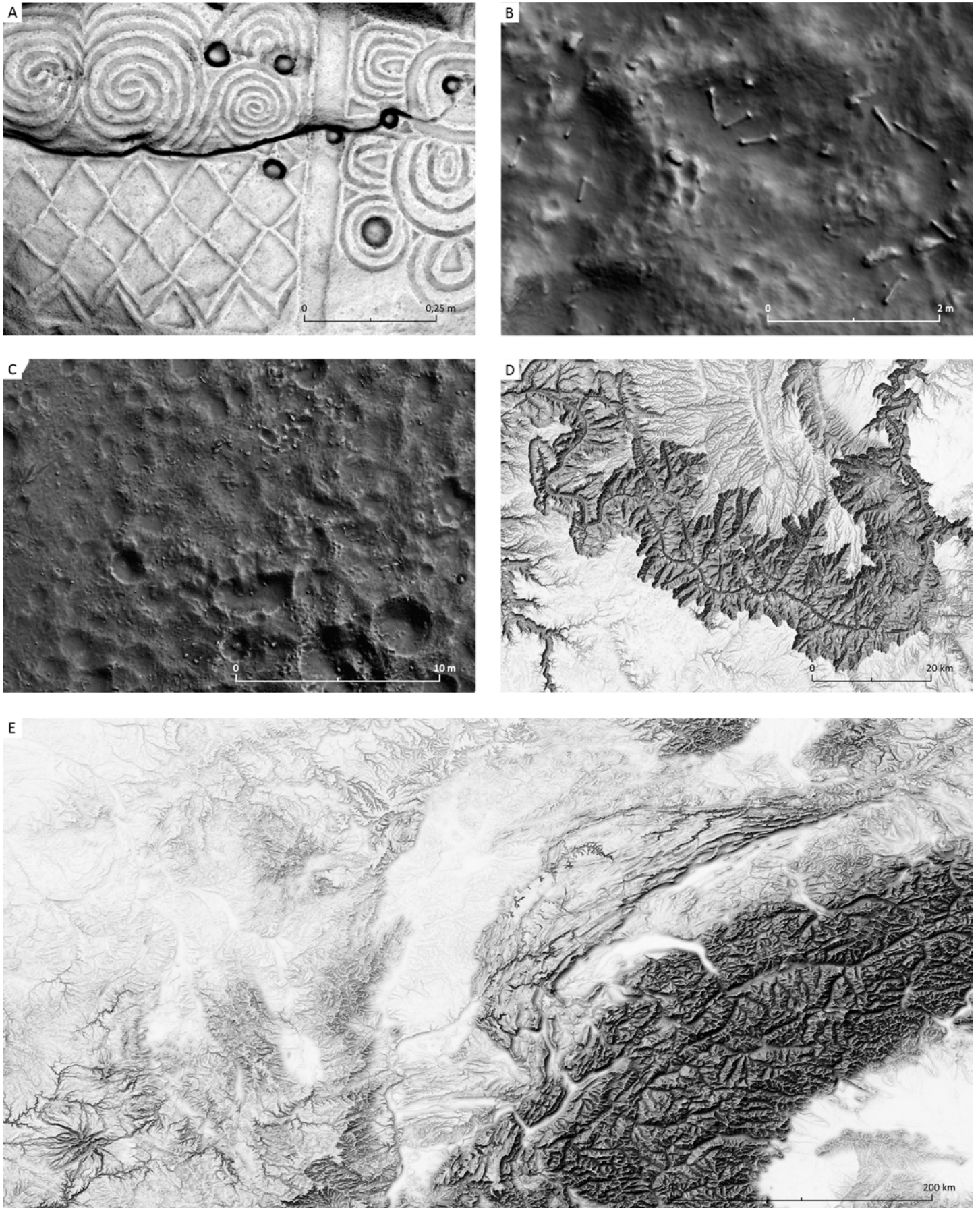


Figure 22: Different scales of observation. Sky-view factor image of a detail from a richly decorated kerbstone from Newgrange, Ireland, produced with Structure-from-Motion of hand held photographs (A). Scattered bones (B) and looting traces (C) on a desert floor in Peru. The elevation model was computed from images taken with a camera on a pole and is presented here with a combination of local dominance and shaded relief. Grand Canyon (D) as evidenced by 30 m SRTM data presented with a combination of sky-view factor and shaded relief. Central Massif, the Jura and the Alps (E) presented with a combination of anisotropic sky-view factor and shaded relief.

3|4 What's in a name?

Metadata about data processing has to follow the lidar dataset to the visualization intended for detection and interpretation and on to the final product – a thematic map. Lidar Base Specification (Heidemann 2014) provides specifications to acquire and procure lidar data and is a good source of information on what metadata should be stored. It specifies that metadata deliverables should include (Heidemann 2014: 13):

- collection report detailing mission planning and flight logs,
- survey report detailing the collection of control and reference points used for calibration and QA/QC including control and calibration points,
- processing report detailing calibration, classification, and product generation procedures,
- a QA/QC report, detailing procedures for analysis, accuracy assessment and validation of the point data, bare-earth surface, and other optional deliverables,
- georeferenced, digital spatial representation of the precise extents of each delivered dataset,
- product metadata files for the overall project, each scanning mission, and each deliverable product group.

It also gives a descriptive template and a completed example in Appendix 3, 'Lidar Metadata Example' and Appendix 4, 'Lidar Metadata Template.' Metadata specifications, however, usually only cover the hardware and software used to process or create the dataset, with additional explanations possibly given in the data quality sections (*e.g.* inclusion or omissions of features). Processing parameters for filtering and visualization are rarely given. If not explicitly demanded by the financier, few technicians and

Table 16: Metadata required when presenting DEM visualisations.

visualisation technique	mandatory parameters	ancillary parameters
shaded relief	illumination azimuth	illumination elevation vertical exaggeration factor histogram stretch
slope	histogram stretch (minimum/maximum slope)	
trend removal and LRM	low pass filter radius	histogram stretch / colour code type of low pass filter
openness	positive/negative greyscale / inverted greyscale search radius	number of search directions histogram stretch
sky-view factor	search radius	number of search directions histogram stretch
local dominance	search radius	observer height histogram stretch
cumulative visibility	search radius	observer/target height angular resolution
accessibility		search radius number of search directions
MSII	reference vector (if not zero)	number of scales minimum and maximum radius histogram stretch
Laplacian-of-Gaussian	filter radius	greyscale / inverted greyscale histogram stretch

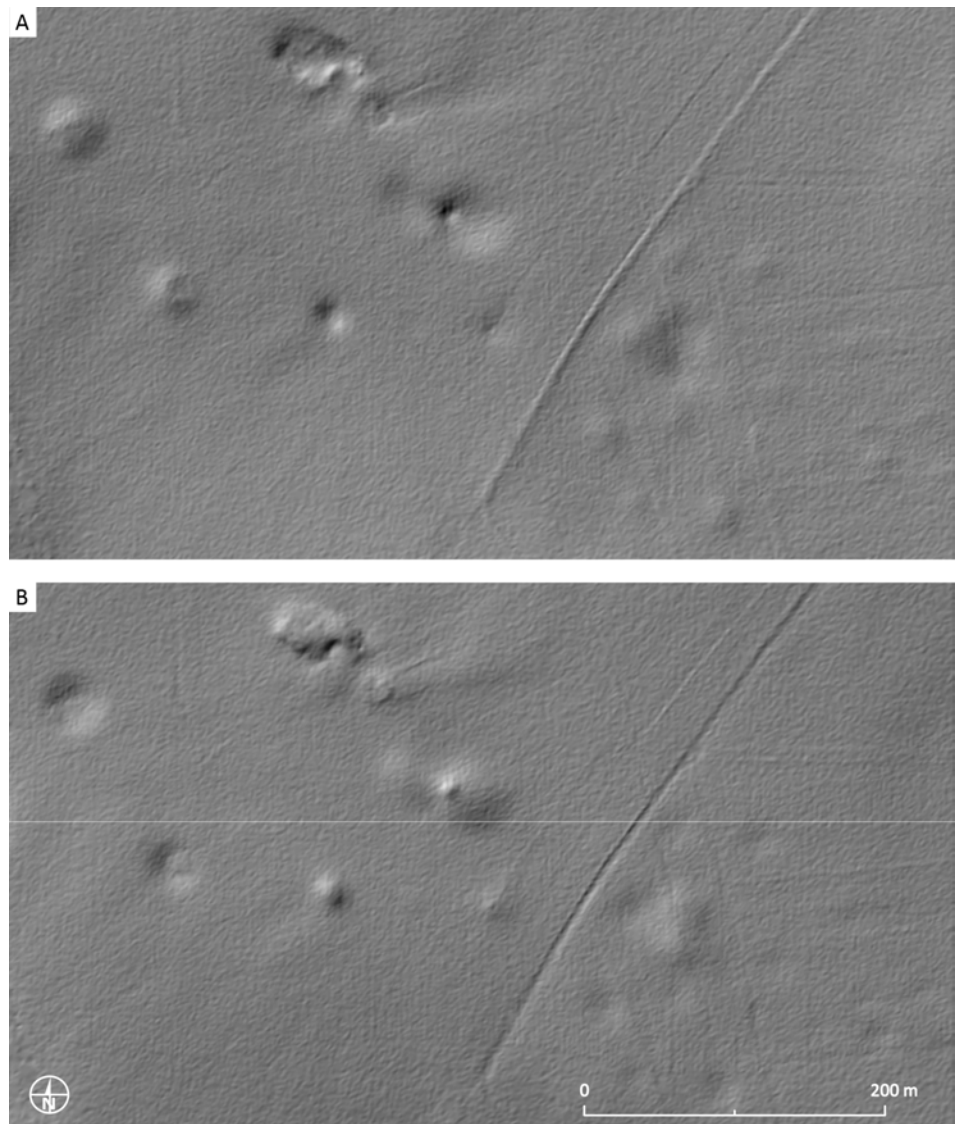


Figure 23: Is it a burial mound or a hole in the ground, a quarry or a hill? Someone observing the image needs to know the direction of the light source, because it has a definitive impact on the perception of the landscape. 315° azimuth illumination (A) and 135° azimuth (B). Terrain features seem inverted on (B).

scientist input all the required fields, let alone the optional fields into the metadata scheme. Nevertheless, entering the following records can assist the interpretation process at several stages:

- data acquisition: lidar sensor make and model, nominal scanning density, nominal swath overlap, date of data collection;
- description of post-collection processing: method(s) used, parameter settings, description of the processing goal (*e.g.* production of a terrain model, removing just the vegetation, production of a surface model), elevation model spatial resolution;
- visualization: method(s) used, parameter settings (see below and Table 16);
- interpretation process: aims of interpretation (*e.g.* identifying locations of individual burial mounds and marking their circumference), reliability of the results (qualitative if quantitative evaluation is not possible, *e.g.* low to high, description of each class is recommended).

A minimum metadata requirement for visualization is the applied algorithm and the settings of its principal parameters. Providing all details may often not be practical when preparing images for publications.

Table 16 lists the mandatory and ancillary parameters. The necessity of providing the ancillary parameters depends largely on the purpose of presenting the image: if the aim is solely to provide a visual illustration, many parameters may be omitted. However, if the aim is a quantitative analysis of specific features, a discussion of feature details, or a comparison of different visualisations, more parameters have to be provided for the reader to understand the image and to be able to reproduce the process of image creation. Sometimes a seemingly trivial parameter, such as shaded relief illumination azimuth, can have a huge impact on the perception of the landscape and has to be known to the observer (Figure 24).

It is very easy to repeatedly calculate visualizations with varied settings. A good practice is to store the applied visualization technique and settings of the

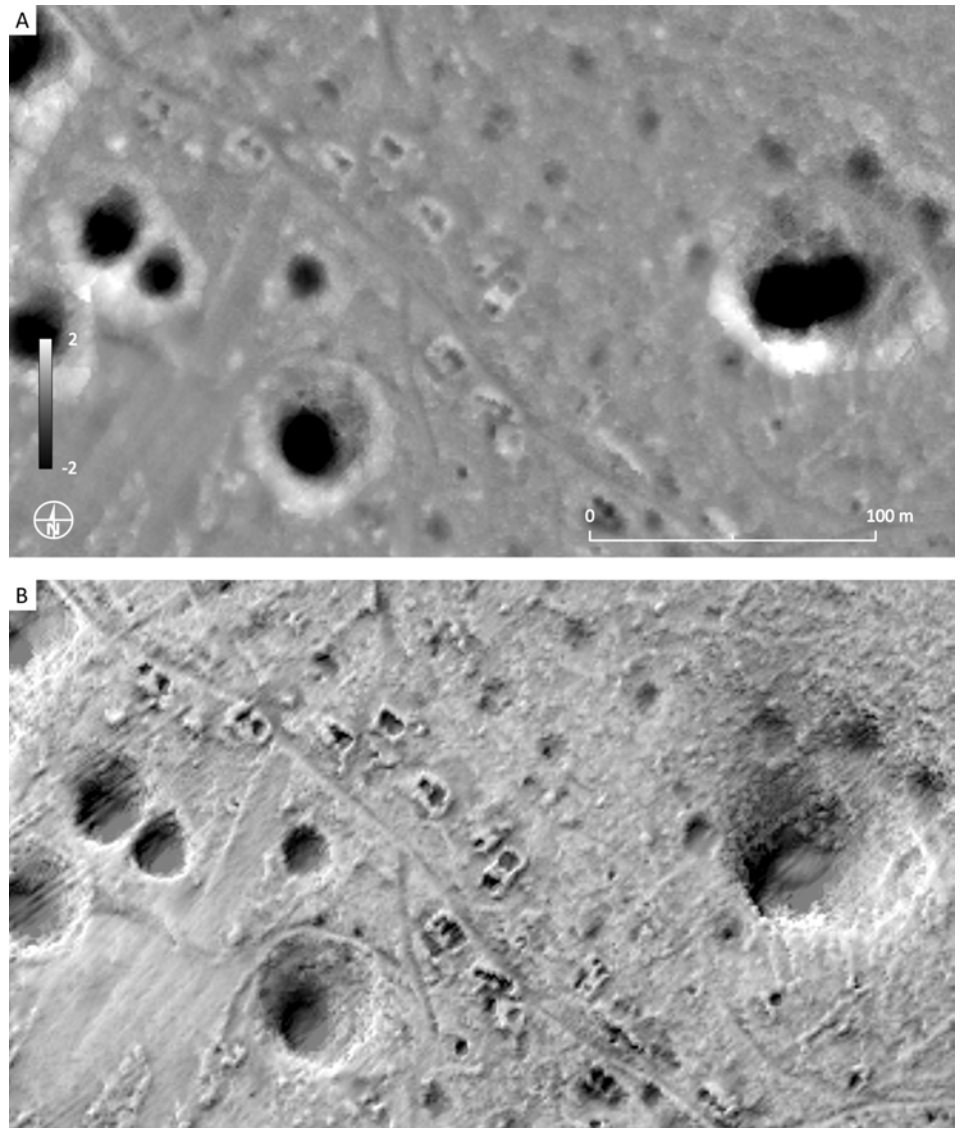


Figure 24: Overgrown remains of an abandoned village Novi Breg (Naubacher), Slovenia, as represented by local relief model technique with a filter radius of 25 m (A). Remains of houses can be seen as bright rectangles. Big black blobs are dolines. It is straightforward to replicate such an image with the minimum data that is provided. However, when reproduction or relative comparison across areas is not required, combinations of visualizations can give images that are easier to read, and details about visualizations may be omitted (B). 1 m resolution lidar data © ARSO, Slovenia.

main parameters in the name of the output file, as well as to store all the settings in a processing log.

From a filename `Novi_Breg_DTM_1m_LRM_FSc_lin_FR10_MR25.tif` it is quite obvious that the local relief model visualization was applied to a 1 m resolution digital terrain model (Figure 24A). The settings applied were:

- FSc – filter shape: circular
- llin – interpolation method: linear
- FR – filter radius [px]: 10
- MR – maximum range [px]: 25

Such filenames may seem strange at a first, but are the best safeguard for

remembering the necessities when producing images for publications or trying to replicate the process with other data.

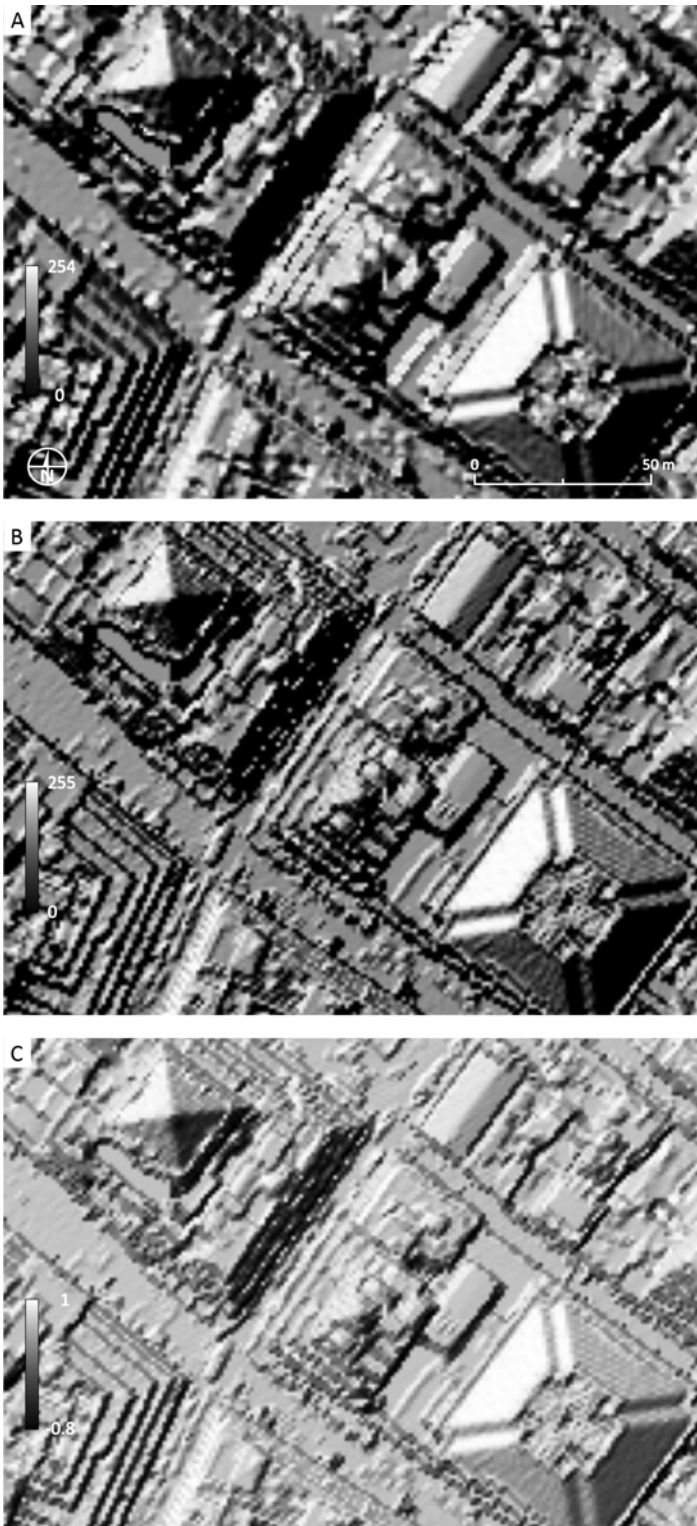
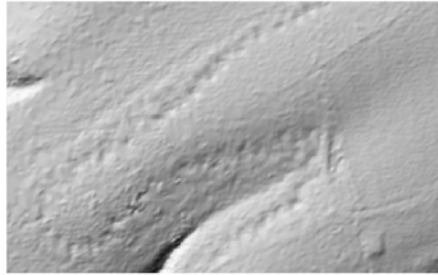


Figure 25: Hillshading algorithms in ArcMap (ArcMap 2012) and RVT use the same method (Yoëli 1965), but the results are quite different as evident from the image of skyscrapers in Lower Manhattan. The hillshading image calculated with ArcGIS (A) seems to be less clear (as if using a DEM of a lower resolution) than the one calculated with RVT (B). Note the distinctly visible elevation steps on (B), especially the steps on the facade of the lower right skyscraper (B), which are completely missing on (A). Both (A) and (B) have saturated high and low values (completely white and black areas). However, RVT calculates hillshading with a full range of values therefore details in black areas are revealed to a great extent on the original unsaturated image (C). The same is true for the difference in calculation of sky-view factor with RVT and SAGA GIS. All figures are calculated with 35° Sun elevation and 315° azimuth using the same DEM. 1 m spatial resolution lidar data © USGS.

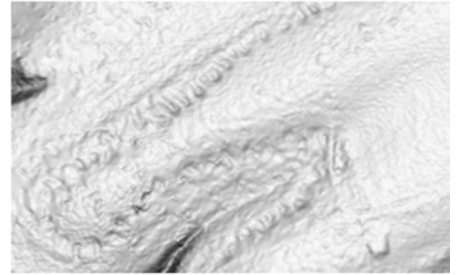
Medieval iron ore mining traces near Owen, Germany. 1 m spatial resolution lidar data © IGL Baden-Württemberg.

0 100 m

Shaded relief
(azimuth 315°, sun elevation 35°)



Slope severity



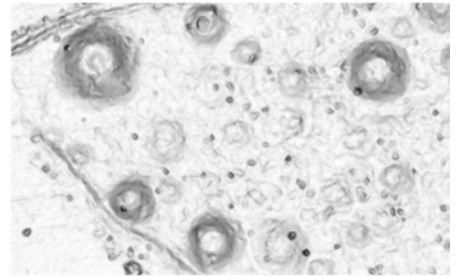
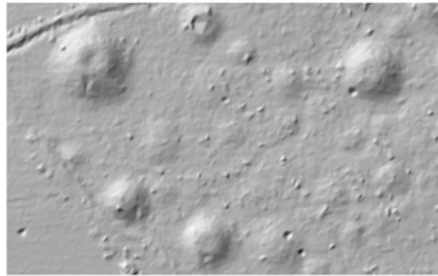
Overlapping field systems near Hügelsheim, Germany. 1 m spatial resolution lidar data © IGL Baden-Württemberg.

0 100 m



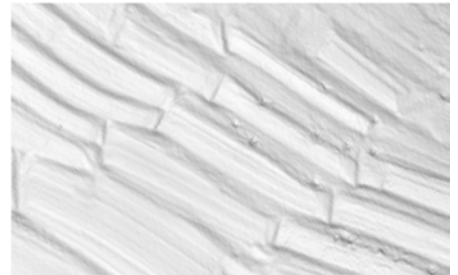
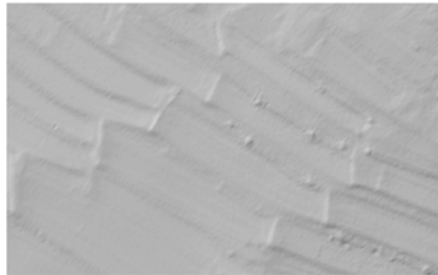
Early Iron Age barrow cemetery in Pivola, Slovenia. 1 m spatial resolution lidar data © ARSO, Slovenia.

0 100 m



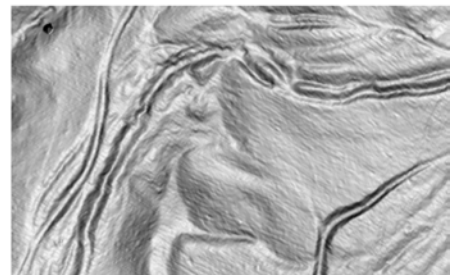
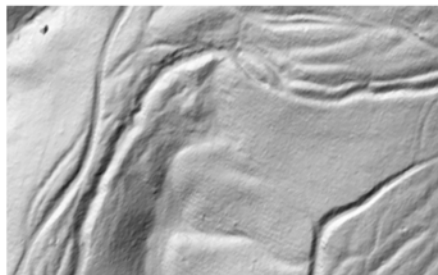
Alpine terraces at Rodine, Slovenia. 1 m spatial resolution lidar data © ARSO, Slovenia.

0 100 m



Hollow ways and headstreams near Rova, Slovenia. 0.5 m spatial resolution lidar data © Občina Domžale, Slovenia.

0 100 m



Ridge and furrow south of Harlaston, Staffordshire, UK. 1 m spatial resolution lidar data © Environment Agency, UK.

0 100 m

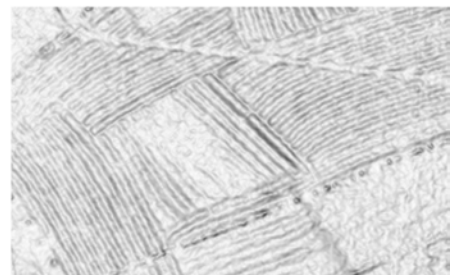
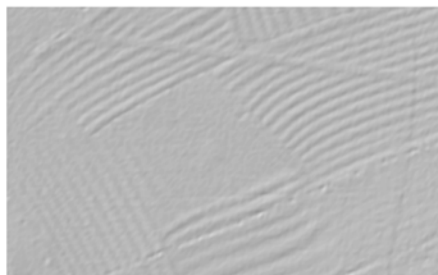
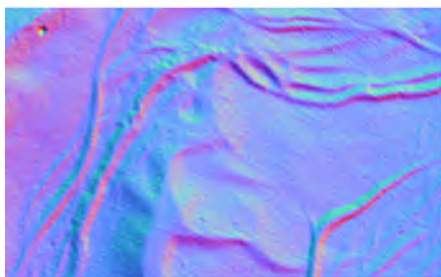
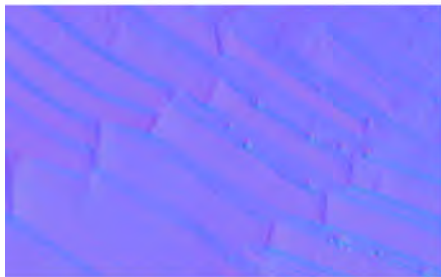
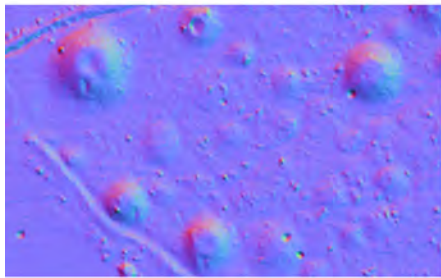
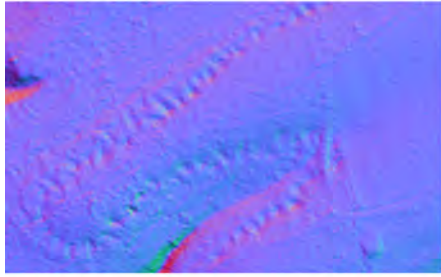
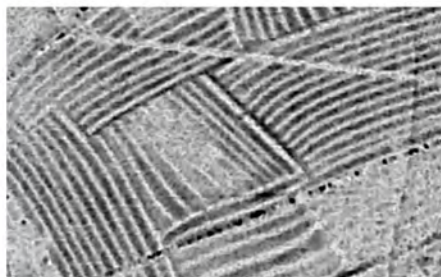
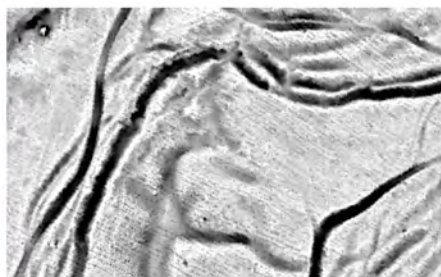
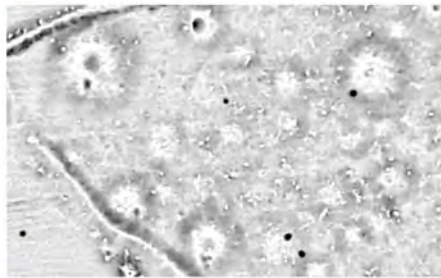
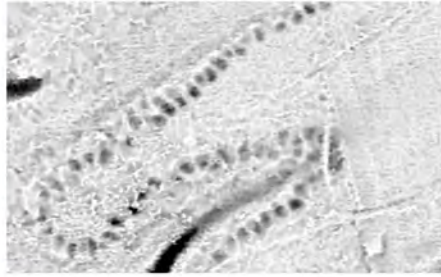


Figure 26: Visualization techniques with different relief features. Continues on next page.

Principal Components Analysis
(sun elevation 35°)



Openness
(radius 10 m, 16 search directions)



Sky-view factor
(radius 10 m, 16 search directions)

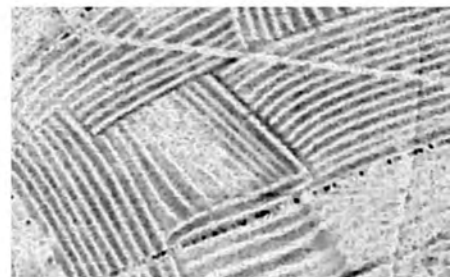
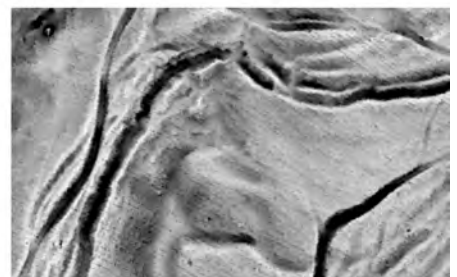
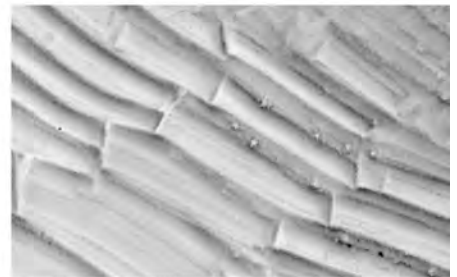
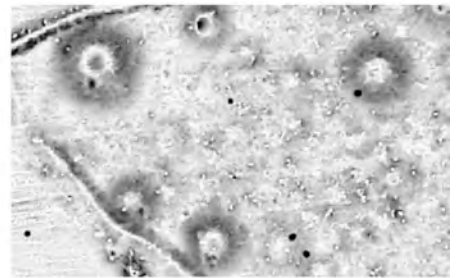
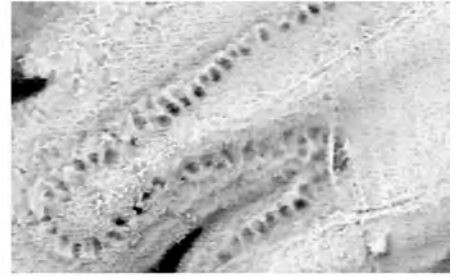
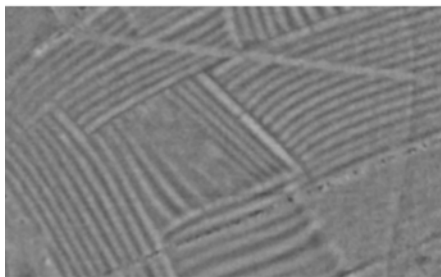
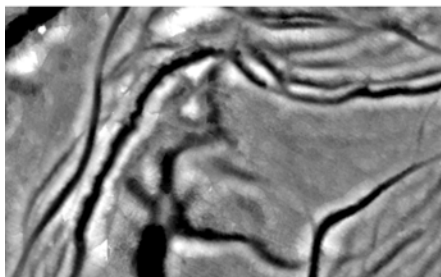
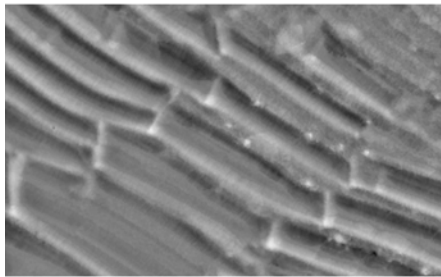
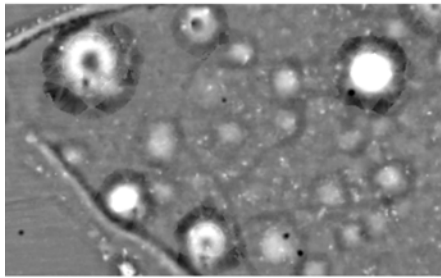
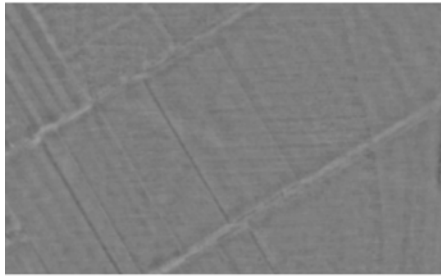
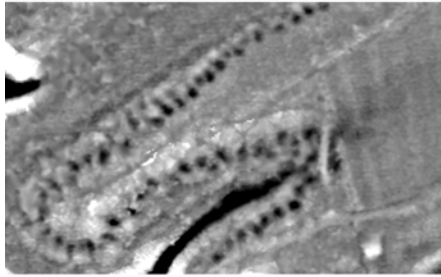
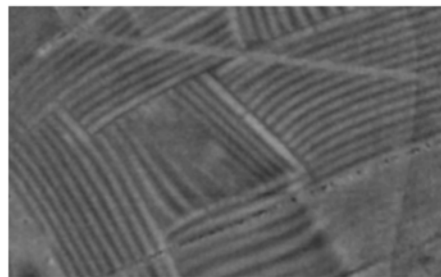
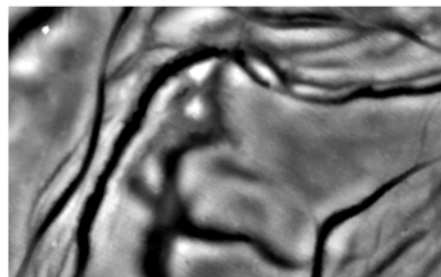
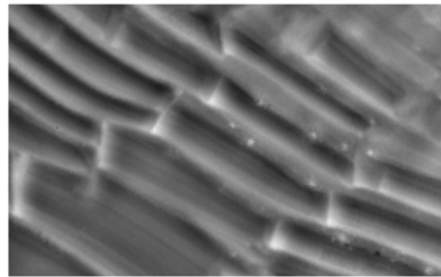
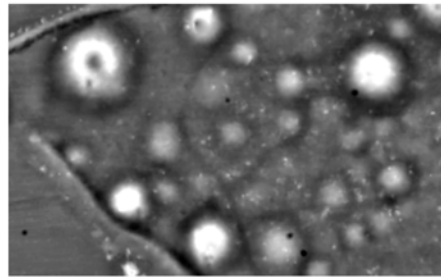
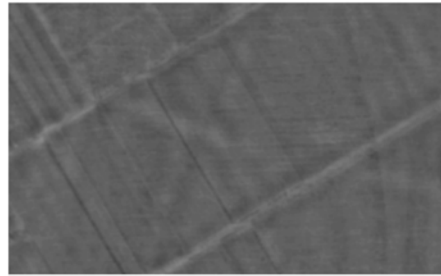
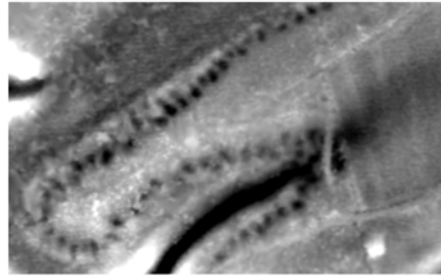


Figure 26 continued.

Local Relief Model
(filter radius 10 m)



Local dominance
(radius 10-20 m)



Cumulative visibility
(radius 10-20 m)

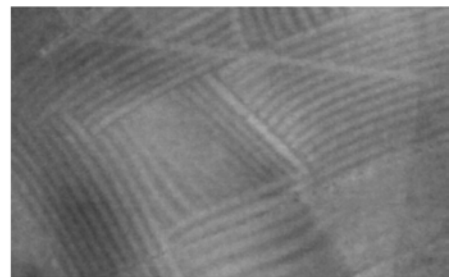
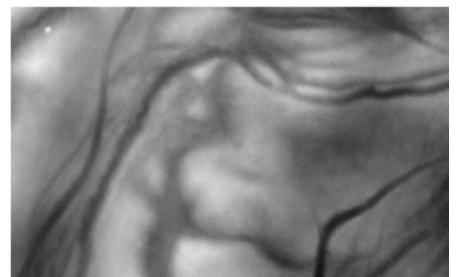
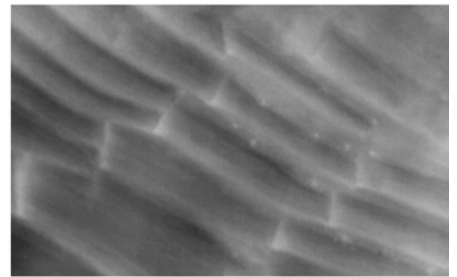
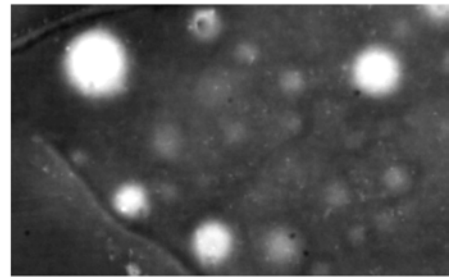
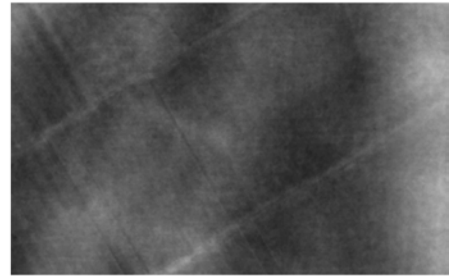
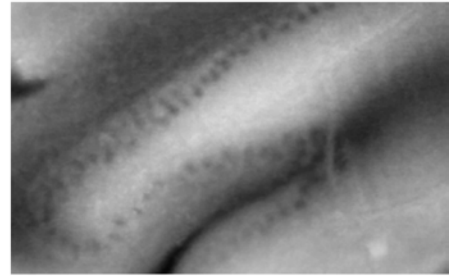
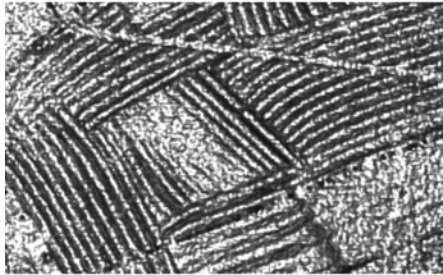
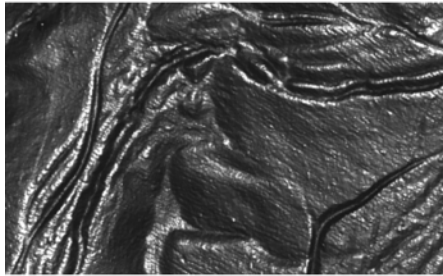
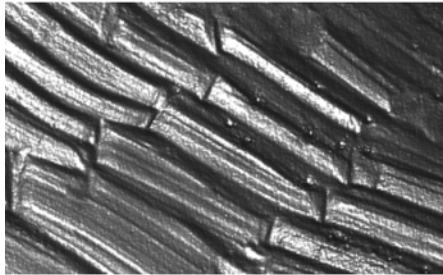
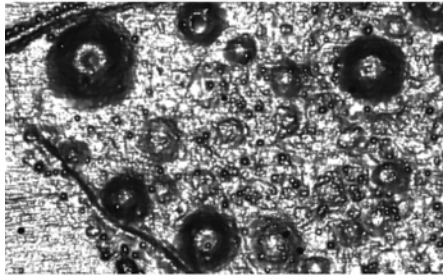
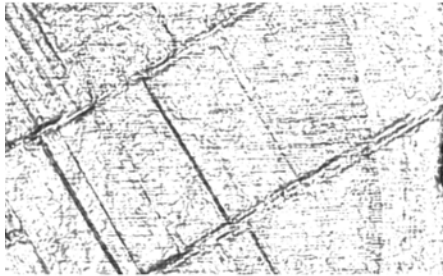
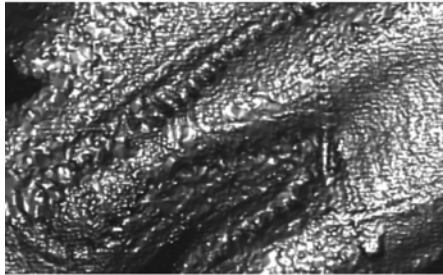
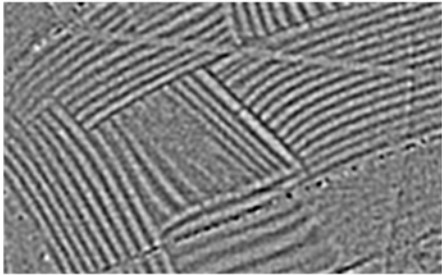
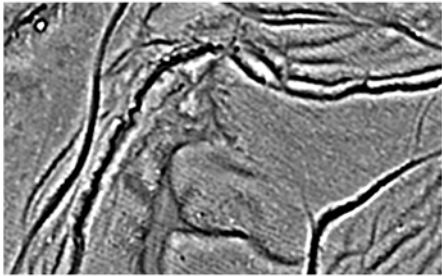
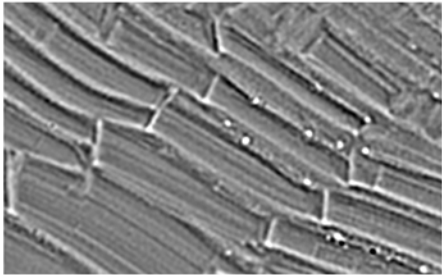
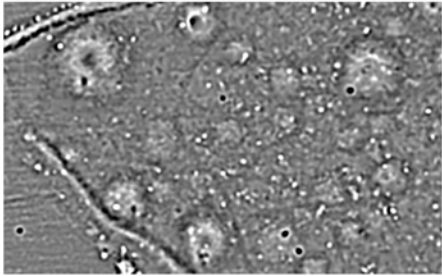
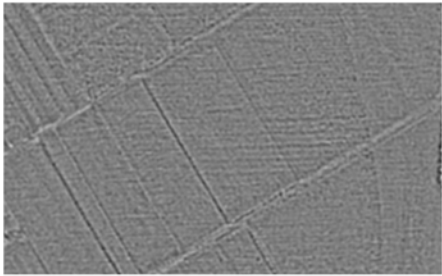
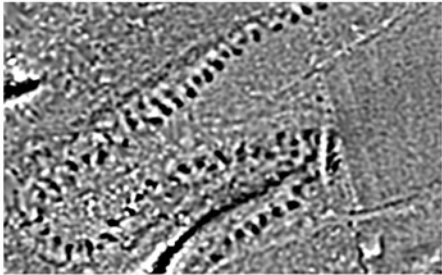


Figure 26 continued.

Accessibility
(radius 10-20 m)



Multi-scale integral invariants
(filter size 3 m)



Laplacian-of-Gaussian
(filter size 3 m)

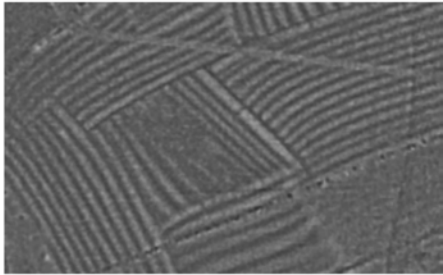
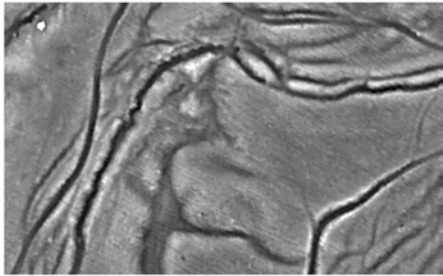
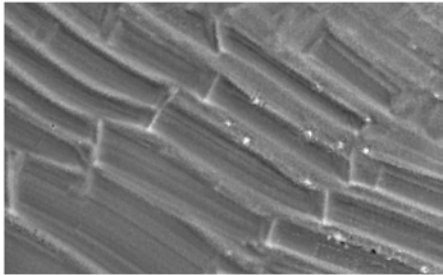
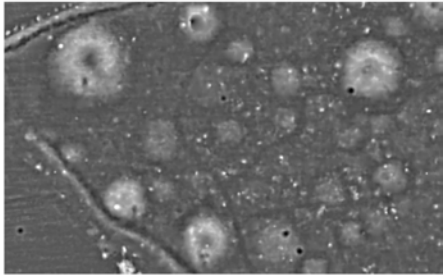
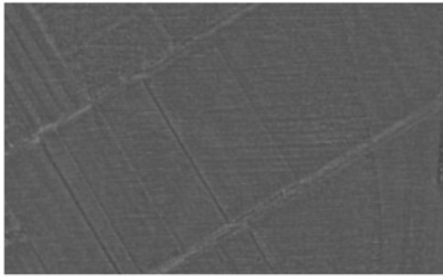
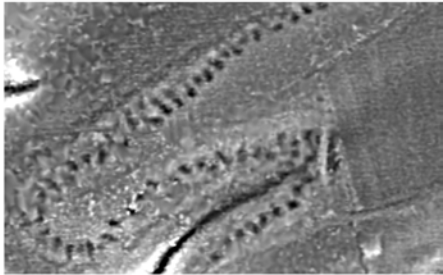


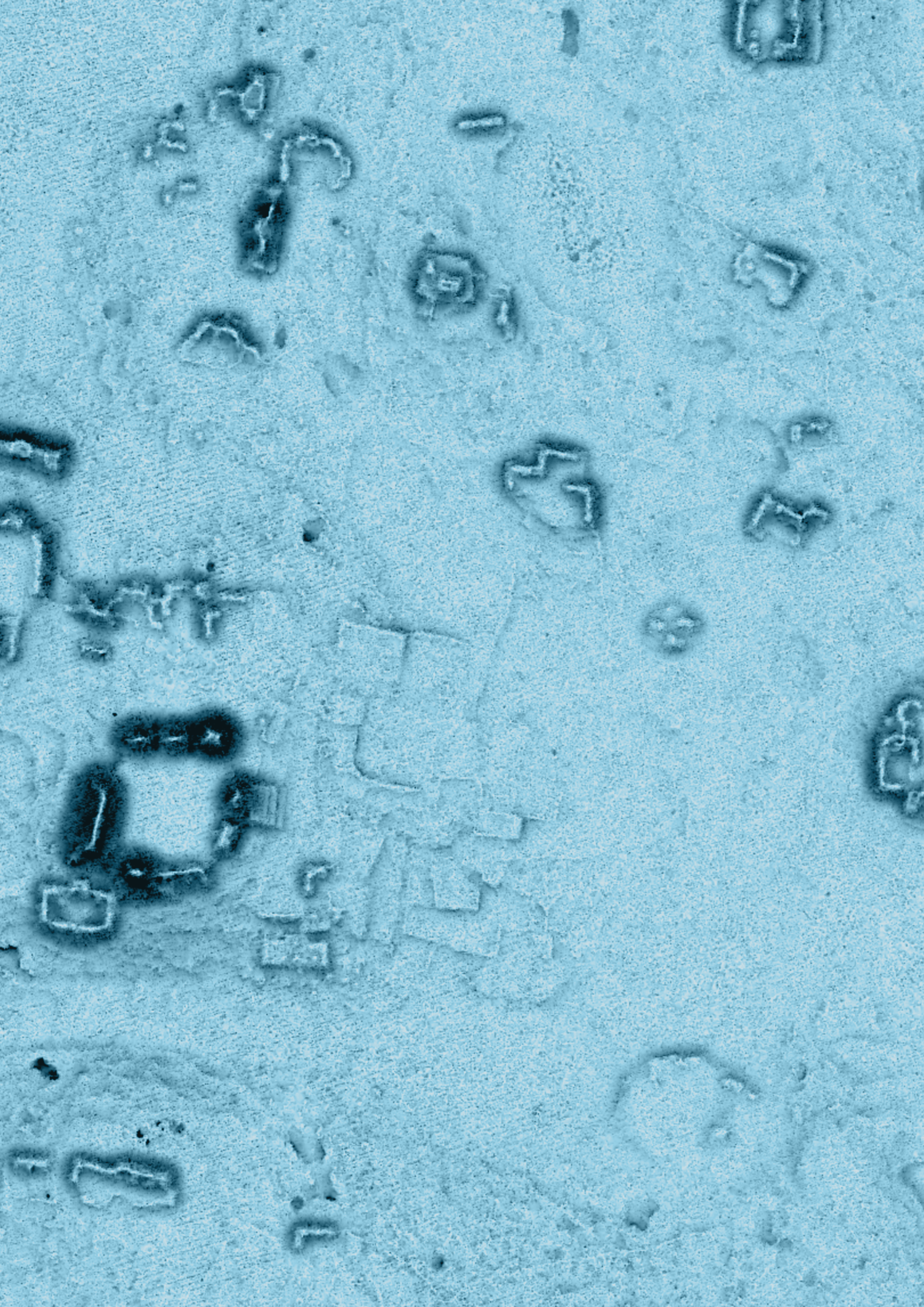
Figure 26 continued.



4



Tools



4

Two toolboxes with implemented methods that give scientifically sound results, and are documented and supported by research papers.

Researchers can only very recently benefit from free software for calculation of advanced visualization techniques. Two such examples are Relief Visualization Toolbox (RVT) and Lidar Visualization Toolbox (LiVT), both free, easy-to-use applications to create visualisations from high-resolution digital elevation data derived from aerial laser scanning (lidar) or other sources, *e.g.* structure-from-motion photogrammetry. The second is oriented towards more advanced users with some knowledge in data processing and geographic information systems, while the first is tailored also for the very beginners in relief interpretation. Implemented methods give scientifically sound results, and are documented and supported by research papers. Both toolboxes should work on any ordinary office computer. With large files, there could be issues with RAM and TIFF size limits. Should you want to process very large files (*e.g.* larger than 40 km² at 1 m resolution), you will most probably have to tile them.

Other raster processing software solutions, such as QGIS, SAGA GIS, GRASS, or ArcGIS, have also started to provide access to at least some of the described visualizations techniques, but are not discussed here, as we have not thoroughly tested the implemented methods. Testing is essential because software solutions can give diverse results despite using the same method and small differences in implementation can have a huge impact on the representation of features (Figure 25).

4|1 Relief Visualization Toolbox (RVT)

Relief Visualization Toolbox (available at <http://iaps.zrc-sazu.si/en/rvt>) is a standalone toolbox that does not require external software to run. It provides a narrowed range of methods and their settings are limited to the most important. The selected techniques have been proven effective for detection of small-scale features and default values are set to do this task. Some techniques (*e.g.* sky-view factor and openness) tile large datasets.

RVT (v 1.3) can process all GDAL (GDAL Development Team 2014) supported raster formats (*e.g.* GeoTIFF, generic binary file, Erdas Imagine file, ENVI file, Arc/Info ASCII Grid, ASCII gridded XYZ, JPEG2000...). It can process multiple files from various folders and all techniques in one go. It is possible to run it without opening the graphical user interface, on a list of files, and with predefined settings.

Visualizations output a pair of GeoTIFFs per each selected visualization. One file gives a precise calculated result, and the other a simplified result ('a picture'), optimized for viewing in non-GIS software, *e.g.* by Windows Photo Viewer or by Preview for Mac users. All output files are written into the folder of the input file. Output file names for visualizations are composed of the input file name, and suffixes describing the selected method and processing parameters. Each

execution of the program also generates a processing log file per input file, thus automatically assembling metadata.

The toolbox supports elevation raster file data conversion. It is possible to convert all frequently used single band raster formats into GeoTIFF, ASCII gridded XYZ, Erdas Imagine file and ENVI file formats. RVT can thus be used to convert DEM files in your favourite format to formats supported by LiVT, *e.g.* ENVI, and to convert results of LiVT back to a more widely supported format, *e.g.* GeoTIFF.

RVT can also mosaic tiled raster data and visualizations with selected settings can be executed on a predefined list of files without running the Graphical User Interface (GUI). For more information, see the RVT Manual (Instructions for use) available from RVT web page.

4|2 Lidar Visualization Toolbox (LiVT)

Lidar Visualization Toolbox (available at <http://sourceforge.net/projects/livt>) can compute all of the techniques described in Chapter Description of techniques and has settings for intricate manipulation of the parameters for each algorithm. For example, when computing a Local Relief Model options allow setting the filter shape (circular or square), filter radius, interpolation method (inverse distance, nearest neighbour, average, linear, or

bilinear), and a maximum range. It is limited in terms of file types it supports and can presently only process and outputs generic BIL (band interleaved by line) files and ENVI raster files.

LiVT also includes a tool to rasterize ASCII XYZ point clouds (e.g. last return lidar data) with four different interpolation methods.

It runs on Windows and requires the Microsoft .NET Framework version 4. It does not include a viewer; additional software (GIS) will therefore be necessary to display the processing results. All algorithms output floating point binary raster maps. For viewing them in GIS, greyscale or colour coding will have to be applied. In addition, appropriate contrast/histogram stretches may be necessary to produce optimal results.

File size limits vary from algorithm to algorithm and range from 30 to 144 million pixels per file. Computation times depend, in addition to the chosen algorithm, also on the selected parameters and of course the processing power of the CPU. LiVT only uses one processor core, but several instances of LiVT can work on separate cores in a multi-processor PC. Simpler algorithms are generally much faster than more complex ones. Where filter or search radius can be specified, doubling the radius will approximately double the computation time for the same input file in a radial algorithm (one that considers pixels along a limited number of radial lines) but will quadruple the computation time in an algorithm which considers all pixels within the radius.

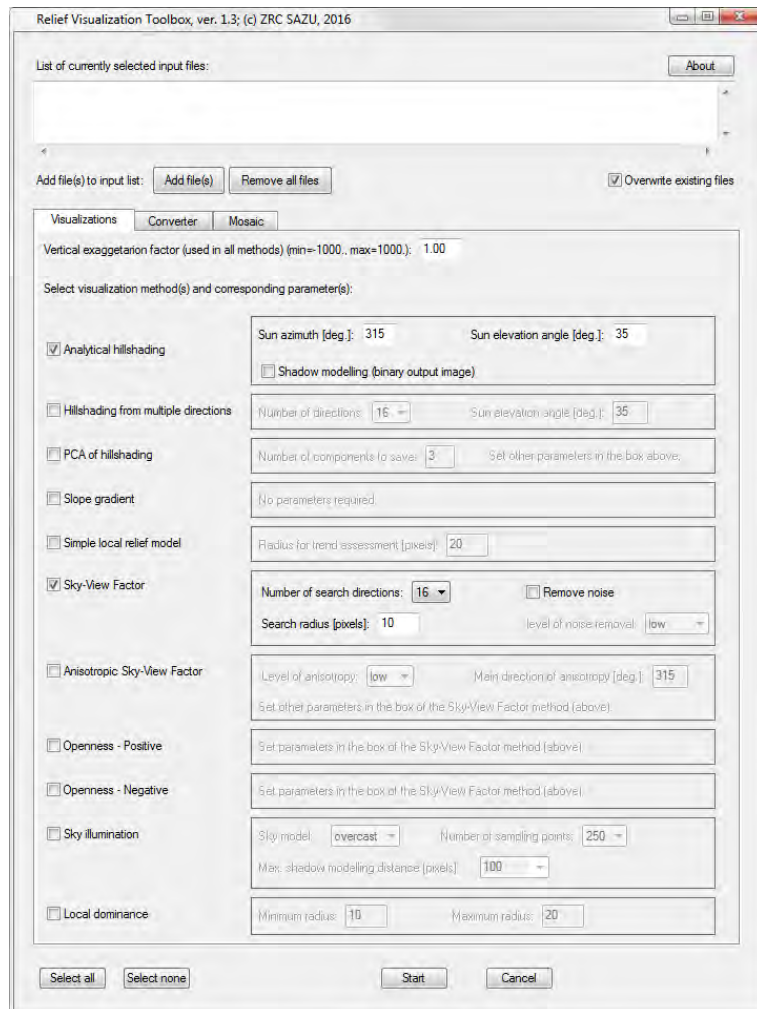


Figure 27: Relief Visualization Toolbox (RVT) offers a range of only the best techniques with just the essential options. It is extremely easy to use and can process multiple files and all techniques in one go.

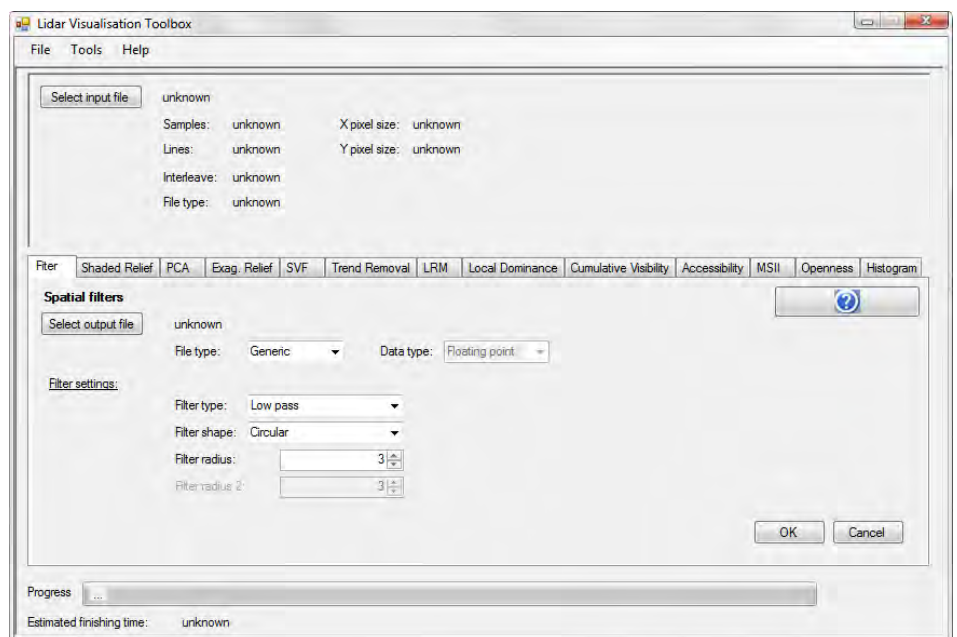
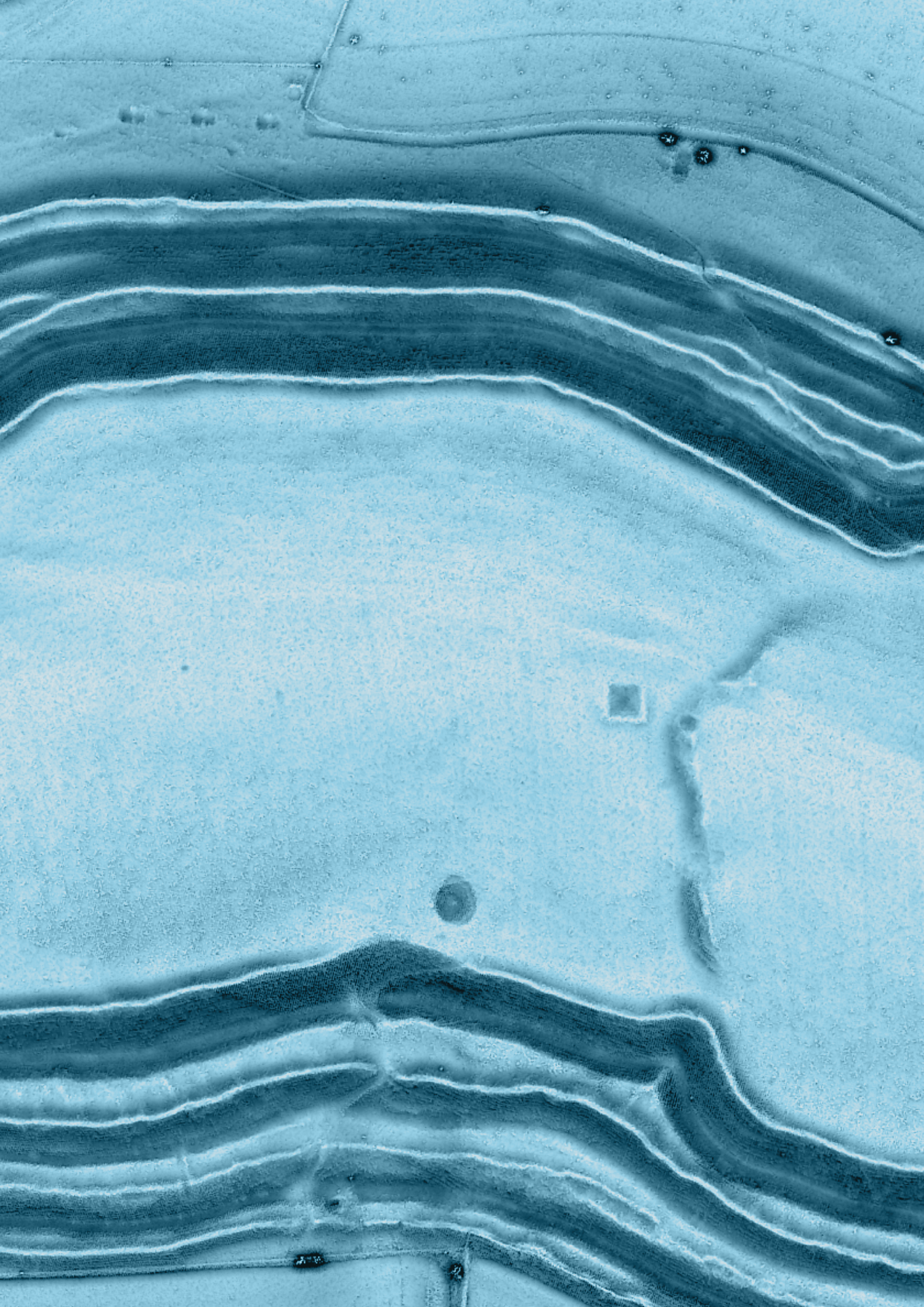


Figure 28: Lidar Visualization Toolbox (LiVT) supports calculation of various techniques with intricate options to manipulate the settings.



5

Case studies



5

The following chapters focus on some typical studies where lidar visualizations have helped archaeologists and geomorphologists better understand their areas of interest.

Archaeologists are highly involved in the interpretation of microrelief features from lidar data because precise relief models allow for a detailed mapping and measurements of overgrown archaeological structures (dams, ramparts, ditches, pits, quarries, remains of houses, etc.) (Kershaw 2003; Devereux *et al.* 2005), fossil fields and cultivation terraces (Sittler 2004), former land division (*e.g.* Roman centuriatio), abandoned quarries and mining pits, burial tumuli and ancient roads (*e.g.* Roman, medieval), and other remains of former cultural landscapes in specific environments where other techniques or field surveying do not give satisfactory results (Challis 2006; Challis *et al.* 2008; Crutchley 2009a; Crutchley 2009b), even in extreme conditions, such as mapping of features under a dense canopy of a tropical forest (Fernandez-Diaz *et al.* 2014).

Aerial laser scanning data is also used in geomorphology, either directly in a form of elevation data for detecting the surface discontinuities (*e.g.* breaklines, lineaments) and forms (*e.g.* fans, lava flows), or indirectly by classification of surface features relevant for geomorphological processes. High-resolution relief models enable:

- mapping of geomorphological features (*e.g.* drainage network and channel heads (Passalacqua *et al.* 2010), fallout deposits, epiclastic sediments and lava flows (Fornaciai

et al. 2010), coastal dunes (Woolard and Colby 2002), glacial forms (Smith *et al.* 2006)),

- modelling of processes (*e.g.* glacial, periglacial (Smith *et al.* 2006), fluvial (French 2003), and aeolian processes (Sankey *et al.* 2010), soil erosion and deposition (Chiverrell *et al.* 2008)), and furthermore
- natural hazards risk assessment (for *e.g.* landslides (Metternicht *et al.* 2005), rock falls (Lan *et al.* 2010), glacial debris (Conway *et al.* 2010)).

flowing, the first material to be laid down is usually coarse, with fine sands and silts toward the edges.

Alluvial fans are of practical and economic importance to society, particularly in arid and semi-arid areas where they may be the principal groundwater source for irrigation farming and the sustenance of life. The use of desert fans as permanent sources of water is limited, however, because periodic rainfall or snowmelt provides only a very slow rate of recharge.

Creating a settlement on an alluvial fan can be dangerous, because they are prone to flooding. Rushing water, mud, and debris can threaten communities many kilometres away from the apex of the alluvial fan. Lidar data reveals details of the intricate drainage system formed on the fan and is often used for hydrological studies of groundwater sources and flood modelling.

5|1 Alluvial fan at Craig canyon, Saline Valley, California, USA

The alluvial fan that stretches out of Craig canyon at the edge of the Inyo Mountains onto the floor of the Saline Valley in California, USA, is a typical fan-shaped deposit of unconsolidated water-transported material (alluvium). Alluvial fans typically form at the base of topographic features where there is a marked break in slope. The apex (the narrow part) of each fan is just within a canyon mouth that serves as the outlet for a mountain drainage system. Sediment from erosion within the mountains is moved by these drainage systems to the adjacent basin, forming the wide triangle – the fan's apron. Since the rivers that deposit alluvial fans tend to be fast

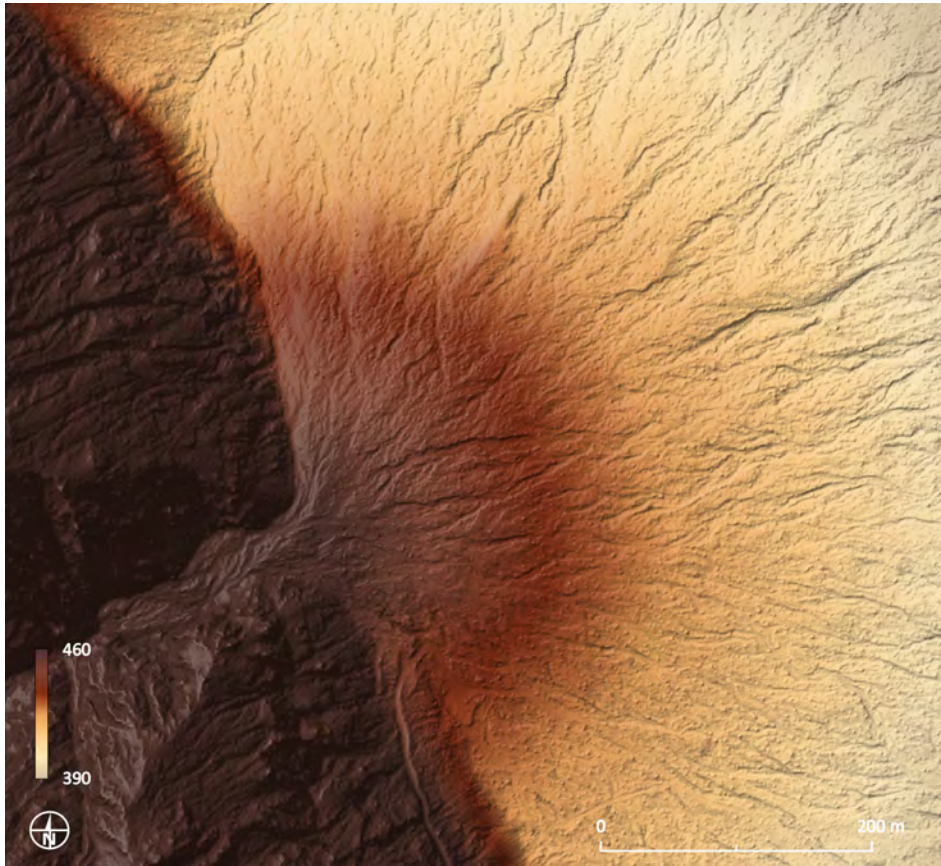


Figure 29: Craig canyon alluvial fan (California, USA) as evident on 0.5 m spatial resolution lidar data (California, USA). Coloured stretched elevations over SVF and shaded relief provide a detailed view of the intricate drainage system of the fan's apron. The typical shape of the fan is also easily recognizable. © Plate Boundary Observatory by NCALM, USA.

Table 17: Lidar scanning parameters of Craig canyon alluvial fan (California, USA)¹.

	parameter value
scanner type	Optech GEMINI
platform	fixed wing
date	between 18 th April and 24 th April 2008, exact date unknown
average last and only returns per m ² on a combined dataset	3.6
spatial resolution of the final elevation model [m]	0.5

¹ Lidar data acquired by Plate Boundary Observatory by NCALM, USA. PBO is operated by UNAVCO for EarthScope and supported by the National Science Foundation (No. EAR-0350028 and EAR-0732947).



Figure 30: Alluvial fan's apron at the foot of Craig Canyon in the Saline Valley, USA. Photo by Brian Lockett, Air-and-Space.com.

5|2 Hollow ways at Volčji Potok, Slovenia

Historical hollow ways or sunken paths are routes that have been eroded down to bedrock by the flow of people, animals, and carts, so that they are recessed beneath the level of the surrounding landscape. They form in the soft stone, not on the hard rock. Regular trampling by people or livestock suppresses the growth of vegetation on trails and reduces the water infiltration rate. This results in increased surface runoff along trails, especially on steep slopes. During the dry season, trampling displaces surface soil, providing a source of sediment during the rainy season. The trails become a conduit for surface runoff and a source of sediment, resulting in increased erosion rates (George *et al.* 2004). As the roads deepened, they became natural waterways. Rain drained into and down them; storms turned them into temporary rivers, sluicing away the loose rock debris and cutting the roads still further below the meadows and the fields. Water erosion speeded the hollowing-out process and made some lanes muddy and impassable. When this happened, alternative routes

were taken by people traveling along them, leading in some places to formation of river-like braided channels, branching and converging (Edgeworth 2011: 109).

“Instead of fragments of transport networks connecting fixed points in the landscape, hollow ways are rather ‘messy’ landscapes of movement, interwoven swarms of different scrapes and traces of movement, almost biological shapes, ‘organic’ entanglement of lines that emerges from growth and differentiation through rhythms of human and animal movement, change of seasons, water dynamics... They are not about getting somewhere, from point A to point B, but about being in the landscape, living the daily life. People inhabit the landscape along these paths. They are lines along which past landscapes were created, in a messy way, from things and features encountered along the path.” (Mlekuž 2013: 41).

Most have through time become unpassable, so overgrown by nettles, brambles, and scrub that they are

impossible to walk on, and have gone unexplored for decades. Their changing direction and position on slopes make them difficult to visualize on lidar data. A combination of several techniques is necessary to do this properly (Figure 32).

Table 18: Lidar scanning parameters of Žiški vrh and Volčji Potok, Slovenia.

	parameter value
scanner type	Riegl LMS-Q780
platform	helicopter
date	July 2014 to March 2015
average last and only returns per m ² on a combined dataset	3.0
spatial resolution of the final elevation model [m]	0.5



Figure 31: Parallel hollow ways in a forest NW of Volčji Potok, Slovenia. Photo by Žiga Kokalj.

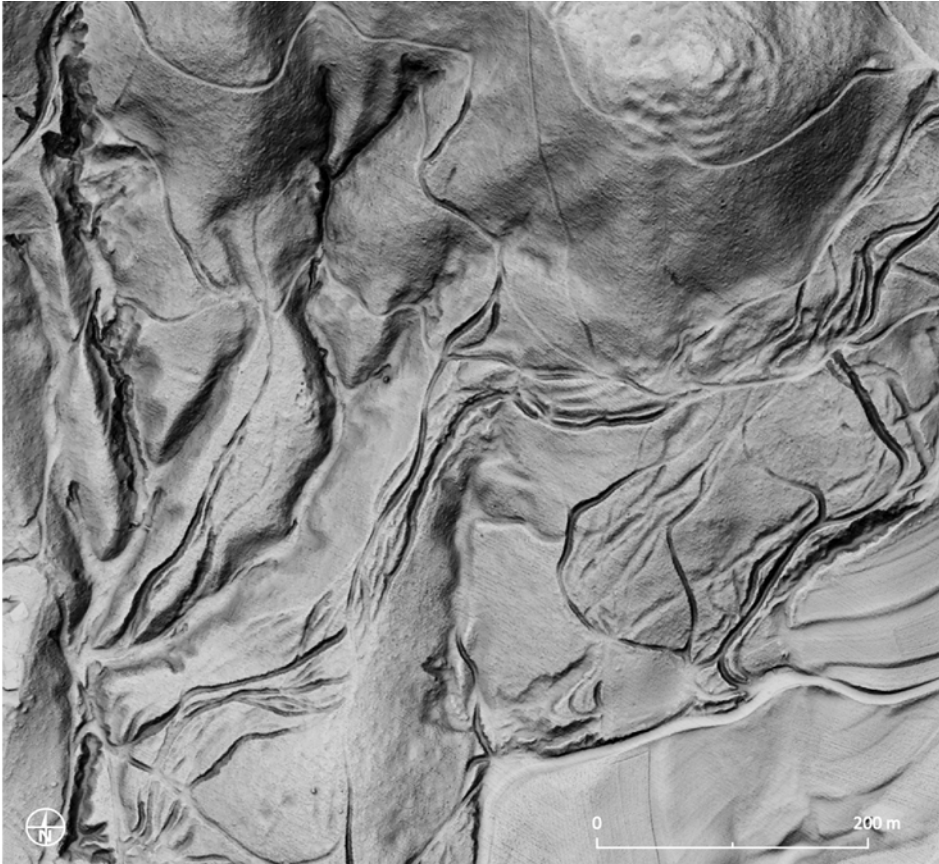


Figure 32: Hollow ways and headstreams below a hillfort on Žiški vrh, northern Slovenia, as evident on a combination of sky-view factor (0.65-1.0, 25 % opacity, multiply), positive openness (70-93, 50 % opacity, overlay), slope (0-45°, 50 % opacity, luminosity) and hillshading. 0.5 m spatial resolution lidar data © ARSO, Slovenia.



Figure 33: Hollow ways developed on a narrow passageway along the river Volčji Potok, northern Slovenia. 0.5 m spatial resolution lidar data © ARSO, Slovenia.

5|3 Prehistoric and Roman settlement above Knežak, Slovenia

Gradišče nad Knežakom hillfort from the Iron and Roman Age was once a central settlement in the Pivka area, Slovenia. It sits on the top of a ridge and is today totally covered by impenetrable forest. Its shape is oval-triangular, demarcated by well-preserved ramparts on the western, southern, and eastern side, and steep slopes on its northern edge. On the north-western boundary the settlement is fortified by a tower. The plateau is slowly reducing in height towards the south in low terraces. Small depressions on them are most probably traces of partially-buried structures (Laharnar 2012: 66–67).

Absence of Roman military finds and traces of military engagement from the Late Republican period, and the continuous occupation of old settlements

indicate loyalty of these communities to the Roman state (Laharnar 2012: 243–244).

Countries, states, and regions increasingly offer their lidar datasets for free and open use. There is thus a growing opportunity for development of products and services based on high-resolution elevation models. However, data users still need at least the basic knowledge about how these data were acquired, processed, and can be developed or improved according to their requirements. The Slovenian national lidar dataset is of a generally high quality,

but much of the data point cloud contains double entries and negative outlier points that are classified as ground (erroneous points lying below true ground). The data was also processed with a specific requirement to classify buildings. Experts interested in true representation of the ground and small-scale features specifically, can gain much by even just reprocessing the data with different software (see Figures 35 and 36).

Table 19: Lidar scanning parameters of Gradišče nad Knežakom, Slovenia.

	parameter value
scanner type	Riegl LMS-Q780
platform	helicopter
date	between February 11 th and November 21 st 2014, exact date unknown
average last and only returns per m ² on a combined dataset	4.2
spatial resolution of the final elevation model [m]	0.5



Figure 34: Gradišče nad Knežakom hillfort in the centre of the image is today totally covered by impenetrable forest. Photo by Boštjan Laharnar.

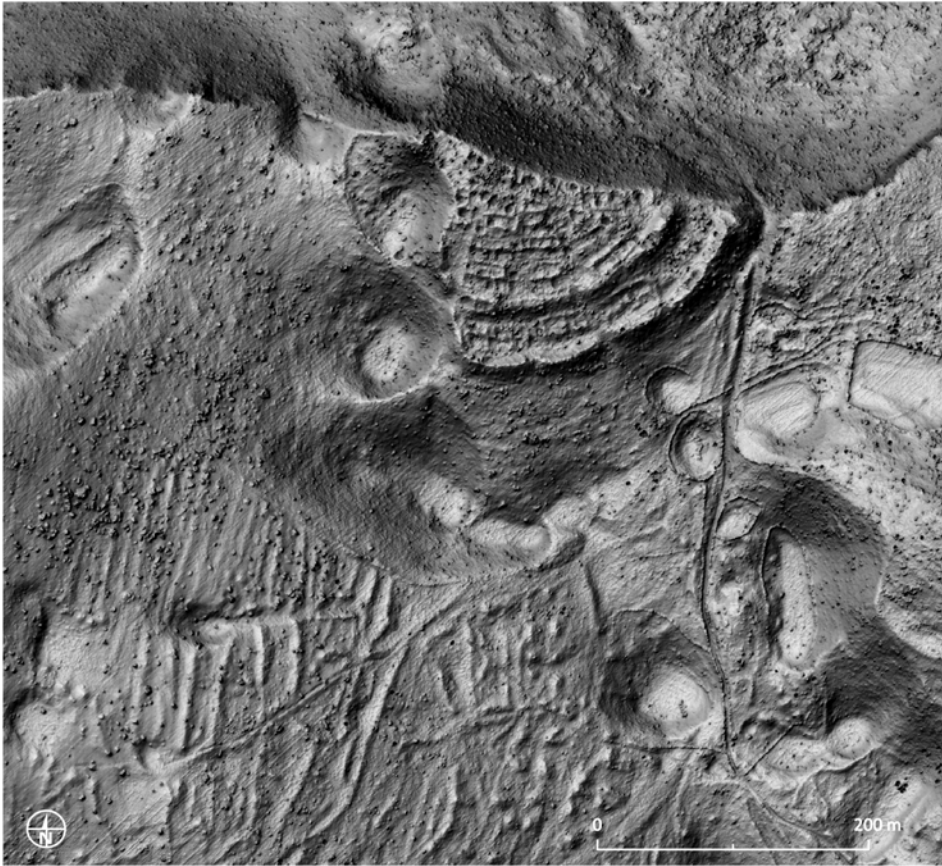


Figure 35: Iron Age settlement above Knežak and its surroundings as evident on the classified Slovenian national lidar data (GKOT, © ARSO, Slovenia) which has been processed by gLidar software, rasterized to a 0.5 m grid. Many small bumps and non-existent holes are visible (see also Figure 18C). The image is a combination of sky-view factor (0.7-1.0, 70 % opacity, multiply), slope (0-55°, 100 % opacity, overlay) and hillshading.



Figure 36: The same as in Figure 35, but processed with different software (LASTools). Even with minimal effort (default settings), the resulting image gives a clearer picture of the archaeological and natural topography, despite losing some of the 'sharpness'. Clearance cairns and field boundaries can be seen on the lower part of the image. 0.5 m spatial resolution lidar data © ARSO, Slovenia.

5|4 Barrow cemetery in Pivola, Slovenia

The burial site at Pivola, on the Drava plain at the foothills of the Pohorje Mountains in Slovenia, contains dozens of mounds. It is part of a large area where dwellers of the fortified hillfort at Poštela were buried in the Early Iron Age (8th to 6th century BC). As a consequence of ideological and religious changes, burial in mounds became a new practice at the beginning of the Early Iron Age, with warriors becoming the most prominent social stratum (Gulič and Črešnar 2012). In their study based on lidar data Mlekuž and Črešnar (2014) have investigated the prominence and deliberateness of positioning different groups of burial mounds around Poštela hillfort into the landscape.

“The Pivola group is situated in a compact visual envelope of the valley, in a shallow depression delimited by natural low ridges to the north and south. The barrows

are positioned deliberately, so as to change the visual structure of the landscape, to dominate the foreground or short distance view, being immediate, close and engaging to all senses. When inside this group, a viewer would find himself in a well-bounded visual envelope and dominated by an immediate presence of barrows (Figure 40). They are less striking in the middle distance, but still represent an important compositional element of the landscape” (Mlekuž and Črešnar 2014: 205).

Based on this study they have found that the landscape around Poštela had a critical role as a medium, because it became a cultural landscape, a polygon for expressing ideas and messages. Respecting, relating to, or changing the existing spatial order was a powerful message, which reproduced or subverted the existing social identities and power relations (Mlekuž and Črešnar 2014: 209).

Table 20: Lidar scanning parameters of Pivola burial mounds, Slovenia.

	parameter value
scanner type	Riegl LMS-Q780
platform	helicopter
date	between 12 th March and 20 th October 2014, exact date unknown
average last and only returns per m ² on a combined dataset	4.7
spatial resolution of the final elevation model [m]	0.5



Figure 37: One of the burial mounds at Pivola. Except in late winter, dense brambles make it very difficult to move around. Photo by Žiga Kokalj.

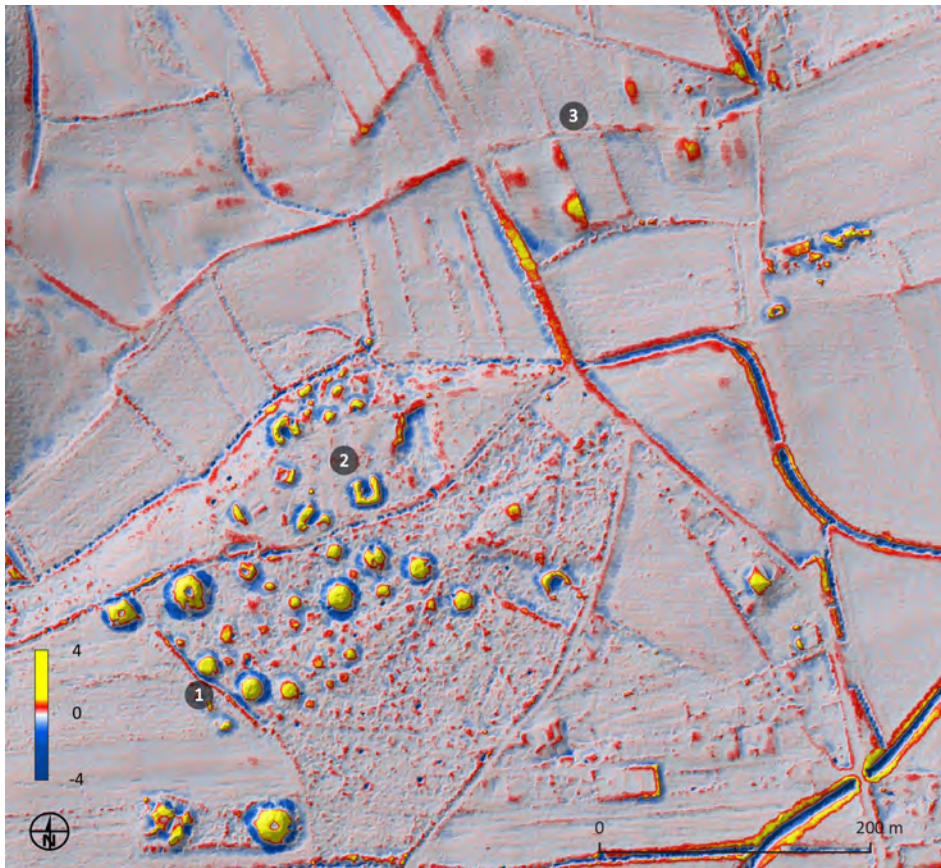


Figure 38: Burial mounds at Pivola as displayed by a Local Relief Model transparently overlaid on a sky-view factor image and shaded relief. The state of preservation of the mounds differs significantly. The ones in the forest are well preserved (1), mounds in the Botanical Garden were damaged when the location served as a military base (2), and the mounds in the fields have been nearly completely levelled (3). 0.5 m spatial resolution lidar data © ARSO, Slovenia.



Figure 39: Visual structure of landscape as represented by Higuchi's foreground range total viewshed around Pivola barrow group. 1 m spatial resolution lidar data © ARSO, Slovenia. Reproduced with permission by D. Mlekuž.

5|5 WWII anti-glider defences at Culbin, Scotland

Peter Crow and Matt Ritchie; Forest Research and Forestry Commission Scotland

The tidal lagoon at Culbin, on the coast of the Moray Firth in Scotland (NH 969 625), is dotted with regular lines of poles that were built in 1940 in order to deter enemy gliders from landing. The poles were erected by digging a hole, inserting an old herring barrel, dropping in the pole and securing it using stones and sand. Hundreds of poles remain standing within a tidal lagoon, protected by sand dunes and forest. However, many have been reduced to little more than stumps. In an attempt to record those remaining before they are lost to the elements, a lidar survey of the coastal area was commissioned by Forestry Commission Scotland, with survey parameters specifically designed to ensure that each upstanding post would be recorded.

The general surviving layout of the anti-glider defences can now be appreciated – particularly the ranked lines intended to dissuade gliders from landing along the beach. The points depicting the location of the posts have not been checked on the ground – they represent features detected by lidar standing 0.2 m or higher within a flat tidal environment. The data was manipulated by cropping the lidar models to remove the surrounding forest before subtracting the digital terrain model (DTM) from the digital surface model (DSM) to produce a normalized digital surface

model (nDSM), which represents heights of features relative to the ground. Features with a height range between 0.2 m to 4 m were selected, selecting (by hand) those features likely to be posts (*i.e.* discrete points away from obvious patches of tall vegetation). Posts shorter than 0.2 m were not plotted as it was difficult to distinguish them from any vegetation present (Forestry Commission Scotland 2012: 34–36). Sky-view factor is particularly useful for visualizing the posts and other ‘pointed’ features because they appear as distinct black stars on an image.

Table 21: Lidar scanning parameters of anti-glider defences at Culbin, Scotland.

	parameter value
scanner type	Optec ALTM 3033
platform	fixed wing
date	7 th October 2009, low tide
average last and only returns per m ² on a combined dataset	4, with a 0.9 m footprint
spatial resolution of the final elevation model [m]	0.5 m

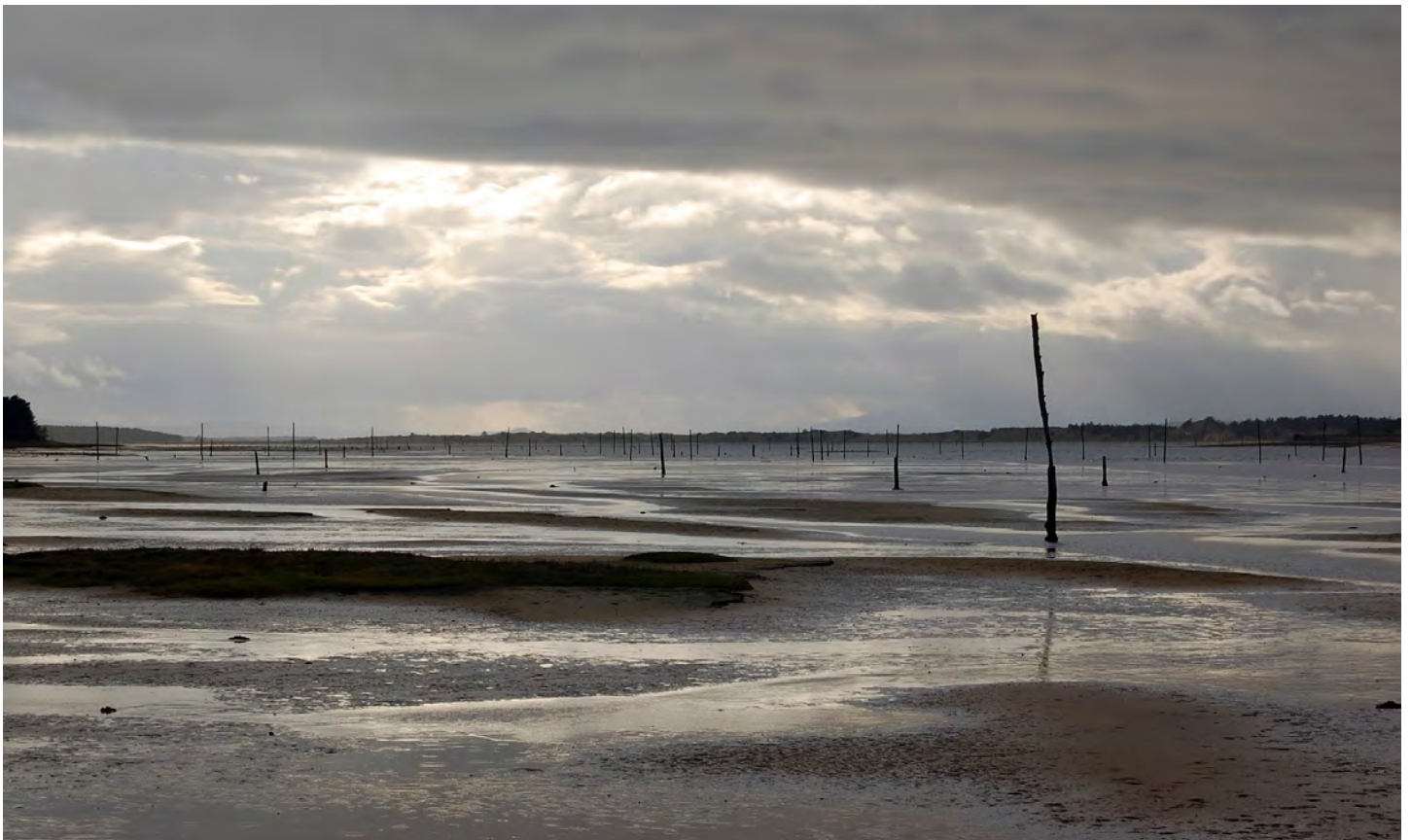


Figure 40: Lines of poles at Culbin Sands. Photo © Forestry Commission Scotland.

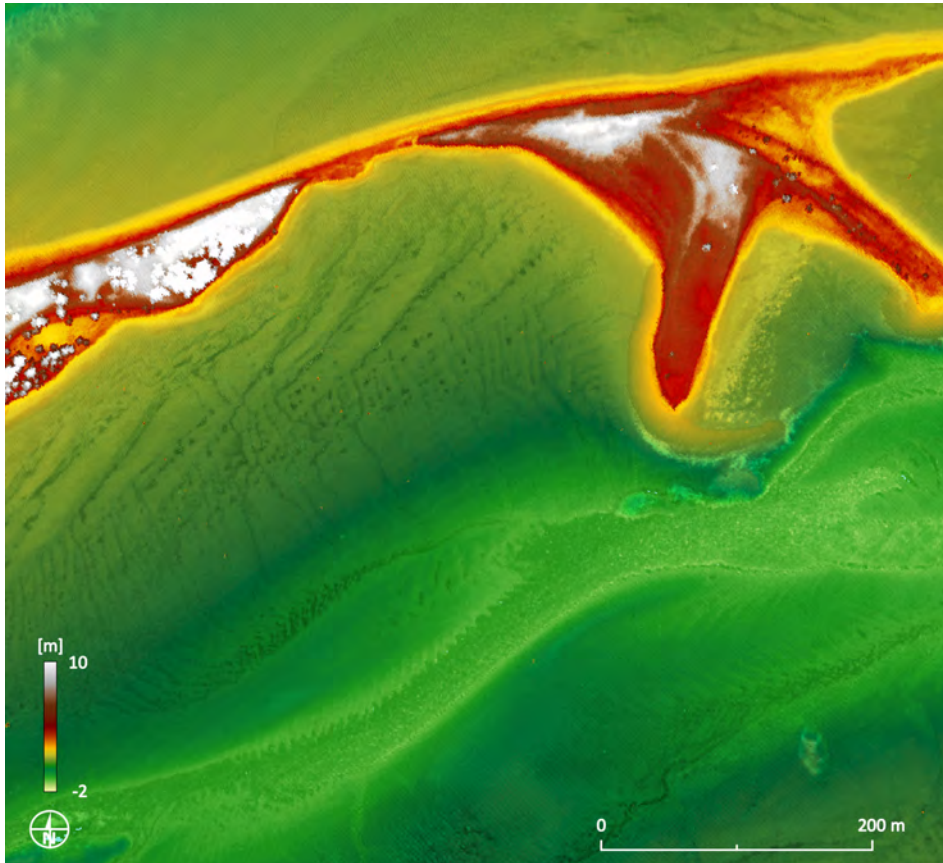


Figure 41: Changes in elevation with added intensity information, Culbin Sands. Lidar intensity is usually recorded at the time of scanning and can provide additional discriminating information about the landscape. However, poles are too narrow to be readily recognised on the elevation image. 0.5 m spatial resolution lidar data © Forestry Commission Scotland.

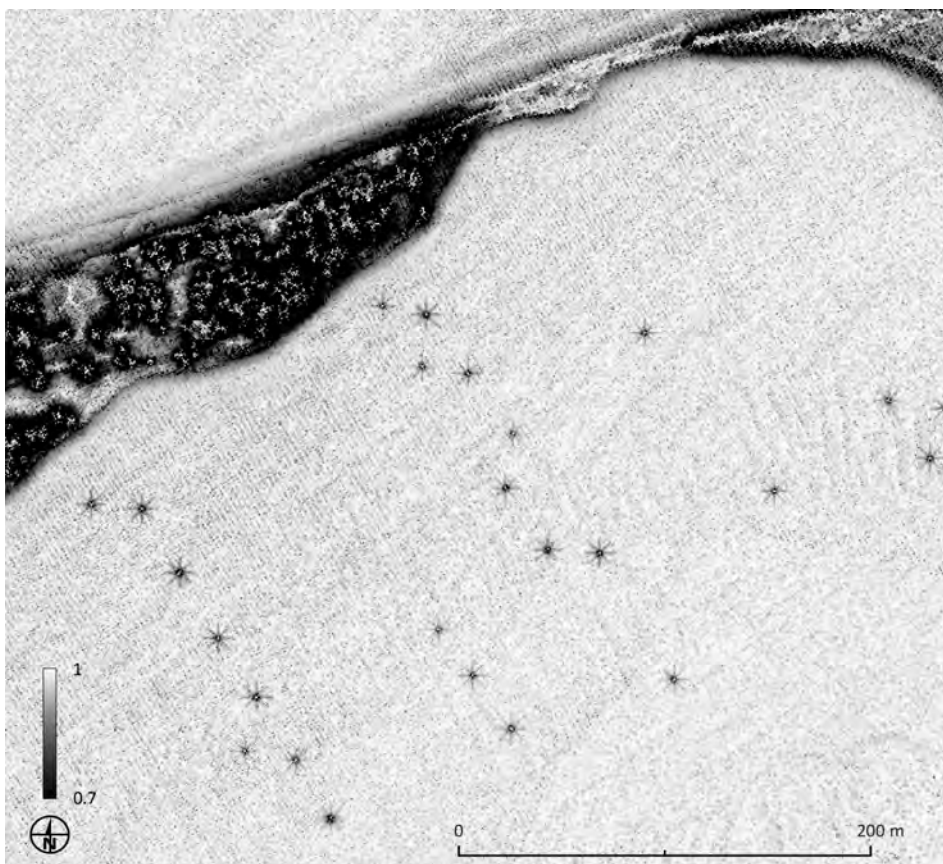


Figure 42: A close-up view of Culbin Sands as seen on a sky-view factor image calculated in 8 directions. Poles are easily identifiable as black stars. 0.5 m spatial resolution lidar data © Forestry Commission Scotland.

5|6 Geological features in the Julian Alps, Slovenia

The Julian Alps are the biggest and highest Alpine mountain chain in Slovenia, rising to 2864 m at Mount Triglav. They are mostly built by 200-million-year-old layers of limestone and dolomite that are up to 2 km deep. The landscape is characterized by an extraordinary diversity of geomorphology, especially glacial, fluvial, and karstic forms of outstanding beauty that preserves a cultural backdrop. Endemic, rare, and threatened plant and animal species are protected in the Triglav national park that covers most of the area.

Lidar has become an indispensable tool in geomorphological and geological studies that traditionally rely heavily on visual interpretation of the landscape. One example of geomorphological beauty is Velika vrata (*big door*) area (Figure 44), a high mountain pass between the Trenta

Valley and the Triglav Lakes Valley. The area is important especially because of its numerous corrosion and glacial erosion forms at various developmental stages. High-mountain dipping limestone pavements (*podji*) are areas of wrinkled, glacially transformed karstic plateaus with a rocky surface, usually above the tree line. They are full of other intricate surface structures, such as clints, grikes, and karren tables, but also subterranean features like vertical caves. Karren tables stand out among the glacial karstic shapes in Velika vrata because the area is their *locus typicus* in Slovenia.

The ridge between mountains Planja (1964 m) and Bavški Grintavec (2333 m) testifies to the powerful tectonic processes in the Cenozoic that have shifted the limestone strata almost vertically. They now lie almost 2 km above the valley floor and the underlying rock is still not exposed (Planina 1954: 192). The location between Vrh Brda and Vrh Rut is known as Ribežni ('slicers') (Figure 43) because of the exposed strata, which are beautifully shown on an appropriate lidar visualization (Figure 45).

Table 22: Lidar scanning parameters of Velika vrata and Vrh Brda, Slovenia.

	Velika vrata	Vrh Brda
scanner type	Riegl LMS-Q780	Riegl LMS-Q780
platform	helicopter	helicopter
date	July 2014 to January 2015	July 2014 to January 2015
average last and only returns per m ² on a combined dataset	4.7	5.0
spatial resolution of the final elevation model [m]	0.5	1.0



Figure 43: A view across the ridge towards Vrh Brda and Bavški Grintavec in the background. Photo by Jovan Cukut.

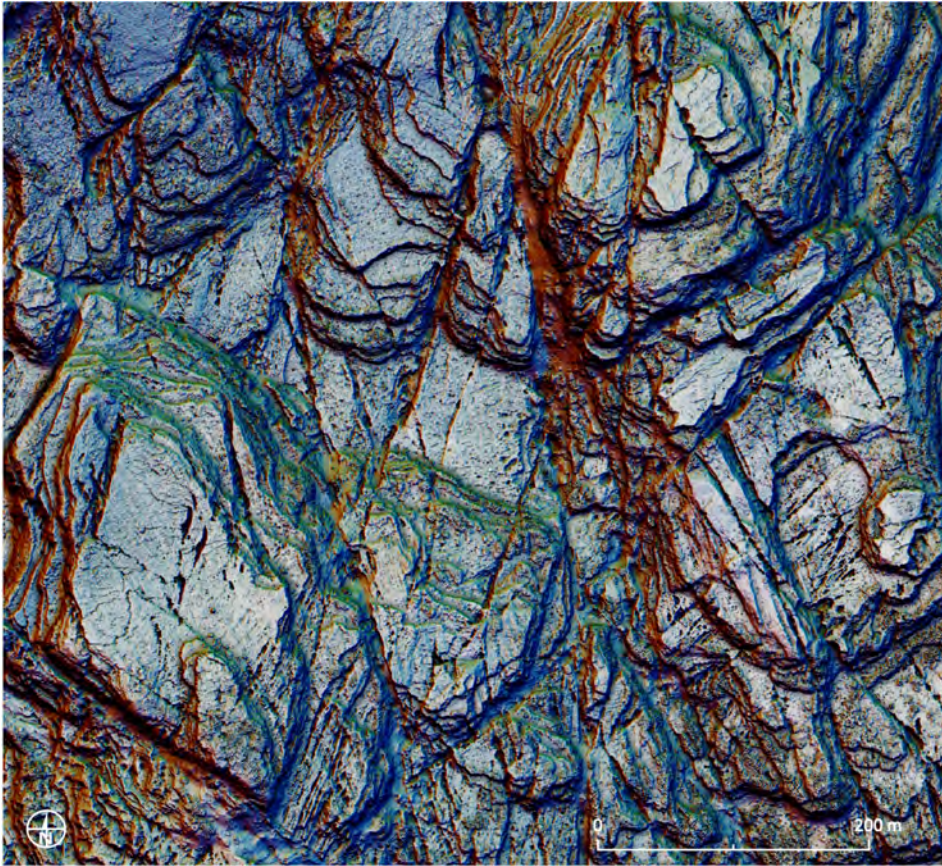


Figure 44: Glacially transformed karstic plateau at Velika vrata, Slovenia. Flat areas of clints are presented in light colours while grikes, crevices, and steep slopes are dark. The image is a combination of sky-view factor (0.5-1.0, 70 % opacity, multiply), slope (0-65°, 80 % opacity, overlay) and RGB image of hillshading from three directions (R: 315°, G: 15°, B: 75°), all computed on a digital surface model. 0.5 m spatial resolution lidar data © ARSO, Slovenia.

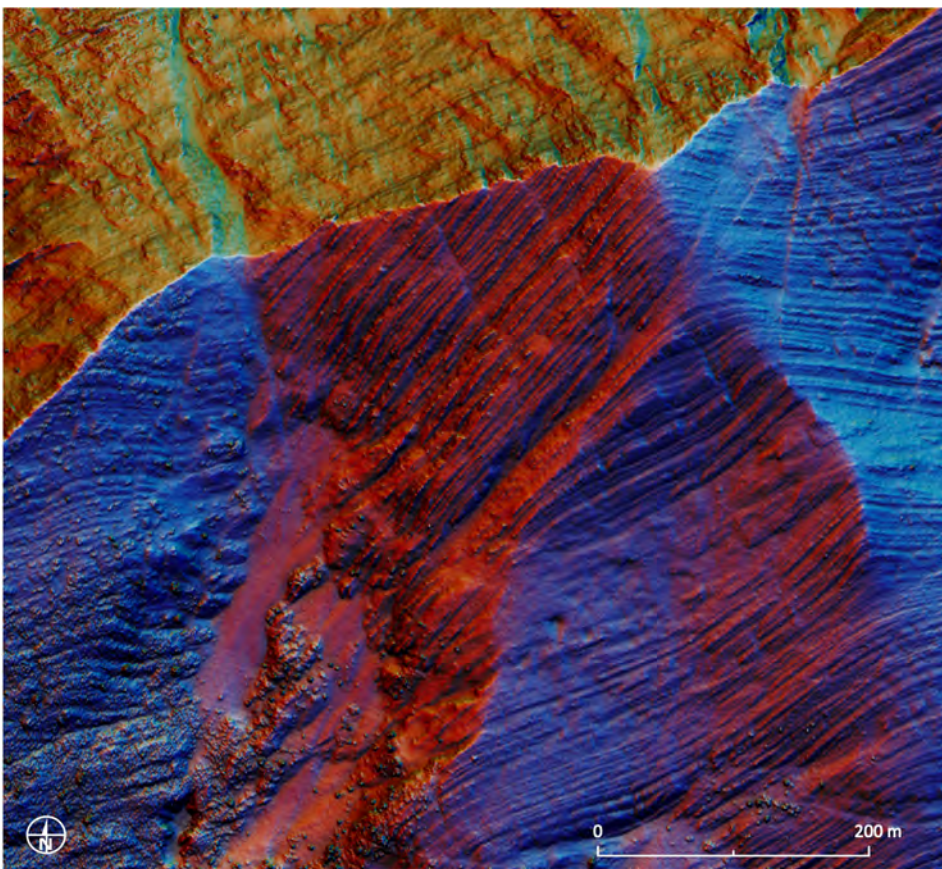


Figure 45: Dachstein limestone strata and scree fields exposed at Vrh Brda (1952 m). The top of the ridge is highlighted in white, while white colours represent different orientation of the slopes. The visualization is a combination of sky-view factor (0.55-1.0, 30 % opacity, multiply), positive openness (65-95, 50 % opacity, overlay), slope (0-65°, 80 % opacity, luminosity) and RGB image of hillshading from three directions (R: 315°, G: 15°, B: 75°). 1 m lidar data © ARSO, Slovenia.

5|7 The Granite Dells, Arizona, USA

The Granite Dells is a geological feature north of Prescott, Arizona, USA. The Dells consist of exposed bedrock and large granite boulders that have eroded into rounded bumpy and unusual shapes giving the rocks a rippled appearance (Figure 46). Dells' granite formed 1.4 billion years ago at a depth of 2-3 km and has since been eroded away. Weathering along joints produced rounded shapes and other unusual rock formations that characterize the Granite Dells. The process is known as spheroidal weathering and is common in granitic terrains. Also characteristic of the area are precariously balanced rocks (PBRs) that are present in a range of sizes, masses, geometric configurations, and precariousness. Haddad and Arrowsmith (2011: 145) have found that the emergence of precariously balanced rocks is affected by changes in the rates of soil production and transport; high soil transport rates

speed up the geomorphic lifecycle of precariously balanced rocks while high soil production rates completely decompose the rocks in the subsurface. This is linked to the density of joints; high joint densities create small boulders that completely decompose prior to exposure while low joint densities create relatively large and stable boulders.

Table 23: Lidar scanning parameters of Granite Dells, Arizona, USA².

	parameter value
scanner type	Optech Gemini
platform	fixed wing
date	November 9 th 2009
average last and only returns per m ² on a combined dataset	6.7
spatial resolution of the final elevation model [m]	0.5

² Lidar data acquired by the NCALM at the University of Houston and the University of California, Berkeley, on behalf of David E. Haddad (Arizona State University) as part of an NCALM graduate student Seed Grant: Geologic and Geomorphic Characterization of Precariously Balanced Rocks. NCALM is funded by the National Science Foundation's Division for Earth Sciences, Instrumentation, and Facilities Program.



Figure 46: Granite Dells at Watson Lake. Photo by Michael Wilson.

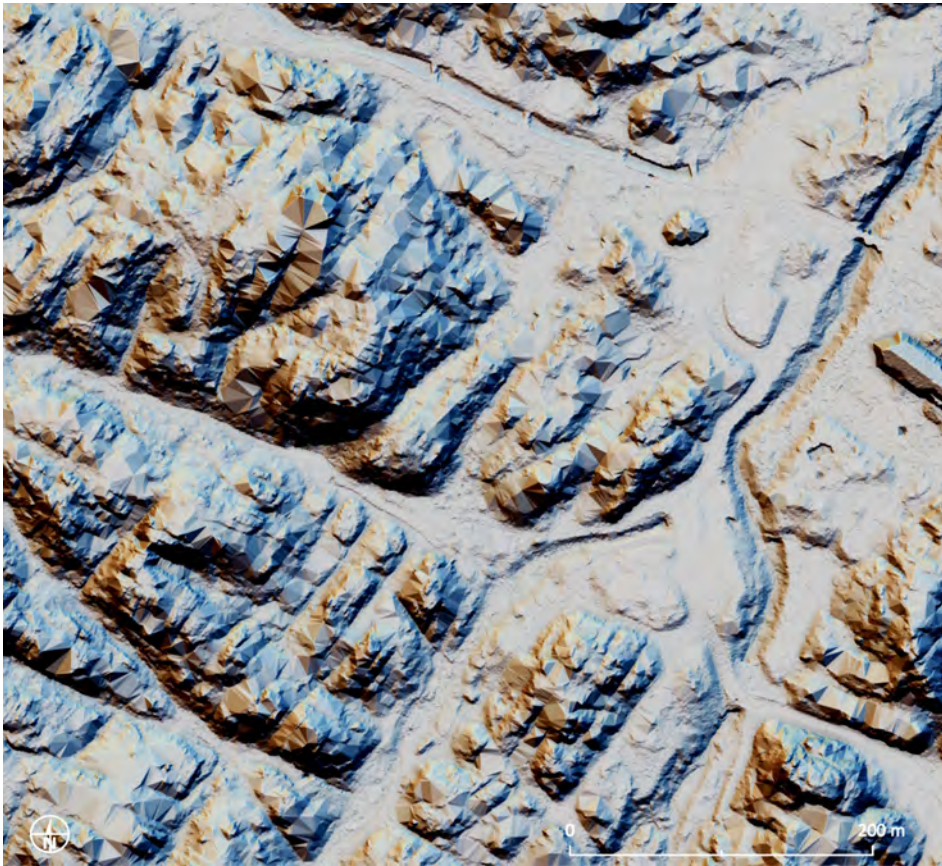


Figure 47: Digital terrain model (DTM) of Granite Dells, Arizona, USA. Much of the detail in the landscape is lost despite dedicated processing. A combination of anisotropic sky-view factor (0.2-1.0, 40 % opacity, multiply), slope [0-80°, 60 % opacity, overlay] and RGB image of hillshading from three directions (R: 337.5°, G: 0°, B: 22.5°). 0.5 m spatial resolution lidar data © NCALM, USA.

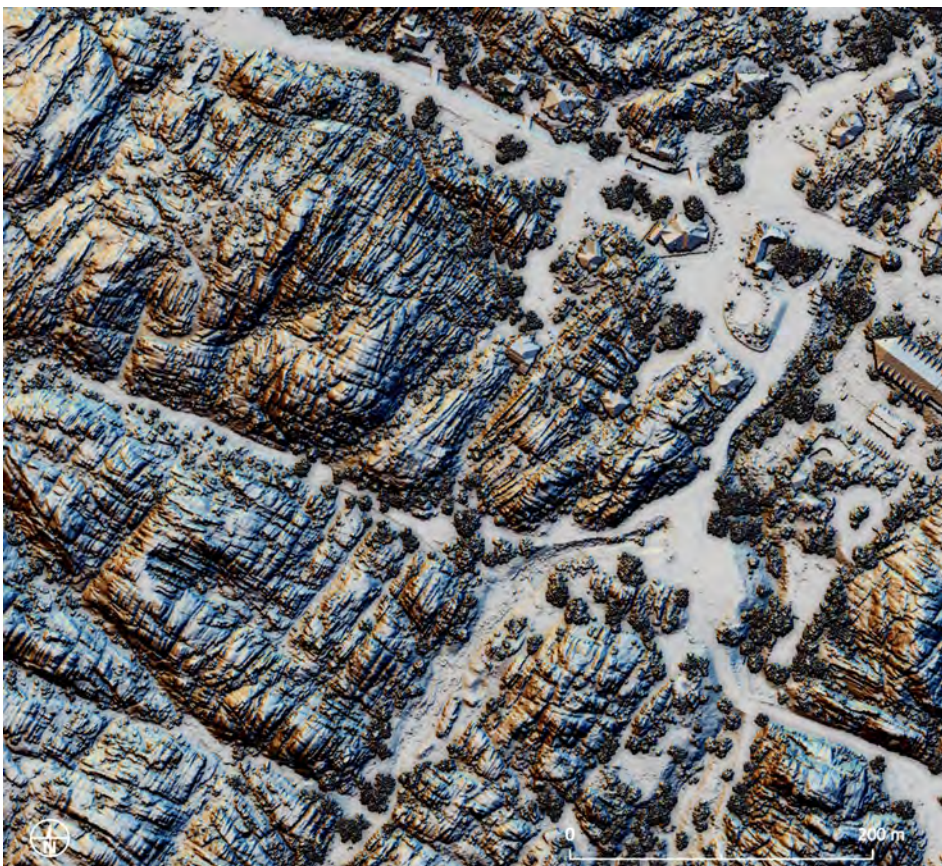


Figure 48: Digital surface model (DSM) of the same area as in Figure 47. Choosing a DSM over a DTM is wise in open landscapes without extensive tree and bush cover, because we can produce a raster image considering a higher number of lidar points, thus getting a 'sharper' result. In case of this figure the DSM makes visible trees, houses, and cars, but more importantly also the joints in granite that are characteristic of the Dells. 0.5 m spatial resolution lidar data © NCALM, USA.

5|8 Cinder cones and lava flows on Mauna Loa, Hawaii, USA

The world's largest volcano, Mauna Loa on Hawai'i Big Island, has come to epitomize shield-stage volcanism. Its volume is in the range 65,000-80,000 km³ of lava flows, vent deposits, and intrusions that extend from the ocean floor to the 4169 m high summit (Sherrod *et al.* 2007). Lava eruptions from Mauna Loa are silica-poor, and very fluid; eruptions tend to be non-explosive and the volcano has relatively shallow slopes. Its most recent eruption was in 1984.

Cashman *et al.* (2013) report that lidar data are revolutionizing both the visual and quantitative analysis of lava flows. Visualizations allow accurate mapping of flow boundaries, particularly in vegetated areas and areas that are difficult to access due to temperature (active flows)

or rough and jagged surfaces (older flows). Detailed relief models permit mapping and morphometric analysis of flow components, such as channels, surface folds, cracks, blocks, and surface roughness, as well as along-flow variations in flow type. Differencing of pre-eruptive and post-eruptive DEMs allows analysis of flow thickness variations, which can be related to the dynamics of lava emplacement. Dieterich *et al.* (2015) have studied lidar data of the Hawai'i and

have found that the spatial and volumetric distributions of lava reflect the effusion rate and interactions with topography. The main channel serves to transport, rather than store, lava and the pre-existing topography exerts a primary control on the (3D) spatial distribution of individual lava flows.

Table 24: Lidar scanning parameters of Mauna Loa, Hawaii, USA³.

	parameter value
scanner type	Optech Gemini
platform	fixed wing
date	June 21 st – 27 th 2009
average last and only returns per m ² on a combined dataset	6.0
spatial resolution of the final elevation model [m]	0.5

³ Lidar data acquisition and processing completed by the National Center for Airborne Laser Mapping (NCALM). NCALM funding is provided by NSF's Division of Earth Sciences, Instrumentation and Facilities Program (EAR-1043051). Grant NSF EAR-0739153 and a NASA subcontract to the Jet Propulsion Laboratory (Award #1290138) also supported this data collection.



Figure 49: View of Mauna Loa from Mauna Kea with cinder cones in the foreground. Photo by Lawrence Goldman.



Figure 50: Lava flows on the Mauna Loa shield volcano are difficult to observe from the ground because they are either hot, have rough and jagged surfaces, or are covered by vegetation. Many vents and cinder cones are visible on this hill-shaded image of 1 m spatial resolution lidar data © NCALM.



Figure 51: This visualization provides a very plastic representation of the surface and reveals an intricate system of cinder cones, vents, cracks, folds, and channels of a lava field on the north-eastern slope of Mauna Loa. The visualization is a combination of positive openness (65-95, 50 % opacity, darken), sky-view factor (0.65-1.0, 50 % opacity, multiply), slope (0-50°, 100 % opacity, overlay) and hillshading. 0.5 m spatial resolution lidar data © NCALM.

5|9 Blind valley Odolina, Slovenia

Odolina at the foothills of Brkini hills is Slovenia's most characteristic blind valley. It is a special valley with corrosion widened bottom, a typical contact karst morphological form shaped by a surface river when it reaches the karst. Brsnica sinking stream drains a 4.3 km² large water basin and forms a normal fluvial landscape on the flysch Brkini hills (Figure 53). When it reaches limestone on Matarsko podolje, it developed Odolina, about a kilometre long and up to 300 m wide valley, with sharply outlined, high, and rocky slopes, ending in an amphitheatre. It was named after a small hamlet with a castle located at its northern part. Close to the contact of flysch and limestone the valley is 150 m deep, and on the southern end it is carved some 60 m deep into the karst plain. The valley

bottom is covered by the sediments, gravel and sands, cut by some younger, up to 25 m deep alluvial ponors and sinkholes, and the riverbed of the brook. During the normal water levels the brook sinks in the riverbed immediately after reaching the limestone, while during higher water levels it flows a kilometre further into a 117 m deep ponor cave composed of potholes and shorter channels (Figure 54) (Mihevc 1994: 102–103).

Table 25: Lidar scanning parameters of Odolina blind valley, Slovenia.

	parameter value
scanner type	Riegl LMS-Q780
platform	helicopter
date	February 2014, exact date unknown
average last and only returns per m ² on a combined dataset	9.8
spatial resolution of the final elevation model [m]	1.0



Figure 52: Blind valley Brezovica. A view to the north. Ločica stream that formed the valley sinks underground in the foreground of the photograph. Photo by Žiga Kokalj.

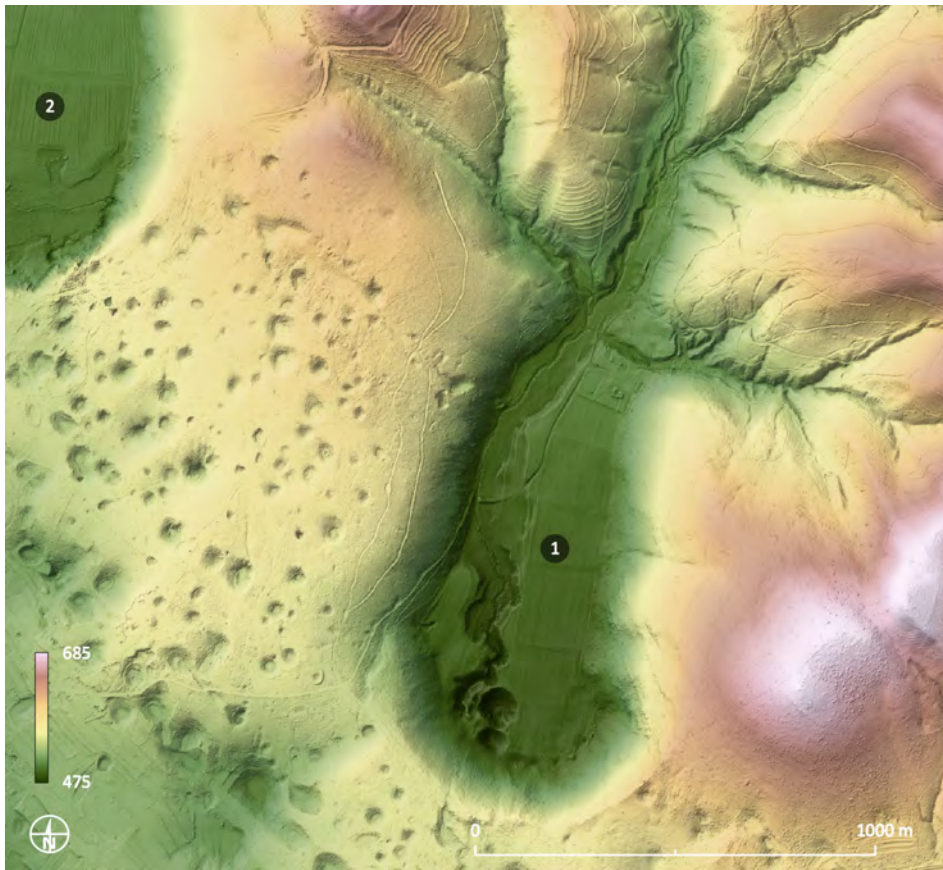


Figure 53: Odolina (1) and Brezovica (2) blind valleys. Contact borderline between flysch and limestone runs NW to SE and is very clearly recognizable. The brooks form a normal fluvial relief on flysch and form corrosion widened valleys on limestone before disappearing underground. Dolines, sinkholes, and other typical karst forms are also easy to identify. 1 m spatial resolution lidar data © ARSO, Slovenia.



Figure 54: A close-up view of the end of blind valley Odolina. On such a location and without prior knowledge about the area someone would expect a stream source. The abyss where Brsnica disappears underground at high water, carrying with it tons of sediment and wood, is marked with an arrow. 1 m spatial resolution lidar data © ARSO, Slovenia.

5|10 Lake floor morphology, Lake Constance, Germany, Switzerland, and Austria

Due to increasing erosion and conservation concerns, a large number of lakeshore settlements dating from the Neolithic to the Bronze Age are subject of archaeological research. Many of these settlements at Lake Constance are now inscribed in the multinational UNESCO World Heritage Site called 'prehistoric pile dwellings around the Alps.'

In the years 2013 and 2014, the topography of the lake floor was surveyed using bathymetric lidar for the shallow near-shore areas and sidescan sonar for the deeper portions of the lake. The resulting digital model, with a resolution of 3 m, is freely available under the

Creative Commons Attribution 3.0 Unported license (IGKB - Internationale Gewässerschutzkommission für den Bodensee 2015) and documents the morphology of the lake bottom in unprecedented detail. While bathymetric models are commonly presented as depth contours and/or by colour coding, the high-resolution data now available allow the application of enhanced visualization techniques. This opens new perspectives for the analysis of the sub-aqueous geomorphology regarding *e.g.* wave erosion or mass movements.

An unexpected detail that now becomes visible are numerous iceberg scour marks (Sacchetti *et al.* 2012) which are most prominently seen on an up to 1.5 km wide and, almost horizontal (approx. 1° slope) bench in the southern half of the lake. This bench lies at a depth of 110 to 130 m below present-day lake surface. Because of geological limitations at the lake outflow, lake water level during the Late Glacial may have been somewhat higher but

cannot have been more than a few metres lower than today. This implies that large icebergs with a thickness of more than 110 m were calving from the retreating Rhine Glacier while it still occupied the eastern portion of today's lake basin.



Figure 55: With a surface area of approximately 570 km² and a maximum depth of 252 m, Lake Constance is one of the largest and deepest lakes in Europe. It was formed by glacial erosion during the last Ice Ages. Large drumlin fields, mainly north of the lake, document the direction of ice flow during the last glaciation. When the glaciers retreated, the basin filled with water and became Lake Constance. Photo by Frank Numrich.

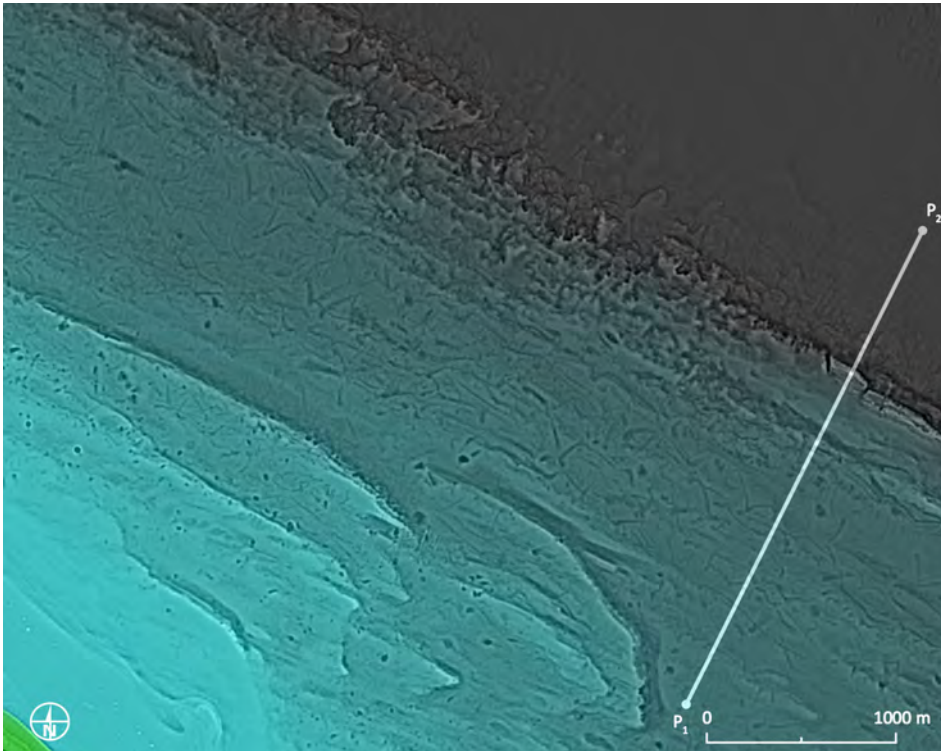


Figure 56: Iceberg scour marks (curvilinear features) and mass movement deposits (lobate features at the foot of the steep slope) in Lake Constance. Visualisation: Laplacian-of-Gaussian overlaid by colour-coded bathymetry. 3 m spatial resolution bathymetric model © IGKB (2015).

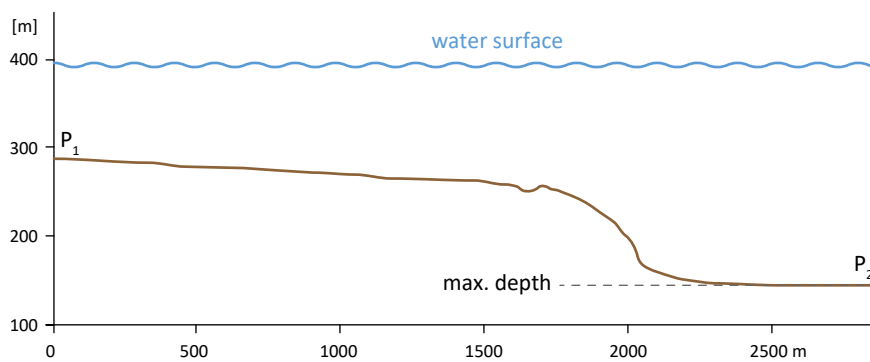


Figure 57: Bathymetric profile (P₁-P₂) from data shown in figure 56 reveals the flat subaqueous bench on which most iceberg scour marks occur. 3 m spatial resolution bathymetric model © IGKB (2015).

5|11 High-rise buildings in New York, USA

New York City is made up of five boroughs sitting where the Hudson River meets the Atlantic Ocean: The Bronx, Brooklyn, Manhattan, Queens, and Staten Island. When people think of New York City, Manhattan – the island in its core –, is often the first place they picture. A densely populated borough is among the world's major commercial, financial, and cultural centres. It is home to big-name attractions, world-class museums, restaurants, and concert halls. Amid its iconic sites are many of the skyscrapers, such as the Empire State Building, the Chrysler Building, the Woolworth Building, Rockefeller Center, and One World Trade Center.

Urban planners use lidar data for inquiry about resources and environment, and for integrating new developments on vacant land with the existing fabric of people, structures, and infrastructure. The magnificent height of the buildings is usually lost in 2D representations and maps because it is difficult to reproduce with analytical hillshading and colour coding (Figure 59). As an alternative, we used an artistic approach of conveying depth with a cast shadow (Figure 60). An overcast sky illumination model nicely renders outlines of buildings and provides a beautiful background image. The less locally obstructed a part of the scene

is – *i.e.* the fewer nearby objects cast a shadow over it, the brighter it is displayed. An added cast shadow from the southeast direction simulates shadows cast by a morning Sun in the northern hemisphere. The elevation angle of the imaginary Sun has to be fine-tuned to the height and density of structures as well as the prevailing topography. The overcast sky illumination model with a cast shadow can be combined with hillshading, or some other visualization technique to add detail, and the elevation model to add colour.

Table 26: Lidar scanning parameters of Manhattan, New York, USA.

	parameter value
scanner type	Leica ALS70
platform	fixed wing
date	August 5 th – 15 th 2013
average last and only returns per m ² on a combined dataset	6.6
spatial resolution of the final elevation model [m]	1.0



Figure 58: Brooklyn bridge across the East River with skyscrapers of Lower Manhattan in the background. Photo by Žiga Kokalj.

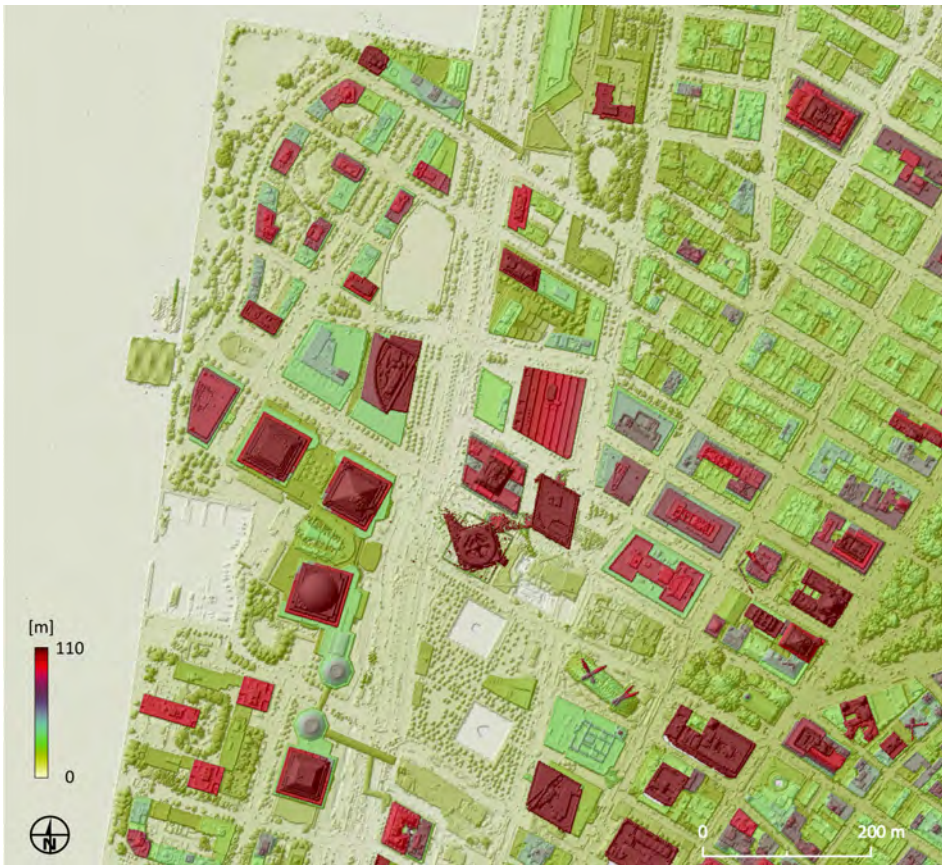


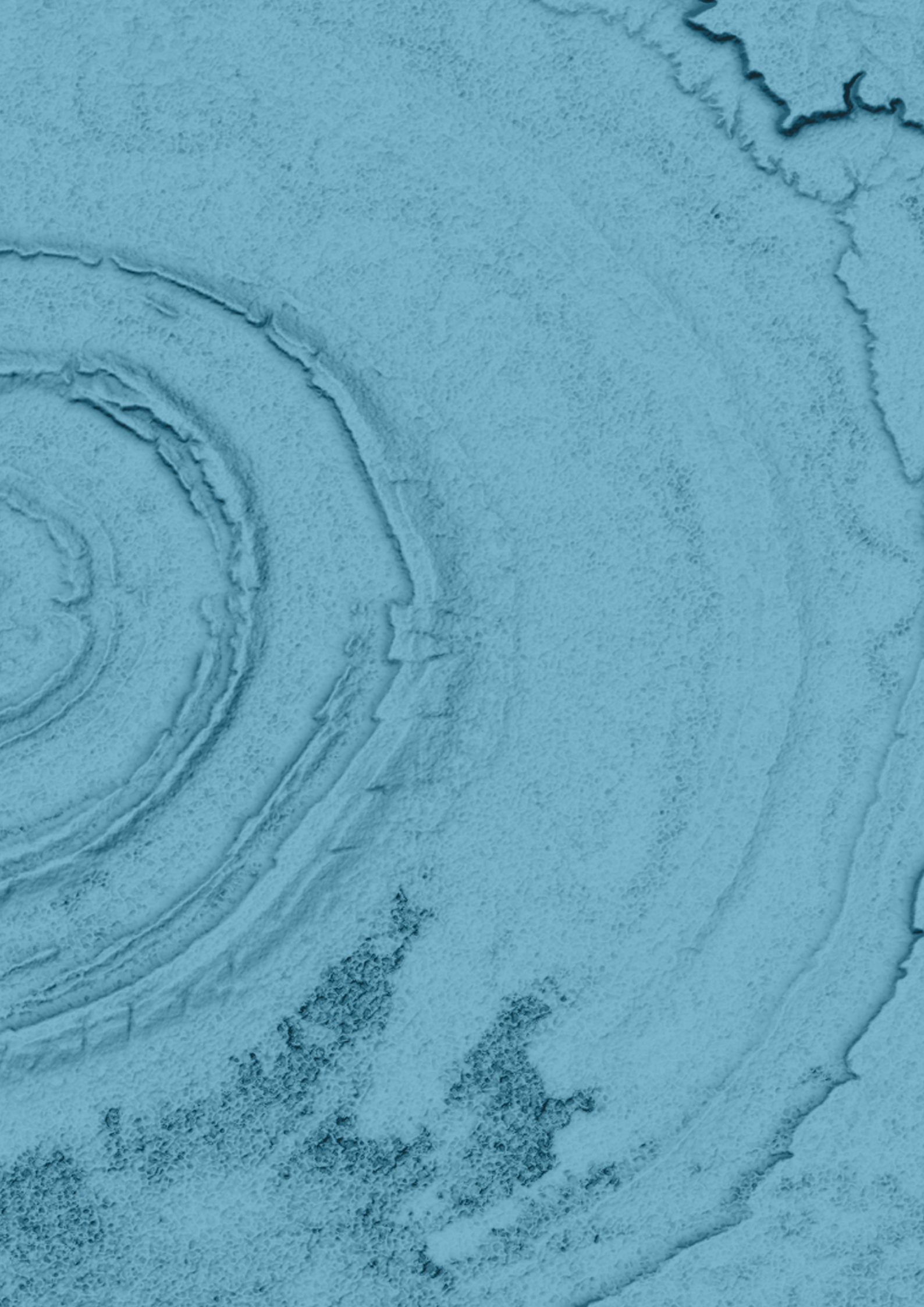
Figure 59: A combination of colour coded elevations and unsaturated shaded relief. This would be a typical two dimensional representation of a city scene. While heights of buildings can be determined to a certain extent, all the values higher than 110 m had been clipped to get a better distribution of colours. Even though the image presents Lower Manhattan with many buildings exceeding 50 m in height, their magnificence is not evident. 1 m spatial resolution lidar data © USGS.



Figure 60: This image is less colourful than Figure 59 but the shadows give a more grandeur feeling of the high-rise buildings. A combination of an overcast Sky Illumination Model (100 m shadow modelling distance) and a cast shadow (35° Sun elevation and 135° azimuth). 1 m spatial resolution lidar data © USGS.

The background of the page is a microscopic image of biological tissue, likely a cross-section of a plant stem or root. It shows various cellular structures, including a large, circular vascular bundle on the right side with distinct concentric layers. On the left side, there is a prominent, dark, branching structure that resembles a vascular cambium or a similar growth zone. A solid white vertical bar is positioned on the left side of the page, partially overlapping the tissue image.

Glossary of terms and abbreviations



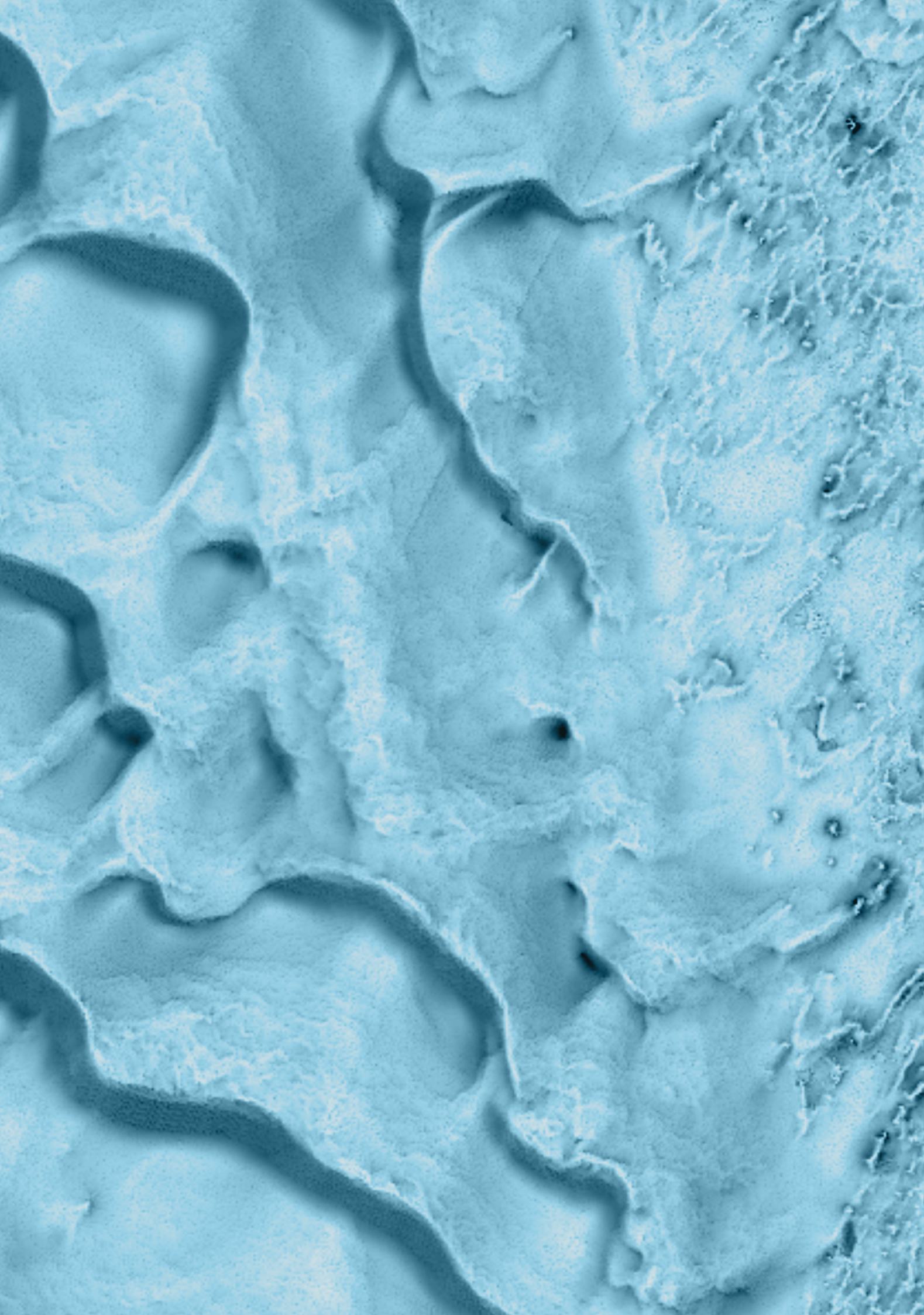
Glossary of terms and abbreviations

ALS	Aerial laser scanning is a surveying technique that uses a lidar scanner on an airborne platform, <i>e.g.</i> a helicopter, a fixed wing aircraft, or an unmanned aerial system.	DTM	A digital terrain model is an ordered set of sampled data points that represent the spatial distribution of various types of information on the terrain (both topographic and non-topographic), <i>e.g.</i> elevation, slope, slope form, rivers, ridge lines, break lines, etc. It usually represents the elevation of 'bare earth', <i>i.e.</i> the shape of terrain without any objects on it.
azimuth	An azimuth is an angular measurement in a spherical coordinate system. The vector from an observer (origin) to a point of interest is projected perpendicularly onto a reference plane; the angle between the projected vector and a reference vector on the reference plane is called the azimuth. The reference plane for an azimuth is typically true north, measured as a 0° azimuth. Moving clockwise on a 360 degree circle, east has azimuth 90°, south 180°, and west 270°.	elevation angle	The angle of the light source above the horizon. The elevation angle (also altitude) is expressed in positive degrees, with 0° at the horizon and 90° directly overhead.
cuneiform tablets	Clay tablets with wedge-shaped marks that represent one of the earliest systems of writing invented by Sumerians.	fovea	A small, central pit in the eye retina responsible for sharp central vision, which is necessary in humans for activities where visual detail is of primary importance.
DEM	A digital elevation model is a subset of a digital terrain model and its most fundamental component. It usually refers to the elevation data organized in the form of a matrix. It usually represents the elevation of 'bare earth'.	GIS	A geographic information system is a system designed to capture, store, manipulate, analyse, manage, and present spatial or geographical data.
DSM	A digital surface model contains elevations of natural terrain features including objects on it, <i>i.e.</i> vegetation and cultural features such as buildings, bridges, and power lines.	histogram	A histogram is a graphical representation of the distribution of numerical data. It therefore presents the frequency of elevations by vertical rectangles, with widths equal to class interval (<i>e.g.</i> one meter) and heights equal to the frequency of elevations in that interval.
		histogram saturation	A method in image processing of contrast adjustment using the image's histogram where the low and/or high values are clipped. No details can therefore be perceived below the lower clipping value (percentage) and above the higher clipping value (percentage), however the rest of the values become more contrasted.

histogram stretch	Histogram stretch is a method in image processing of contrast adjustment using the image's histogram.	RGB	Additive red, green, and blue colour model, where red, green, and blue light are added together in various ways to reproduce a broad array of colours.
LiVT	Lidar Visualisation Toolbox is software for computing visualizations from raster elevation models.	RVT	Relief Visualization Toolbox is software for computing visualizations from raster elevation models.
LoG	Laplacian-of-Gaussian is a filtering approach that combines a Gaussian smoothing filter with a Laplacian edge enhancing filter.	SAR	Synthetic Aperture Radar, a microwave radar remote sensing technology that allows the creation of DSMs.
LRM	Local relief model is a result of a procedure that separates local small-scale features from large-scale landscape forms.	SfM	Structure-from-Motion. A multi-image digital photogrammetry approach to create three-dimensional models.
MSII	Multi-scale integral invariants is a visualization technique that has low noise sensitivity and is especially useful for revealing very subtle topography.	shaded relief	A visualization technique based on shading the digital terrain model with a constant Sun azimuth and elevation angle.
nDSM	Normalised digital surface model represents heights of features relative to the ground.	SVF	Sky-view factor is a geophysical parameter that represents the portion of the sky visible from a certain point.
noise	Noise in the digital elevation model degrades the interpretability of the data. It can result from measurement or production errors, and can usually be observed as an irregularity in the data.	TIN	Triangulated Irregular Network is a digital data structure used in a geographic information system (GIS) for the representation of a surface. The TIN model represents a surface as a set of contiguous, non-overlapping triangles. Within each triangle the surface is represented by a plane. The triangles are made from a set of points called mass points.
openness	Openness is a visualization method based on estimating the mean horizon elevation angle within a defined search radius.	viewshed	The geographical area that is visible from a location. It includes all surrounding points that are in line-of-sight with that location and excludes points that are beyond the horizon or obstructed by terrain and other features (<i>e.g.</i> buildings, trees).
PCA	Principal component analysis is a mathematical procedure that convert a set of observations of possibly correlated variables into a set of values of linearly uncorrelated variables.		
px	A pixel or picture element is a physical point in a raster image. Pixels are normally arranged in a regular two-dimensional grid, and are usually, but not necessarily, square. Each pixel is a sample of an original image; more samples typically provide more accurate representations of the original – we say the image have a higher resolution. In geographical space the pixel carries spatial information; it defines the spatial resolution of an image.		



**Bibliography and lists of
figures and tables**



Bibliography and further reading

- Adams, D. 1982. *Life, the Universe and Everything*. London: Pan Books.
- ArcMap. 2012 (version 10.1). Redlands (CA): Esri Inc.
- Batson, R. M., E. Edwards and E. M. Eliason. 1975. Computer Generated Shaded Relief Images. *Journal of Research of the U.S. Geological Survey* 3 (4): 401–408.
- Blinn, J. F. 1977. Models of Light Reflection for Computer Synthesized Pictures. *SIGGRAPH Computer Graphics* 11 (2): 192–198.
- Boeree, G. 2009. General Psychology: Perception and Interaction. <http://webspace.ship.edu/cgboer/genpsyperception.html>.
- Cashman, K. V., S. A. Soule, B. H. Mackey, N. I. Deligne, N. D. Deardorff and H. R. Dietterich. 2013. How Lava Flows: New Insights from Applications of Lidar Technologies to Lava Flow Studies. *Geosphere* 9 (6): 1664–1680.
- Challis, K. 2006. Airborne Laser Altimetry in Alluviated Landscapes. *Archaeological Prospection* 13 (2): 103–127.
- Challis, K., P. Forlin and M. Kinsey. 2011. A Generic Toolkit for the Visualization of Archaeological Features on Airborne Lidar Elevation Data. *Archaeological Prospection* 18 (4): 279–289.
- Challis, K., Ž. Kokalj, M. Kinsey, D. Moscrop and A. J. Howard. 2008. Airborne Lidar and Historic Environment Records. *Antiquity* 82 (318): 1055–1064.
- Chiverrell, R. C., G. S. P. Thomas and G. C. Foster. 2008. Sediment–landform Assemblages and Digital Elevation Data: Testing an Improved Methodology for the Assessment of Sand and Gravel Aggregate Resources in North-Western Britain. *Engineering Geology* 99 (1–2): 40–50.
- Conrad, O., B. Bechtel, M. Bock, H. Dietrich, E. Fischer, L. Gerlitz, J. Wehberg, V. Wichmann and J. Böhner. 2015. System for Automated Geoscientific Analyses (SAGA) v. 2.1.4. *Geoscientific Model Development* 8 (7): 1991–2007.
- Conway, S. J., A. Decaulne, M. R. Balme, J. B. Murray and M. C. Towner. 2010. A New Approach to Estimating Hazard Posed by Debris Flows in the Westfjords of Iceland. *Geomorphology* 114 (4): 556–572.
- Crutchley, S. 2009a. Using LiDAR in Archaeological Contexts: The English Heritage Experience and Lessons Learned. In *Laser Scanning for the Environmental Sciences*, edited by G. Heritage and A. Large, 180–200. Chichester: Wiley-Blackwell.
- . 2009b. Ancient and Modern: Combining Different Remote Sensing Techniques to Interpret Historic Landscapes. *ICT and Remote Sensing for Cultural Resource Management and Documentation* 10, Supplement 1: e65–e71.
- Devereux, B. J., G. S. Amable and P. Crow. 2008. Visualisation of LiDAR Terrain Models for Archaeological Feature Detection. *Antiquity* 82 (316): 470–479.
- Devereux, B. J., G. S. Amable, P. Crow and A. D. Cliff. 2005. The Potential of Airborne Lidar for Detection of Archaeological Features under Woodland Canopies. *Antiquity* 79 (305): 648–660.
- Dietterich, H. R., S. A. Soule, K. V. Cashman and B. H. Mackey. 2015. Lava Flows in 3D. In *Hawaiian Volcanoes: From Source to Surface*, edited by E. Carey, V. Cayol, M. Poland and D. Weis, 483–505. Hoboken, NJ: John Wiley & Sons, Inc.
- Doneus, M. 2013. Openness as Visualization Technique for Interpretative Mapping of Airborne LiDAR Derived Digital Terrain Models. *Remote Sensing* 5: 6427–6442.

- Edgeworth, M. 2011. *Fluid Pasts: Archaeology of Flow*. London: Bristol Classical Press.
- Fernandez-Diaz, J. C., W. E. Carter, R. L. Shrestha and C. L. Glennie. 2014. Now You See It... Now You Don't: Understanding Airborne Mapping LiDAR Collection and Data Product Generation for Archaeological Research in Mesoamerica. *Remote Sensing* 6 (10): 9951–10001.
- Forestry Commission Scotland. 2012. Archaeological Measured Survey on Scotland's National Forest Estate. Inverness: Forestry Commission Scotland. <http://scotland.forestry.gov.uk/supporting/strategy-policy-guidance/historic-environment>.
- Fornaciai, A., M. Bisson, P. Landi, F. Mazzarini and M. T. Pareschi. 2010. A LiDAR Survey of Stromboli Volcano (Italy): Digital Elevation Model-Based Geomorphology and Intensity Analysis. *International Journal of Remote Sensing* 31 (12): 3177–3194.
- French, J. R. 2003. Airborne LiDAR in Support of Geomorphological and Hydraulic Modelling. *Earth Surface Processes and Landforms* 28 (3): 321–335.
- GDAL Development Team. 2014. *GDAL - Geospatial Data Abstraction Library*. Windows (version 1.11.0). Open Source Geospatial Foundation.
- George, M. R., R. E. Larsen, N. K. McDougald, K. W. Tate, J. Gerlach John D. and K. O. Fulgham. 2004. Cattle Grazing Has Varying Impacts on Stream-Channel Erosion in Oak Woodlands. *California Agriculture* 58 (3). <http://www.escholarship.org/uc/item/72s9c4v2>.
- Gulič, A. and M. Črešnar, ed. 2012. *Arheološka pot po Mariboru z okolico. Odsek I: Zgornje Radvanje – Spodnje Hoče. Vodnik po najdiščih / Archaeological Trail of Maribor and its Surroundings. Section I: Zgornje Radvanje – Spodnje Hoče. Guide to Sites*. Ljubljana, Maribor: Zavod za varstvo kulturne dediščine Slovenije; Društvo mladih raziskovalcev MRM Maribor.
- Haddad, D. E. and J. R. Arrowsmith. 2011. Geologic and Geomorphic Characterization of Precariously Balanced Rocks. Contributed report CR-11-B. Tucson: Arizona Geological Survey.
- Heidemann, H. K. 2014. Lidar Base Specification. In *Book 11, Collection and Delineation of Spatial Data, Chap. B4*, ver. 1.2, 67. U.S. Geological Survey Techniques and Methods. <http://dx.doi.org/10.3133/tm11B4>.
- Hesse, R. 2010. LiDAR-Derived Local Relief Models - a New Tool for Archaeological Prospection. *Archaeological Prospection* 17 (2): 67–72.
- . 2016. Visualisierung Hochauflösender Digitaler Geländemodelle Mit LiVT. In *Computeranwendungen Und Quantitative Methoden in Der Archäologie*. 4. Workshop Der AG CAA 2013, edited by U. Lieberwirth and I. Herzog, Edition Topoi, 109–128. Berlin Studies of the Ancient World. Berlin: Topoi.
- Hobbs, K. F. 1995. The Rendering of Relief Images from Digital Contour Data. *The Cartographic Journal* 32 (2): 111–116.
- . 1999. An Investigation of RGB Multi-Band Shading for Relief Visualisation. *International Journal of Applied Earth Observation and Geoinformation* 1 (3–4): 181–186.
- Horn, B. K. P. 1981. Hill Shading and the Reflectance Map. *Proceedings of the IEEE* 69 (1): 14–47.
- IGKB - Internationale Gewässerschutzkommission für den Bodensee. 2015. IGKB-Tiefenschärfe-Bodensee Digitale Geländemodelle Mit 10 m Und 3 m Auflösung. doi: 10.1594/PANGAEA.855987 <https://doi.pangaea.de/10.1594/PANGAEA.855987>.
- Imhof, E. 1982. *Cartographic Relief Presentation*. Berlin, New York: Walter de Gruyter.
- Kershaw, A. 2003. Hadrian's Wall National Mapping Programme - a World Heritage Site from the Air. *Archaeological Prospection* 10 (2): 159–161.
- Kokalj, Ž., K. Zakšek and K. Oštir. 2011. Application of Sky-View Factor for the Visualization of Historic Landscape Features in Lidar-Derived Relief Models. *Antiquity* 85 (327): 263–273.
- Laharnar, B. 2012. Notranjska med prazgodovino in antiko. Ljubljana: Univerza v Ljubljani, Filozofska fakulteta.
- Lan, H., C. D. Martin, C. Zhou and C. H. Lim. 2010. Rockfall Hazard Analysis Using LiDAR and Spatial Modeling. *Geomorphology* 118 (1–2): 213–223.
- Mara, H., S. Krömker, S. Jakob and B. Breuckmann. 2010. GigaMesh and Gilgamesh: 3D Multiscale Integral Invariant Cuneiform Character Extraction. In *Proceedings of the 11th International Conference on Virtual Reality, Archaeology and Cultural Heritage*, 131–138. Paris, France: Eurographics Association.
- Metternicht, G., L. Hurni and R. Gogu. 2005. Remote Sensing of Landslides: An Analysis of the Potential Contribution to Geo-Spatial Systems for Hazard Assessment in Mountainous Environments. *Remote Sensing of Environment* 98 (2–3): 284–303.
- Mihvec, A. 1994. Contact Karst of Brkini Hills. *Acta Carsologica* 23: 99–109.
- Miller, G. 1994. Efficient Algorithms for Local and Global Accessibility Shading. In *Proceedings of the 21st Annual Conference on Computer Graphics and Interactive Techniques*, 319–326. ACM.
- Minnaert, M. 1961. Photometry of the Moon. In *Planets and Satellites*, edited by G. P. Kuiper and B. M. Middlehurst, 213–248. Chicago: The University of Chicago Press.
- Mlekuž, D. 2013. Roads to Nowhere? Disentangling Meshworks of Holloways. In *Aerial Archaeology and Remote Sensing from the Baltic to the Adriatic*, edited by Z. Czajlik and A. Bödocs, 37–41. Budapest: Eötvös Loránd University.

- Mlekuž, D. and M. Črešnar. 2014. Landscape and Identity Politics of the Poštela Hillfort. In *Studia Praehistorica in Honorem Janez Dular*, edited by S. Tecco Hvala, 197–211. Opera Instituti Archaeologici Sloveniae 30. Založba ZRC.
- Passalacqua, P., P. Tarolli and E. Fofoula-Georgiou. 2010. Testing Space-Scale Methodologies for Automatic Geomorphic Feature Extraction from LiDAR in a Complex Mountainous Landscape. *Water Resources Research* 46 (11): W11535.
- Planina, J. 1954. Soča (Slovenia). A Monograph of a Village and Its Surroundings (in Slovenian). *Acta Geographica* 2: 187–250.
- Reitberger, J., P. Krzystek and U. Stilla. 2008. Analysis of Full Waveform LIDAR Data for the Classification of Deciduous and Coniferous Trees. *International Journal of Remote Sensing* 29 (5): 1407–1431.
- Sacchetti, F., S. Benetti, C. Ó Cofaigh and A. Georgiopoulou. 2012. Geophysical Evidence of Deep-Keeled Icebergs on the Rockall Bank, Northeast Atlantic Ocean. *Geomorphology* 159–160: 63–72.
- Sankey, J. B., N. F. Glenn, M. J. Germino, A. I. N. Gironella and G. D. Thackray. 2010. Relationships of Aeolian Erosion and Deposition with LiDAR-Derived Landscape Surface Roughness Following Wildfire. *Geomorphology* 119 (1–2): 135–145.
- Sherrod, D. R., J. M. Sinton, S. E. Watkins and K. M. Brunt. 2007. Geologic Map of the State of Hawai'i. Open-File Report 2007–1089. Reston: U.S. Geological Survey. <http://pubs.usgs.gov/of/2007/1089/>.
- Sittler, B. 2004. Revealing Historical Landscapes by Using Airborne Laser-Scanning - A 3D-Modell of Ridge and Furrow in Forests near Rastatt (Germany). *International Archives of the Photogrammetry, Remote Sensing and Spatial Information Sciences* 36 (8/W2): 258–261.
- Smith, M. J., J. Rose and S. Booth. 2006. Geomorphological Mapping of Glacial Landforms from Remotely Sensed Data: An Evaluation of the Principal Data Sources and an Assessment of Their Quality. *Geomorphology* 76 (1–2): 148–165.
- Wagner, W., M. Hollaus, C. Briese and V. Ducic. 2008. 3D Vegetation Mapping Using Small-footprint Full-waveform Airborne Laser Scanners. *International Journal of Remote Sensing* 29 (5): 1433–1452.
- Woolard, J. W. and J. D. Colby. 2002. Spatial Characterization, Resolution, and Volumetric Change of Coastal Dunes Using Airborne LIDAR: Cape Hatteras, North Carolina. *29th Binghamton Geomorphology Symposium: Coastal Geomorphology* 48 (1–3): 269–287.
- Yarbus, A. L. 1967. *Eye Movements and Vision*. Translated from the Russian edition (Moscow, 1965) by Basil Haigh. New York: Plenum Press.
- Yoëli, P. 1965. Analytische Schattierung. Ein Kartographischer Entwurf. *Kartographische Nachrichten* 15 (5): 141–148.
- Yokoyama, R., M. Shirasawa and R. J. Pike. 2002. Visualizing Topography by Openness: A New Application of Image Processing to Digital Elevation Models. *Photogrammetric Engineering and Remote Sensing* 68: 251–266.
- Zakšek, K., K. Oštir and Ž. Kokalj. 2011. Sky-View Factor as a Relief Visualization Technique. *Remote Sensing* 3: 398–415.
- Zakšek, K., K. Oštir, P. Pehani, Ž. Kokalj and E. Polert. 2012. Hill Shading Based on Anisotropic Diffuse Illumination. In *Symposium GIS Ostrava 2012*, 1–10. Ostrava: Technical University of Ostrava.
- ZRC SAZU. 2010. IAPS ZRC SAZU | Institute of Anthropological and Spatial Studies ZRC SAZU. <http://iaps.zrc-sazu.si/en/svf> 2010.

List of figures

- Figure 1: Angle dependence of analytical hill-shading: 315° azimuth illumination (A), and 225° azimuth (B), both with 35° Sun elevation. Note the difference of the relief perception and the structures that can be observed. Overgrown cultural terraces near Koboli in Slovenia as evidenced by 1 m spatial resolution terrain model. See also Figure 23. 17
- Figure 2: Very low light source angles expose features of extreme subtleness: a standard 45° Sun elevation (A) and (B), and low light 5° Sun elevation (C), all with 45° azimuth. However, this only works in areas with very gentle relief morphology, such as this example of the Site A embanked enclosure(s) in Brú na Bóinne World Heritage Site in Ireland. 1 m spatial resolution lidar data used with permission of Meath County Council and the Discovery Programme. Local histogram saturation is used to present (B) and (C). The first to show the difference this makes when compared with normally presented shaded relief (A), and the second because the image is otherwise too dark to expose any details. 18
- Figure 3: An RGB image of hill-shadings from three directions (315°, 0°, and 45° azimuth with 35° Sun elevation) (A), a composite of the first two components (B) and RGB composite of the first three components of a principal component analysis of analytical hill-shading from 16 directions with 35° Sun elevation (C). A late Roman camp at St. Helena, west of Kobarid, Slovenia. 0.5 m spatial resolution lidar data © Walks of Peace in the Soča river Foundation. 18
- Figure 4: Slope image of Žerovinšček Iron Age hillfort near Bločice, Slovenia (A). The elevation profile (B) refers to the CD line in (A). Note that the structure the profile line crosses can be quite easily – and wrongly – interpreted as convex instead of concave. 1 m spatial resolution lidar data. 19
- Figure 5: (A 1) A histogram of the whole data range – elevations between 263 m and 536 m. As we are interested only in a very narrow range of values between 271 m and 278 m – marked by a dark arrow on (A) –, it makes sense to stretch only this range to the whole ‘colour’ palette (B). (A 2) A histogram of stretched values of the area shown on Figure 5. Instead of everything being concentrated in a ‘dark corner’ of the histogram, the values are much more evenly distributed and differences in colour shade can be more easily perceived. 20
- Figure 6: Histogram stretch to a narrow range of values. Past riverbeds of Nadiža. 0.5 m spatial resolution lidar data, West of Kobarid in NW Slovenia. 20
- Figure 7: A hill-shaded image (A) and a histogram stretch (B) of a local relief model, and the LRM presented with a purposely designed colour ramp overlaid on a hill-shaded image (Hesse 2010) (C). 1 m spatial resolution lidar data Žerovinšček Iron Age hillfort near Bločice, Slovenia © ZRC SAZU. 21
- Figure 8: Sky-view factor image (10 m search radius in 16 directions) (A) and anisotropic sky-view factor image (B) of Žerovinšček Iron Age hillfort. Many

details can be perceived despite the variable relief morphology.

22

Figure 9: Sky-view factor image (10 m search radius in 16 directions) of ridge and furrow near Neudingen, Germany (A). Omitting the nearest pixels from the calculation can reduce the noise in the data so that features can be perceived more clearly (B). 1 m spatial resolution lidar data © LGL in Baden-Württemberg.

23

Figure 10: Positive (A) and negative (B) openness image (10 m search radius in 16 directions) of a late Antiquity settlement of Tonovcov grad, Slovenia. The very complex terrain seems flattened. Tops of protruding features are well delineated on positive openness image, while negative openness delineates the bottoms of hollows and lower edges of cliffs.

24

Figure 11: Local dominance image (10-20 m search radius) of former field boundaries, roads, and ridge and furrow near Hügelsheim, Germany. Ridge and furrow is only preserved in areas that are today covered by forest. Some other features on the image include bomb craters, earth covered bunkers, and trenches. 1 m resolution lidar data © LGL in Baden-Württemberg.

25

Figure 12: Cumulative visibility image of burial mounds (high values) and dolines (low values) on the Swabian Alb. 1 m resolution lidar data © LGL in Baden-Württemberg.

25

Figure 13: Accessibility image (20 m maximum radius) of very narrow agricultural terraces with vineyards near Jeruzalem, Slovenia. 0.5 m resolution lidar data © ARSO, Slovenia.

26

Figure 14: Multiscale integral invariants image of a late Roman camp at St. Helena, west of Kobarid, Slovenia. 0.5 m resolution lidar data © Walks of Peace in the Soča river Foundation.

26

Figure 15: Image of a late Roman camp at St. Helena, west of Kobarid, Slovenia as evident on a 0.5 m resolution lidar data filtered by a Laplacian-of-Gaussian convolution filter with a radius of 3 pixels (*i.e.* 1.5 by 1.5 m).

27

Figure 16: Lidar data density maps of Castle Montfaucon east of Besancon, France. Density of all points (A), vegetation points (B) and ground points (C) calculated per every pixel (0.5 m) but plotted per m². Density of ground points calculated and plotted per m² (D). 0.5 m resolution lidar data © University of Franche-Comte.

28

Figure 17: Anisotropic sky-view factor image of elevation models produced with different rasterization (interpolation) algorithms. Note the difference in interpolation of the castle area and the south-eastern slope leading to it. Natural Neighbours (NN) (A) generates a very smooth terrain, Inverse Distance Weighted (IDW) (B) introduces steps, TIN with Repetitive Interpolation (REIN) (C) introduces triangles, and splines (D) create a range of artefacts.

28

Figure 18: 'Fish scales' are a result of direct point cloud rasterization (A). 0.5 m spatial resolution lidar data of an area around Besancon, France, © University of Franche-Comte. Black stars typically form around small protruding features on a sky-view factor (SVF) image when calculating it with 8 or 16 directions (B). 0.5 m spatial resolution lidar data of World War I trenches near Kobarid in Slovenia. © Walks of Peace in the Soča river Foundation. 1 m spatial resolution lidar data full of false depressions (C). They are a result of poor data processing that classified many below-ground lidar points as true ground. Poštela burial mounds can be seen in the upper left corner of (C). © ARSO, Slovenia. All images display SVF calculated in 8 directions with a 10 m search radius.

29

Figure 19: Wave-like features are a consequence of poor registration of scan lines (A). Charcoal burning platforms can be seen in (A). 0.5 m spatial resolution lidar data of an area around Besancon, France, © University of Franche-Comte. Severe strip misalignment and over-ambitious resolution setting result in scrub-like artefacts and fictional steps in terrain (B). 1 m spatial resolution lidar data of an area close to Tauberbischofsheim © LGL in Baden-Württemberg. Both images display SVF calculated in 8 directions with a 10 m search radius.

29

Figure 20: An original image where only a minimum-maximum histogram stretch has been applied – a whole range of values is displayed with relative differences between values preserved (A). Images displayed with different techniques of histogram stretch: histogram equalisation (B), standard deviation 2.5 σ (C), 0.5 % saturation of minimum and maximum (D).

33

Figure 21: Visualization techniques in different topographic settings. (A) Plough headlands on a flat plain near Endingen am Kaiserstuhl. 1 m lidar data © LGL in Baden-Württemberg. (B) Three different types of World War I trenches with shelters on gentle NE slopes of Črni hribi, near Renče, Slovenia. 1 m lidar data © ARSO,

- Slovenia. (C) Charcoal burning platforms in the hills of the Black forest. 1 m lidar data © LGL in Baden-Württemberg. (D) A late Roman campo on a rocky outcrop with a church of St. Helena, west of Kobarid, Slovenia. 0.5 m lidar data © Walks of Peace in the Soča river Foundation. 36
- Figure 22: Different scales of observation. Sky-view factor image of a detail from a richly decorated kerbstone from Newgrange, Ireland, produced with Structure-from-Motion of hand held photographs (A). Scattered bones (B) and looting traces (C) on a desert floor in Peru. The elevation model was computed from images taken with a camera on a pole and is presented here with a combination of local dominance and shaded relief. Grand Canyon (D) as evidenced by 30 m SRTM data presented with a combination of sky-view factor and shaded relief. Central Massif, the Jura and the Alps (E) presented with a combination of anisotropic sky-view factor and shaded relief. 38
- Figure 23: Is it a burial mound or a hole in the ground, a quarry or a hill? Someone observing the image needs to know the direction of the light source, because it has a definitive impact on the perception of the landscape. 315° azimuth illumination (A), and 135° azimuth (B). Terrain features seem inverted on (B). 39
- Figure 24: Overgrown remains of an abandoned village Novi Breg (Naubacher), Slovenia, as represented by local relief model technique with a filter radius of 25 m (A). Remains of houses can be seen as bright rectangles. Big black blobs are dolines. It is straightforward to replicate such an image with the minimum data that is provided. However, when reproduction or relative comparison across areas is not required, combinations of visualizations can give images that are easier to read, and details about visualizations may be omitted (B). 1 m resolution lidar data © ARSO, Slovenia. 40
- Figure 25: Hillshading algorithms in ArcMap (ArcMap 2012) and RVT use the same method (Yoëli 1965), but the results are quite different as evident from the image of skyscrapers in Lower Manhattan. The hillshading image calculated with ArcGIS (A) seems to be less clear (as if using a DEM of a lower resolution) than the one calculated with RVT (B). Note the distinctly visible elevation steps on (B), especially the steps on the facade of the lower right skyscraper (B), which are completely missing on (A). Both (A) and (B) have saturated high and low values (completely white and black areas). However, RVT calculates hillshading with a full range of values therefore details in black areas are revealed to a great extent on the original unsaturated image (C). The same is true for the difference in calculation of sky-view factor with RVT and SAGA GIS. All figures are calculated with 35° Sun elevation and 315° azimuth using the same DEM. 1 m spatial resolution lidar data © USGS. 41
- Figure 26: Visualization techniques with different relief features. 42
- Figure 27: Relief Visualization Toolbox (RVT) offers a range of only the best techniques with just the essential options. It is extremely easy to use and can process multiple files and all techniques in one go. 49
- Figure 28: Lidar Visualization Toolbox (LiVT) supports calculation of various techniques with intricate options to manipulate the settings. 49
- Figure 29: Craig canyon alluvial fan (California, USA) as evident on 0.5 m spatial resolution lidar data (California, USA). Coloured stretched elevations over SVF and shaded relief. © Plate Boundary Observatory by NCALM, USA. 53
- Figure 30: Alluvial fan's apron at the foot of Craig Canyon in the Saline Valley, USA. Photo by Brian Lockett, Air-and-Space.com. 53
- Figure 31: Parallel hollow ways in a forest NW of Volčji Potok, Slovenia. Photo by Žiga Kokalj. 54
- Figure 32: Hollow ways and headstreams below a hillfort on Žiški vrh, northern Slovenia, as evident on a combination of sky-view factor (0.65-1.0, 25 % opacity, multiply), positive openness (70-93, 50 % opacity, overlay), slope (0-45°, 50 % opacity, luminosity) and hillshading. 0.5 m spatial resolution lidar data © ARSO, Slovenia. 55
- Figure 33: Hollow ways developed on a narrow passageway along the river. Volčji Potok, northern Slovenia. 0.5 m spatial resolution lidar data © ARSO, Slovenia. 55
- Figure 34: Gradišče nad Knežakom hillfort in the centre of the image is today totally covered by impenetrable forest. Photo by Boštjan Laharnar. 56
- Figure 35: Iron Age settlement above Knežak and its surroundings as evident on the classified Slovenian national lidar data (GKOT, © ARSO, Slovenia) which has been processed by gLidar software, rasterized to a 0.5 m grid. Many small bumps and non-existent holes are visible (see also Figure 18C). The image is a combination of

sky-view factor (0.7-1.0, 70 % opacity, multiply), slope (0-55°, 100 % opacity, overlay) and hillshading.

57

Figure 36: The same are as in Figure 35, but processed with different software (LASTools). Even with minimal effort (default settings), the resulting image gives a clearer picture of the archaeological and natural topography, despite losing some of the 'sharpness'. Clearance cairns and field boundaries can be seen on the lower part of the image. 0.5 m spatial resolution lidar data © ARSO, Slovenia.

57

Figure 37: One of the burial mounds at Pivola, well protected by brambles. Photo by Žiga Kokalj.

58

Figure 38: Burial mounds at Pivola as displayed by a Local Relief Model transparently overlaid on a sky-view factor image and shaded relief. The state of preservation of the mounds differs significantly. The ones in the forest are well preserved (1), mounds in the Botanical Garden were damaged when the location served as a military base (2), and the mounds in the fields have been nearly completely levelled (3). 0.5 m spatial resolution lidar data © ARSO, Slovenia.

59

Figure 39: Visual structure of landscape as represented by Higuchi's foreground range total viewshed around Pivola barrow group. 1 m spatial resolution lidar data © ARSO, Slovenia. Reproduced with permission by D. Mlekuž.

59

Figure 40: Lines of poles at Culbin Sands. Photo © Forestry Commission Scotland.

60

Figure 41: Changes in elevation with added intensity information, Culbin Sands. Lidar intensity is usually recorded at the time of scanning and can provide additional discriminating information about the landscape. 0.5 m spatial resolution lidar data © Forestry Commission Scotland.

61

Figure 42: A close-up view of Culbin Sands as seen on a sky-view factor image calculated in 8 directions. Poles are easily identifiable as black stars. 0.5 m spatial resolution lidar data © Forestry Commission Scotland.

61

Figure 43: A view across the ridge towards Vrh Brda and Bavški Grintavec in the background. Photo by Jovan Cukut.

62

Figure 44: Glacially transformed karstic plateau at Velika vrata, Slovenia. Flat areas of clints are presented in light colours while grikes, crevices, and steep slopes are dark. The image is a combination of sky-view factor (0.5-1.0, 70 % opacity, multiply),

slope (0-65°, 80 % opacity, overlay) and RGB image of hillshading from three directions (R: 315°, G: 15°, B: 75°), all computed on a digital surface model. 0.5 m spatial resolution lidar data © ARSO, Slovenia.

63

Figure 45: Dachstein limestone strata and scree fields exposed at Vrh Brda (1952 m). The top of the ridge is highlighted in white, while colours represent different orientation of the slopes. The visualization is a combination of sky-view factor (0.55-1.0, 30 % opacity, multiply), positive openness (65-95, 50 % opacity, overlay), slope (0-65°, 80 % opacity, luminosity) and RGB image of hillshading from three directions (R: 315°, G: 15°, B: 75°). 1 m lidar data © ARSO, Slovenia.

63

Figure 46: Granite Dells at Watson Lake. Photo by Michael Wilson.

64

Figure 47: Digital terrain model (DTM) of Granite Dells, Arizona, USA. Much of the detail in the landscape is lost despite dedicated processing. A combination of anisotropic sky-view factor (0.2-1.0, 40 % opacity, multiply), slope (0-80°, 60 % opacity, overlay) and RGB image of hillshading from three directions (R: 337.5°, G: 0°, B: 22.5°). 0.5 m spatial resolution lidar data © NCALM, USA.

65

Figure 48: Digital surface model (DSM) of the same area as in Figure 47. Visible are trees, houses, and cars, but more importantly also the joints in granite that are characteristic of the Dells. 0.5 m spatial resolution lidar data © NCALM, USA.

65

Figure 49: View of Mauna Loa from Mauna Kea with cinder cones in the foreground. Photo by Lawrence Goldman.

66

Figure 50: Lava flows on the Mauna Loa shield volcano are difficult to observe on the ground because they are either hot, have rough and jagged surfaces, or are covered by vegetation. Many vents and cinder cones are visible on this hillshaded image of 1 m spatial resolution lidar data © NCALM.

67

Figure 51: This visualization provides a very plastic representation of the surface and reveals an intricate system of cinder cones, vents, cracks, folds, and channels of a lava field on the north-eastern slope of Mauna Loa. The visualization is a combination of positive openness (65-95, 50 % opacity, darken), sky-view factor (0.65-1.0, 50 % opacity, multiply), slope (0-50°, 100 % opacity, overlay) and hillshading. 0.5 m spatial resolution lidar data © NCALM.

67

- Figure 52: Blind valley Brezovica. A view to the north. Ločica stream that formed the valley sinks underground in the foreground of the photograph. Photo by Žiga Kokalj. 68
- Figure 53: Odolina (1) and Brezovica (2) blind valleys. Contact borderline between flysch and limestone runs NW to SE and is very clearly recognizable. The brooks form a normal fluvial relief on flysch and form corrosion widened valleys on limestone before disappearing underground. Dolines, sinkholes, and other typical karst features are also easy to identify. 1 m spatial resolution lidar data © ARSO, Slovenia. 69
- Figure 54: A close-up view of the end of blind valley Odolina. On such a location and without prior knowledge about the area someone would expect a stream source. The abyss where Brsnica disappears underground at high water, carrying with it tons of sediment and wood, is marked with an arrow. 1 m spatial resolution lidar data © ARSO, Slovenia. 69
- Figure 55: With a surface area of approximately 570 km² and a maximum depth of 252 m, Lake Constance is one of the largest and deepest lakes in Europe. It was formed by glacial erosion during the last Ice Ages. Large drumlin fields, mainly north of the lake, document the direction of ice flow during the last glaciation. When the glaciers retreated, the basin filled with water and became Lake Constance. Photo by Frank Numrich. 70
- Figure 56: Iceberg scour marks (curvilinear features) and mass movement deposits (lobate features at the foot of the steep slope) in Lake Constance. Visualisation: Laplacian-of-Gaussian overlaid by colour-coded bathymetry. 3 m spatial resolution bathymetric model © IGKB (2015). 71
- Figure 57: Bathymetric profile (A-B) from data shown in figure 56 reveals the flat subaqueous bench on which most iceberg scour marks occur. 3 m spatial resolution bathymetric model © IGKB (2015). 71
- Figure 58: Brooklyn bridge across the East River with skyscrapers of Lower Manhattan in the background. Photo by Žiga Kokalj. 72
- Figure 59: A combination of colour coded elevations and unsaturated shaded relief. This would be a typical two dimensional representation of a city scene. While heights of buildings can be determined to a certain extent, all the values higher than 110 m had been clipped to get a better distribution of colours. Even though the image presents Lower Manhattan with many buildings exceeding 50 m in height, their magnificence is not evident. 1 m spatial resolution lidar data © USGS. 73
- Figure 60: This image is less colourful than Figure 59 but the shadows give a more grandeur feeling of the high-rise buildings. A combination of an overcast Sky Illumination Model (100 m shadow modelling distance) and a cast shadow (35° Sun elevation and 135° azimuth). 1 m spatial resolution lidar data © USGS. 73
- Chapter 1. Charcoal burning platforms in the Black forest, Germany, as evident on a sky-view factor image (10 m search radius in 16 directions). 1 m resolution lidar data © LGL in Baden-Württemberg. 10
- Chapter 2. Anisotropic sky-view factor image (5 m search radius in 16 directions) of Ajdovščina above Rodik hillfort, Slovenia. 0.5 m resolution lidar data © ARSO, Slovenia. 14
- Chapter 3. Local dominance image (10-20 m search radius) of plough headlands at Endingen am Kaiserstuhl, Germany. 1 m resolution lidar data © LGL in Baden-Württemberg. 30
- Chapter 4. House mounds, palaces, platforms, walls, quarries, a possible water reservoir, and a field system of an unknown Maya settlement in the Calakmul Biosphere Reserve, Campeche, Mexico. A combination of visualizations (sky-view factor, openness, slope, hillshading). 0.5 m resolution lidar data © ZRC SAZU, Slovenia. 46
- Chapter 5. A part of Maiden Castle Iron Age hillfort, United Kingdom, as seen on a sky-view factor image (5 m search radius in 16 directions). 0.5 m resolution surface model lidar data © Environment Agency, UK. 50
- Glossary of terms. Eye of the Sahara or Guelb er Richat is a deeply eroded geologic dome in Mauritania. A combination of visualizations (sky-view factor, slope, hillshading). 30 m SRTM data © USGS. 74
- Bibliography and lists. Sand dunes at Guaiuba, Santa Catarina, Brazil, as seen on a sky-view factor image (10 m search radius in 16 directions). 1 m resolution surface model lidar data © FAPESP grant 2009/17675-5. Grohmann, C.H. and A.O. Sawakuchi. 2013. Influence of cell size on volume calculation using digital terrain models: a case of coastal dune fields. *Geomorphology* 180–181: 130–136. 78

List of tables

Table 1: Some useful resources to go search for free lidar datasets. Host sites will inevitably change and new datasets are becoming available regularly, so use your favourite search engine.	13	Table 13: Typical settings for calculation and visualization of Laplacian-of-Gaussian.	27
Table 2: Typical settings for calculation and visualization of hillshading.	19	Table 14: Matrix for the suitability of visualisation techniques for selected archaeological relief features in different topographic settings.	34
Table 3: Typical settings for calculation and visualization of principal components analysis of hillshading images from multiple directions.	19	Table 15: Suitability of visualisation techniques for representing selected archaeological topographical features.	35
Table 4: Typical settings for visualization of slope.	19	Table 16: Metadata required when presenting DEM visualisations.	39
Table 5: Typical settings for displaying elevation differentiation.	20	Table 17: Lidar scanning parameters of Craig canyon alluvial fan, California, USA.	53
Table 6: Typical settings for trend removal and Local Relief Modelling.	23	Table 18: Lidar scanning parameters of Žiški vrh and Volčji Potok, Slovenia.	54
Table 7: Typical settings for calculation and visualization of sky-view factor.	23	Table 19: Lidar scanning parameters of Gradišče nad Knežakom, Slovenia.	56
Table 8: Typical settings for calculation and visualization of positive and negative openness.	24	Table 20: Lidar scanning parameters of Pivola burial mounds, Slovenia.	58
Table 9: Typical settings for calculation and visualization of local dominance.	25	Table 21: Lidar scanning parameters of Culbin Sands, Scotland.	60
Table 10: Typical settings for calculation and visualization of cumulative visibility.	25	Table 22: Lidar scanning parameters of Velika vrata and Vrh Brda, Slovenia.	62
Table 11: Typical settings for calculation and visualization of accessibility.	26	Table 23: Lidar scanning parameters of Granite Dells, Arizona, USA.	64
Table 12: Typical settings for calculation and visualization of multi-scale integral invariants.	26	Table 24: Lidar scanning parameters of Mauna Loa, Hawaii, USA.	66
		Table 25: Lidar scanning parameters of Odolina blind valley, Slovenia.	68
		Table 26: Lidar scanning parameters of Manhattan, New York, USA.	72

The series *Prostor, kraj, čas* (Space, Place, Time) publishes shorter, thematically rounded studies from diverse aspects of exploration of space and time, that are based on geographical information systems and remote sensing, as well as their social and cultural constructs: how people of various periods and landscapes think about, live, feel, use, and change space and time.

Series editors: Nataša Gregorič Bon and Žiga Kokalj, ZRC SAZU

AIRBORNE LASER SCANNING RASTER DATA VISUALIZATION

A Guide to Good Practice

Žiga Kokalj and **Ralf Hesse**

Žiga Kokalj is a research fellow at the Research Centre of the Slovenian Academy of Sciences and Arts and at the Centre of Excellence for Space Sciences and Technologies. He has general research interest in application of optical imagery and aerial laser scanning, spatial analysis, and modelling of natural processes.

Ralf Hesse works at the State Office for Cultural Heritage Baden-Württemberg where he uses airborne lidar data for large area archaeological prospection. His research focuses on the visualisation and analysis of digital elevation models in the fields of archaeology and physical geography.